

UNIVERSITA' DEGLI STUDI DI TORINO



**DOTTORATO DI RICERCA IN NEUROSCIENZE
XXXIII CICLO**

**Monitoring spontaneous activity and dopamine release from
midbrain dopaminergic neurons through conventional
electrophysiology and diamond-based prototypes: focus on the
effects of exogenous α -synuclein**

Giulia Tomagra

Tutor: Prof.ssa Valentina Carabelli

ANNI ACCADEMICI: 2018 - 2021

*Ai miei genitori
che mi hanno donato forti radici per non dimenticare
ed ali robuste per poter spiccare il volo*

*e a Davide
che ha accettato tutti i miei difetti*

Abstract

Within the central nervous system, dopamine (DA) release from dopaminergic neurons occurs in two regions of the ventral midbrain, the *substantia nigra pars compacta* (SNc) and the ventral tegmental area (VTA). Dopaminergic mesencephalic neurons play an important role in a variety of brain functions, such as motor control, cognitive processes, reward-based learning, motivation. Dysfunctions of the dopaminergic system are associated to neurological disorders including Parkinson's disease (PD), a progressive neuropathology that is diagnosed when neuronal functions are severely damaged, but preceded by a long-lasting asymptomatic phase during which neuronal properties are altered without clearly affecting brain function. Despite different causes may be associated to the onset of the disease, growing evidence focus on the role of alpha-synuclein (aSyn) anomalous aggregation, and the pathogenic effects exerted by aSyn oligomers' spreading from neuron to neuron in the early stages of the disease.

My PhD research has been focused on evaluating the electrophysiological properties of cultured midbrain dopaminergic neurons and the changes of their pattern activity during the network development, through the use of multielectrode arrays (MEA). Using TH-GFP mice as experimental model, I could investigate the role of Cav_{1.2}, Cav_{1.3}, Cav_{2.3} channels in sustaining the spontaneous firing of midbrain DA neurons as well as the Ca²⁺-dependent secretion. Quantal dopamine release and its correlation with spontaneous firing has been quantified taking advantage of diamond-based multielectrode (μ G-SCD-MEA) prototypes, which have been realized to provide an electrochemical mapping of exocytosis from the network undergoing either spontaneous or stimulated activity. By means of μ G-SCD-MEAs, I uncovered a heterogeneous modulation of cultured midbrain neurons by L-DOPA, which caused either a potentiation or an inhibition of the spontaneous firing activity.

Finally, I focused on the effect of exogenous aSyn in modifying the network activity, unravelling a potential role of the MVIIC in counteracting the detrimental effects of aSyn.

Index

ABSTRACT	3
CHAPTER 1	8
INTRODUCTION	8
1.0 Function of basal ganglia	9
2.0 Electrophysiological properties of substantia nigra and VTA neurons	10
2.1 <i>Substantia nigra pars compacta neurons</i>	10
2.2 <i>Substantia nigra pars reticulata neurons</i>	12
2.3 <i>Ventral tegmental area neurons</i>	12
3.0 Dopamine release, uptake and autocrine effect SN on dopaminergic neurons	13
4.0 Role of aSyn in Parkinson's disease	18
5.0 Physiological and pathological properties of aSyn	22
CHAPTER 2	27
MATERIALS AND METHODS	27
1.0 Culture of midbrain dopaminergic neurons	27
2.0 Techniques: Patch clamp, MultiElectrode Arrays (MEA), μ G-SCD MEAs	30
2.1 Patch clamp: voltage clamp, current clamp, capacitance	30
2.2 Microelectrode arrays (MEA): recordings	33
2.3 Micro-Electrode Array: analysis	36
3.0 Amperometric detection of quantal dopamine release by carbon fibers and μ G-SCD-MEAs	40
3.1 μ G-SCD MEAs: micro graphitic single crystal diamond MEAs (<i>Picollo et al., Scientific reports DOI: 10.1038/srep20682</i>)	41
3.2 Acquisition electronic chain	43
3.3 Electrical characterization (Tomagra et al., Sensors, Lecture Notes in Electrical Engineering 539, doi.org/10.1007/978-3-030-04324-7_17)	44
CHAPTER 3	48
FIRING PROPERTIES OF CULTURED MIDBRAIN DOPAMINERGIC NEURONS	48

1.0 The firing mode of midbrain neurons switches from isolated spikes to burst-driven activity along with the network development (Tomagra et al., in preparation)	48
2.0 Modulation of the firing rate and the synchronism by GABAergic and glutamatergic input	53
3.0 Synchronization of midbrain neurons	54
4.0 The pacemaking activity of cultured midbrain dopaminergic neurons	57
CHAPTER 4	60
TIME- AND DOSE-DEPENDENT ALTERATION OF THE FIRING RATE BY EXOGENOUS A-SYNUCLEIN	60
1.0 Effect of aSyn at different concentrations in a mature network (14 DIV)	61
2.0 aSyn is uneffective on young neurons (9 DIV)	64
3.0 aSyn-reduction of the firing rate is reversed by MVIIC	66
4.0 MVIIC restores the firing rate	68
CHAPTER 5	70
ROLE OF CALCIUM CHANNELS IN SUSTAINING THE FIRING AND THE CA²⁺ DEPENDENT SECRETION OF MIDBRAIN DOPAMINERGIC NEURONS (BY MEANS OF CONVENTIONAL ELECTROPHYSIOLOGY)	70
1.0 Role of Cav_{1.3} in sustaining the spontaneous firing activity of midbrain dopaminergic neurons.	72
2.0 Role of Cav_{2.3} sustaining the firing activity of midbrain dopaminergic neurons: SNX-482 inhibits Ca²⁺ current (I_{Ca}) and reduces spontaneous AP firing (<i>Siller et al. e-life 2021, peer review e-Life</i>)	73
3.0 Ca²⁺ channels contribution to the Ca²⁺-dependent secretion in midbrain DA neurons.	76
CHAPTER 6	79
NEW APPROACHES FOR INVESTIGATING MULTISITE DETECTION OF DA RELEASE AND CELL FIRING (DIAMOND-BASED MULTIARRAY PROTOTYPES)	79
1.0 L-DOPA potentiates the stimulus-dependent exocytosis and down-regulates the spontaneous firing activity	79

2.0 The μG-SCD-MEAs: compact and versatile device that allows the measurement of secretion from 16 electrodes	81
3.0 Dopamine detection in the PC12 dopaminergic cells by means of μG-SCD-MEAs (Tomagra et al., <i>Biophysical chemistry</i> 2019 [157])	82
4.0 Detection of quantal DA release from dopaminergic neurons using μG-SCD-MEAs (Tomagra et al., <i>Frontiers in Neuroscience</i> 2019 [9])	85
5.0 L-DOPA-induced modulation of firing dopaminergic neurons and role of D₂-autoreceptors (Tomagra et al., <i>Frontiers in Neuroscience</i> 2019)	87
6.0 D₂-autoreceptor induced inhibition after L-DOPA administration in Current-Clamp Recordings	87
7.0 Dopamine-induced modulation of neuronal firing observed through μG-SCD-MEAs and conventional MEAs: role of D₂ receptor (Tomagra et al., <i>Frontiers in Neuroscience</i> 2019)	90
8.0 Simultaneous amperometric and potentiometric detection of neural signals	95
CHAPTER 7	97
DISCUSSION	97
1.0 Monitoring the maturation of the dopaminergic network maturation	97
2.0 Dopaminergic neurons are more affected by GABAergic control than glutamate control	98
3.0 Synchronization is regulated by the GABAergic and glutamatergic activity	99
4.0 Cav_{1.3} and Cav_{2.3} can play an important role in neuroprotection in PD	101
5.0 μG-SCD-MEAs are efficient to monitor quantal release and electrical activity	102
6.0 The L-DOPA-induced down-modulation of spontaneous firing and the effect is reverted by D₂ autoreceptor	103
7.0 μG-SCD-MEAs are suitable tools for simultaneously performing amperometric and potentiometric measurements	104
8.0 MVIIC restores the impaired firing rates by aSyn	105
CHAPTER 8	109
BIBLIOGRAPHY	109

- aSYN: α -sinuclein protein;
- AC: adenylate cyclase;
- AMPA: acid- α -amino-3-idrossi-5-isoxazol-propionico;
- AP-V, AP-5: acid (2R)-amino-5- fosfonopentanoico;
- BK: large conductance potassium channels;
- cAMP: Cyclic adenosine monophosphate;
- Ctrl: control;
- DA: dopamine;
- DAT: dopamine transporter;
- DIV: days in vitro;
- DNQX: 6,7-dinitrchinossalin-2,3 (1H,4H)-dione;
- DOPA: diidrossifenilalanine;
- GABA: γ - aminobutirric acid;
- GIRK: G protein-coupled inwardly-rectifying potassium channel;
- GP: globus pallidus;
- GPCR: G protein coupled receptor;
- GPe: globus pallidus external;
- GPi: globus pallidus internal;
- HVA: high voltage-activated channes;
- L-dopa: l - DiOxyPhenylAlanine
- KA: kainate;
- MEA: multiElectrode array;
- mGluR: metabotropic glutammatergic receptors;
- NACC: nucleus accumbens;
- NiT: titanium nitride;
- NMDA: N-metil-D-aspartic acid;
- PD: Parkinson disease;
- PKA: protein kinasi A;
- SCH 23390: (R)-(+)-7-cloro-8-idrossi-3-metil-1-fenil-2,3,4,5-tetraidro-1H-3-benzazepine;
- SK: small conductance calcium-activated potassium channels;
- SN: substantia nigra;
- SNARE: SNAP (Soluble NSF Attachment Protein) receptor
- SNCA: Synuclein alpha gene;
- SNPC o SNc: substantia nigra pars compacta;
- SNPR o SNr: substantia nigra pars reticulata;
- STN: subthalamic nucleus;
- TH: tyrosine hydroxylase;
- TTX: tetrodotoxine;
- VGCC: voltage-gated calcium channels;
- VTA: ventral tegmental area.

Chapter 1

Introduction

Midbrain dopaminergic neurons, releasing dopamine (DA), are crucial for regulating important physiological functions in the central nervous system, such as the control of movement, behaviour and reward. There are several dopaminergic pathways, which originate mainly from two mesencephalic nuclei: the *ventral tegmental area* (VTA) and the *substantia nigra* (SN). The latter represents one of the five nuclei that make up the basal ganglia circuit, which controls volunteer movements [1]–[3]. The *substantia nigra* further divides into two distinct parts: the *pars compacta* (SNc) and the *reticulate* (SNr), which mainly contain dopaminergic and GABAergic cells.

Most DA midbrain neurons are found in the *substantia nigra* and ventral tegmental area and have diffuse axonal projections to subcortical and cortical target areas. In particular, the SNc projects its afferents mainly towards the dorsal *striatum* (as shown in Figure 1) [4]. Dopaminergic neurons of the VTA project towards the limbic areas (*nucleus accumbens*, *hippocampus*, *amygdala*) and the cortical regions, constituting the mesolimbic and mesocortical respectively.

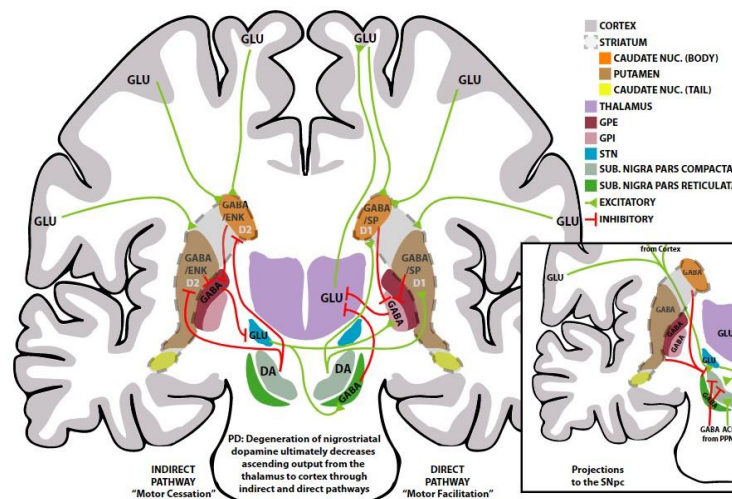


Figure 1 "Overview of basal ganglia neuroanatomy. A schematic overview of the primary motor circuits in the basal ganglia, the indirect (left) and direct (right) pathways. Note, pathways crossing sides does not imply decussation, rather the contralateral connections separate the indirect and direct pathways. Excitatory connections are depicted in green

with triangle ends, inhibitory connections are depicted in red with "T" ends. Not all connections are depicted, including but not limited to, all connections from thalamus to cortex, all connections from cortex to striatum, connections to/from caudate nucleus (tail), connections from cortex to brainstem, and inputs to SNc (pictured in the inset). Inset: a schematic overview of the inputs to SNc. The PPN is located caudal to the substantia nigra and inputs are depicted as such. Inputs from the caudate nucleus (tail) is not pictured, and not all inputs from the cortex are depicted. Merging of signals from the cortex or caudate/putamen are done for illustrative purposes. D1; D1 receptors; D2; D2 receptors; DA dopamine; ENK enkephalin; GLU glutamate; NUC nucleus; PPN pedunculopontine nucleus; SP substance P; SUB substantia" [4].

1.0 Function of basal ganglia

The basal ganglia and related nuclei are made up of a variety of subcortical neuronal groups primarily engaged in motor control, along with a wider variety of roles such as motor learning, executive functions, behaviour, and emotions. The term basal ganglia in the strict sense means the nuclei immersed deep in the cerebral hemispheres (*striatum* or *caudate-putamen* and *globus pallidus*), while the relative nuclei consist of structures located in the diencephalon (*subthalamic nucleus*), midbrain (*substantia nigra*) and bridge (*pedunculo pontine nucleus*). These consist of five closely interconnected entities: the *caudate nucleus* and the *putamen* (form the dorsal *striatum*), the *globus pallidus* (GP), the *substantia nigra* (SN) (divided into *pars compacta* and *reticulata*) and the *nucleus subthalamic* (STN).

Basal ganglia and related nuclei can be classified into: input nuclei, output nuclei and intrinsic nuclei.

Input nuclei receive incoming information from various sources. The *striatum* and *subthalamic nucleus* represent the most important input and reception stations information from the cerebral cortex. The output nuclei send information about the basal ganglia to the thalamus. The inner part of the *globus pallidus* (GP_i) and the *substantia nigra pars reticulata* (SN_r) represent the main output nuclei, protruding towards the thalamus and the brain stem. Finally, the intrinsic nuclei are located between the input and output nuclei in the information relay. These nuclei are the outer segment of the *globus pallidus* (GP_i) and the *substantia nigra pars compacta* [5].

Two distinct pathways, one direct, monosynaptic and inhibitory (*striatum-GP_i* and *striatum-SN_r*) and the other indirect, polysynaptic and excitatory, which includes external part of the *globus pallidus* (GP_e) and *subthalamic nucleus* (STN) (*striatum - GP_e -STN*) [6],

[7], provide synaptic communication between the *striatum* and the nuclei of output (GP_i and SN_r). The output of the basal ganglia consists of GABAergic fibers (from GP_i and SN_r) which terminate in the thalamus and inhibit glutamatergic thalamo-cortical neurons. The strength of thalamic inhibition is believed to depend on the clear prevalence of the direct versus the indirect pathway: the activation of some striatal neurons inhibits GP_i and SN_r through the direct pathway (D₁), while the activation of other striatal neurons may have, through the indirect pathway (D₂), a net excitatory effect on GP_i and SN_r.

As a consequence of this complex modulation, an increase in the output of the basal ganglia (GABAergic) produces a decrease in movement through the inhibition of the glutamatergic neurons of the *cortical thalamus*, while a reduced output of the basal ganglia leads to an increase in movement due to the disinhibition of the thalamic neurons themselves.

In particular, an important internal circuit, consisting of the nigrostriatal dopaminergic projection, provides the source of dopamine (DA) in the dorsal striatum. The SN, located in the ventral midbrain, is an essential site that regulates the overall execution of movements. Is divided in two functional and anatomically distinct areas: *pars compacta*, where they are located neurons that synthesize DA and project towards the *striatum* and *pars reticulata*, where they have originated the outgoing GABAergic neurons directed towards the *thalamus* [8].

2.0 Electrophysiological properties of substantia nigra and VTA neurons

The neurons of the *substantia nigra*, as mentioned, are distributed within the *substantia nigra pars compacta* (SNc) containing mostly dopaminergic neurons, and *substantia nigra pars reticulata* (SNr) mostly GABAergic neurons.

2.1 *Substantia nigra pars compacta neurons*

Dopaminergic neurons in the *substantia nigra compacta* (SNc) are characterized by a short-lasting action potential (AP) (> 1.5 ms), which appears biphasic in most extracellular

recordings made with MEAs (MultiElectrode Array) [9]. The AP is characterized by a post-hyperpolarization phase mediated by a Ca^{2+} -activated potassium conductance [10].

As reported by Berretta et al. [11] in slices, these mesencephalic dopaminergic neurons can be distinguished in high rate (H_R) neurons and low rate neurons (L_R). H_R are mainly identified by a basal firing frequency > 7 Hz and are characterized by a regular pacemaker-like firing pattern defined by an higher-frequency burst firing evoked by glutamatergic input [12].

The low firing frequency are very heterogeneous: it is possible to distinguish low rate pacemaker (LRp), with a typical basal firing rate (1-3 Hz), and low rate non-pacemaker (LRn-p) with a typical basal firing frequency less than 1 Hz [11], [13].

The pacemaker-like firing pattern is mainly regulated by Ca^{2+} currents, particularly L-type, although it has been also recently observed an important component of R-type calcium [14], [15], which support depolarizations that regulate this pacemaker activity [16]. Though, several evidence [17]–[20] demonstrated also a role of Ca^{2+} and Na^+ currents in the pacemaking: others elucidates the role of Kv_4 -mediated A-type current, SK Ca^{2+} -activated potassium current [21]–[24]. Recently, Kimm et al., [25] demonstrated the involvement of BK and Kv_2 channels in spike repolarization, even though the effect on pacemaker is different among slices and dissociated neurons: the role of these two potassium channels in slices is relevant while a consistent effect in dissociated neurons is lacking. One possible explanation could be due to the fact that some channels in the dendrites or axon that can be lost in the dissociation procedures.

In vivo, midbrain dopaminergic neurons may be silent or exhibit regular, infrequent and irregular firing or burst firing. The pacemaker-like activity promotes a tonic release of dopamine, while a burst firing promotes a phasic release [26], [27]; this is very important in voluntary movement control.

Last but not least, a further phenomenon that modulates this firing is the release of dopamine from the soma and dendrites: released DA activates D_2 autoreceptors, providing an inhibition of electrical activity through the activation of K^+ currents linked to G proteins (GIRK) [28]–[30]. These characteristics suggest that the depolarization of dopaminergic cells is able to activate Cav causing a release of dopamine which, in turn, acts on dopaminergic D_2 autoreceptors [29].

It has also been observed that specific activation systems of oscillatory activity in synchronized neuronal populations encode information in both physiological and pathological conditions [11], [31].

2.2 *Substantia nigra pars reticulata neurons*

The neurons of the SNr, unlike those of the SNc, are for the most part GABAergic. They are characterized by a tonic firing that depends on different conductances. Furthermore, they express apamine-sensitive K^+ - Ca^{2+} channels (SK) [32]. SNr neurons show a relatively depolarized membrane potential compared to other neurons; this seems to depend on a tonic incoming current that provides a depolarization of 10 mV and is mediated by TRPC₃ channels [8],[33].

In pathological conditions, such as in Parkinson's disease, the firing is affected and the GABAergic neurons of the SNr and the internal *globus pallidus* acquire a burstly firing mode due, at least in part, to a greater excitatory contribution from the *subthalamic nucleus* [7],[8]. Stimulation of the NMDA receptor activates a non-selective cationic conductance activated by Ca^{2+} (TRPM₂) capable of sustaining burst firing; the latter seems to be further supported by low conductivity K^+ (SK) channels dependent on calcium and high voltage Ca^{2+} (HVA) channels [8].

2.3 *Ventral tegmental area neurons*

Ventral tegmental area (VTA) is characterized by dopaminergic and non-dopaminergic (mainly GABAergic) neurons.

Dopamine (DA) neurons in VTA are implicated in different brain functions: drug addiction, behavioral disorders, cognition, motivation, and locomotor activity. These neurons are characterized by a hyperpolarization activated current (I_h). Electrophysiological properties have confirmed the presence of DA neurons mainly in the lateral and medial VTA. These DA neurons show spike frequency adaptation when the cell membrane is depolarized, and a large voltage “sag¹” when hyperpolarized [34].

Autoreceptor feedback, also in the VTA, is an important regulator in controlling the activity and discharge patterns of dopaminergic cells. A notable exception to this form of

¹ Absolute difference between the steady state decrease in the voltage and the largest decrease in voltage following a hyperpolarizing current step.

lateral inhibition occurs in the mesocortical VTA dopaminergic neurons projecting to the prefrontal cortex. These cells exhibit reduced levels of D₂ receptors and GIRK channels and are therefore insensitive to autoreceptor-mediated feedback inhibition [35], [36]. Recent evidence show that VTA DA neurons can release glutamate as co-transmitter [35], [37]–[39]. In the VTA a subpopulation of GABA and glutamate neurons is also present: it has been estimated that GABA neurons to be around 30-35%, and the glutamate more or less 2-5% [40].

3.0 Dopamine release, uptake and autocrine effect SN on dopaminergic neurons

Dopamine, is released in several brain areas, including the *substantia nigra* and the ventral tegmental area (VTA). Other quantities are found also in the telencephalon, in the accumbens, in the olfactory tubercle, in the central nucleus of the amygdala.

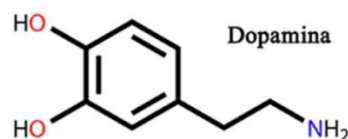
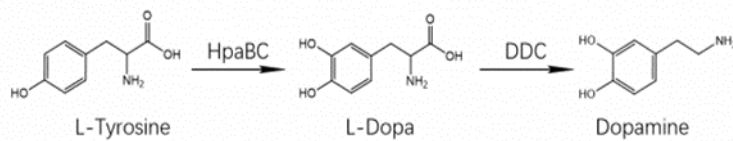


Figure 2 Dopamine

Besides regulating a wide range of neurophysiological functions such as movement control, behavioural functions, dopamine is also involved in some neurological diseases, such as Lewy bodies disease, Parkinson's or schizophrenia, all of which are related to dysfunctions of dopaminergic synapses. Dopamine may act also a hormone, which is released from the *hypothalamus*, it is also known as the euphoria hormone due to its role related to reward mechanisms.

Dopamine belong to the catecholamine family, deriving from the amino acid tyrosine, characterized by the presence of a catechol nucleus (to which they owe their name), via an ethylene bridge.

The synthesis of dopamine occurs in the cytosol of dopaminergic neurons starting from tyrosine. The first step leading to the synthesis of dopamine is carried out by the tyrosine hydroxylase (TH) enzyme, producing dihydroxyphenylalanine (DOPA). The second step involves the DOPA-decarboxylase enzyme, which eliminates the carboxyl group thus forming dopamine. This is the principal way, but dopamine can also be synthesized indirectly from phenylalanine [41], [42], which is the amino acid from which tyrosine is derived by hydroxylation.



Once synthesized, dopamine is stored in vesicles via the monoamine transporter 2 and is released from these following a presynaptic stimulus.

Dopamine-induced effects are mediated by G protein-coupled receptors (GPCRs) consisting of transmembrane 7 α -helices with the N-terminal domain at the extracellular level and the C-terminal domain at the intracellular level.

The physiological effects of dopamine are mediated by five dopaminergic receptors, divided into two groups: the D₁-like (D₁, D₅) and D₂-like (D₂, D₃, D₄) receptors. These are respectively coupled to excitatory G_s/olf and inhibitory G_i/G_o proteins.

D₁-like receptors increase cAMP (adenosine monophosphate cyclic) which acts by stimulating protein kinase A (PKA) and activating a cascade of phosphorylations, while D₂-like receptors cause inhibition of adenylate cyclase (AC), lower cAMP levels and inhibit PKA [43]. The primary action of DA is to activate neurons through D₁-like receptors, this activation is regulated/antagonized by D₂-like receptors [44].

D₁ modulates several ion channels, including voltage-gated Na⁺ (Na_v), K⁺ (K_v), and Ca²⁺ channels (Ca_v); G-protein activated potassium channels (GIRK) and calcium-dependent potassium channels (K_{Ca}) [45]. D₁-like receptors exhibit a higher density at the level of the *striatum* or *caudo-putamen*, of the *nucleus accumbens* (NACC), of the *SN pars reticulata* (SN_r), of the *SN pars compacta* (SN_c) [46], of the *hypothalamus* [46] and of the olfactory

bulb [43], [47]. A moderate presence of the D₁ receptors in the *entopeduncular nucleus* (inner part of the *globus pallidus*).

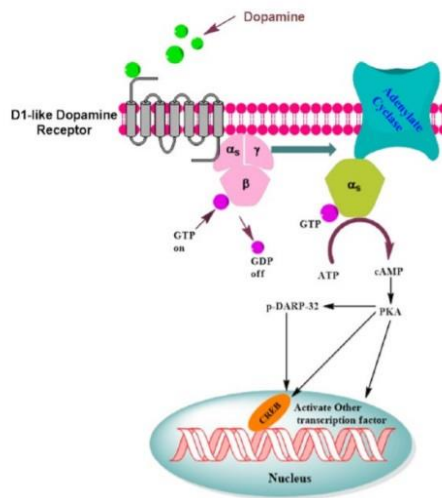


Figure 3 D₁-like receptors function. Adapted from Mishra et al., 2018 [43]

The D₂ receptor is mainly expressed in the *striatum*, in the external *globus pallidus*, in the *nucleus accumbens*, in the amygdala, in the cerebral cortex, in the *hippocampus*, in the pituitary gland. Is present also in the prefrontal, temporal and entorhinal cortex; in the ventral tegmental area (VTA) and in the *substantia nigra pars compacta* (SN_c) [43], [48]. D₂ receptors are autoreceptors expressed at the somatodendritic level, where reduce neuronal excitability, and at the axon terminal, where they reduce the synthesis, the storage and the release of dopamine.

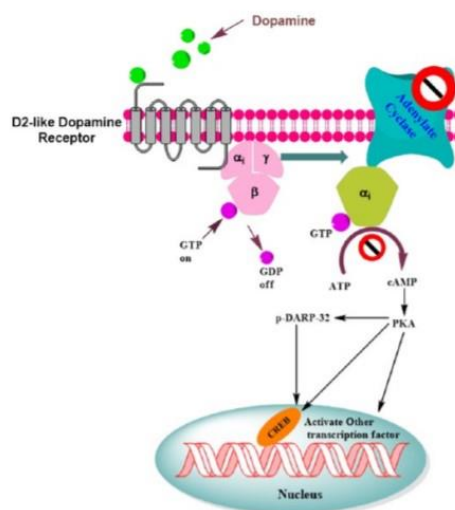


Figure 4 D₂-like receptors function. Adapted from Mishra et al., 2018 [43]

The D₁ and D₂ receptors show a separate expression at the level of the GABAergic medium spiny neurons (MSNs), which are the largest population in the *striatum*. The *striatum* modulates the activity of the basal ganglia by acting on both dopaminergic receptors. MSNs expressing D₁ project directly onto the output nuclei of the basal ganglia, the SNr and the *globus pallidus internus*, via what is termed the direct or D₁-pathway. MSNs expressing D₂ projection to the intermediate nuclei, the external *globus pallidus* which in turn projects to the *subthalamic nucleus* this is known as the indirect pathway. The combined D₁/D₂ activation regulates SNr and *globus pallidus internus*, which control excitation of the cortex through the *thalamus*, promoting or inhibiting locomotion [45]. Neurons expressing D₁ or D₂ have been confirmed to have opposite effects on movement, in fact, the stimulation of the direct pathway facilitates movement, while the activation of the indirect pathway inhibits it [49]. However, a low number of MSNs express both receptor types (D₁ and D₂) adding further complexity to the phenomenon.

The effects of dopamine at the striatal level are regulated by D₂ autoreceptors located at the presynaptic level on dopaminergic terminals and on mesencephalic neurons. Hence the receptors D₂ possess a negative feedback, which by regulating neuronal firing and dopamine synthesis/release, modifies the level of the extracellular neurotransmitter [29].

Dopamine, in addition to being fundamental in the control of movements, also regulates essential cognitive functions. D₁-like receptors are extensively involved in cognitive processes, including behavioural flexibility, working memory, decision-making, learning and memory processes, and act by regulating the excitability of neurons cortical pyramids and regulation of synaptic plasticity at the hippocampal and striatal level [49]. D₂-like receptors are highly expressed in the *striatum* and *hippocampus* and moderately in the prefrontal cortex where they regulate decision-making, behavioural flexibility and also affect long-term memory by modifying the excitability of cortical pyramidal neurons and/or involvement in synaptic glutamatergic plasticity in the *hippocampus* and *striatum*. D₃ receptors are absent in the prefrontal cortex, but indirectly modulate cognitive functions through the inhibition of dopaminergic activity at the cortical level and / or the regulation of cortical acetylcholine levels. Inhibition mediated by these receptors improves functions such as memory and learning.

Finally, D₄ receptors, located in the prefrontal cortex and *hippocampus*, are important in cognitive processes such as object recognition memory [45].

Midbrain dopaminergic neurons in the SNc and VTA, release dopamine (DA) from soma and dendrites [50], [51]. Dopamine neurotransmission starts by the fusion of synaptic vesicles. This process is regulated at many levels: DA synthesis, uptake and vesicular transport [52].

The term "somatodendritic", which historically describes the evoked release of DA in SNc and VTA, is defined in this way as somatic and dendritic release cannot be easily distinguished. As described above in SNc [53]–[55] the D₂ autoreceptor when binding to dopamine regulates the firing rate and pattern of dopaminergic neurons, consequently regulating release in both the dorsal and ventral *striatum* [56]. This local autoinhibition through this link between dopamine and D₂ autoreceptors creates a feedback to limit the release of somatodendritic DA too.

Furthermore, dopamine is released from the dendrites of SNc neurons that protrude ventrally into the adjacent *substantia nigra pars reticulata* (SNr). In this case, dopamine acts on the D₁ receptors of the striatonigral axon terminals (also called direct pathway) in the SNr to enhance the release of gamma-aminobutyric acid (GABA) from these axons in order to amplify the inhibition of the main cells of the SNr, which are mainly GABAergic neurons. It has been shown that there is a calcium dependency linked to somatodendritic release. It has been recognized the very important role of the Cav_{1.3} L-type calcium channel in the regulation of the pacemaker activity in the SNc compared to the dopaminergic neurons of the VTA. It seems that this contributes to the greater vulnerability of the neurons of the SNc. Liss and colleagues further showed a functional link between Cav_{1.3} L-type channels and the desensitizing / non-desensitizing state of the D₂ autoreceptor, which is governed by intracellular levels of neuronal calcium sensor (NCS-1) [28], [57].

The classic mechanism of fusion regulation occurs through synaptic proteins. These proteins belong to the SNARE complex. The neuron's plasma membrane contains two t-SNAREs, (syntaxin and SNAP-25), while the synaptic vesicle membrane contains a single v-SNARE (synaptobrevin). As the vesicle and membrane come together, the SNARE proteins interact with each other to form bundles of four strands. Each beam consists of

two α -helices of SNAP-25, one α -helix of syntaxin and one of synaptobrevin. When the bilayer of the two membranes fuses, the SNAREs that previously protruded from the separate membranes are now in the same cell membrane and the release of the neurotransmitter in the extracellular zone is possible. Another form of regulation is presynaptic macroautophagy. Striatal DA buttons can form autophagic vacuoles which can sequester and degrade synaptic vesicles, resulting in decreased release of evoked DA [52].

The modulation of dopamine release at the somatodendritic level can also occur by synaptic input. In this specific case, glutamate and GABA provide primary synaptic input to DA neurons in the midbrain, with a different balance between excitatory and inhibitory input between SNc and VTA. The GABAergic input predominates in the SNc and glutamate input predominates in the VTA [57].

Therefore, it is easy to understand the important of dopamine in motor control and behaviour, the loss of DA leads to the consequent dysfunction of the ganglia with consequent motor deficits of Parkinson's disease.

4.0 Role of aSyn in Parkinson's disease

Parkinson's disease (PD) is the second most common neurodegenerative disease in the world, about 1-2% of the world population over the age of 65 is affected. The main symptoms are of a motor type: slowness of movement, rigidity, tremor and instability postural; however, non-motor symptoms are also present including fatigue, olfactory disturbances, anxiety, sleep disturbances, depression, memory and learning disorders. Symptoms of the disease appear in most cases as tremors in the upper limbs or in the head, and are caused by the death of dopaminergic neurons of the *substantia nigra pars compacta* (SN_c). There are only palliative therapies, such as the administration of *Levodopa* to compensate for the loss of dopaminergic neurons. No cure has yet been found, as when the first symptoms appear the disease is already in a very advanced stage, in which most of the dopaminergic neurons have been compromised. In addition to the loss of dopaminergic neurons at the SN_c level, neurodegeneration has been observed also in other areas of the brain such as the *locus ceruleus*, the *intralaminar nuclei* of the

thalamus, the *lateral hypothalamus* and the *pedunculopontine nucleus*; these regions are characterized by neurons that do not use dopamine as a neurotransmitter, suggesting that this is not the only cause of degeneration. In many neurons of patients with the disease there is no correct regulation of protein homeostasis, as evidenced by the abnormal accumulation of intracellular protein aggregates in the brains of affected patients. These aggregates, if present at the level of the neuronal soma, are called Lewy bodies (LB); when present at the dendritic or axonal level they are called Lewy neurites (LN).

An important component of this pathology (Lewy pathology) is the phosphorylated α -synuclein (aSyn). However, it is still unclear whether the LB cells represent a cause or an effect of neurodegeneration [58].

The second line of study of Parkinson's disease is based on genetics: one in ten cases of PD is familial, that is, it can be traced by a genetic mutation. Recessive and dominant mutations associated with Parkinson's disease have been identified. Mutations better characterized, recessive and loss-of-function related have been clearly linked to mitochondria, these mutations involving specific PINK1 and PARKIN genes. PARKIN is also involved in biogenesis mitochondrial in which it negatively regulates the PARIS repressor; in the absence of PARKIN the PARIS repressor accumulates leading to the progressive loss of dopaminergic neurons in the CNS. Another gene involved is the DJ-1 gene, this gene is involved in the regulation of defences against oxidation at the mitochondrial and cellular level. Mutations only listed, related to mitochondrial function, increase the likelihood of developing an early form of PD and are not necessarily related to the presence of Lewy bodies.

Autosomal dominant mutations associated with PD have not yet been linked to any particularly via cellular. Mutations or duplications / triplications of copies of SNCA they are associated with the onset of Parkinson's disease at the age of approximately 60, which is defined as the normal course of the disease. SNCA encodes the aSyn protein. Under physiological conditions, aSyn is abundant in synaptic terminals where it could modulate vesicle trafficking and neurotransmitter release [59].

According to some studies, an excessive presence of these proteins or their misfolding could also be associated with familial Parkinson's, although several studies are necessary to investigate this phenomenology. It would appear that these aSyn oligomers can behave like a prion and catalyze the formation of new oligomers and / or fibrils that spread from neuron to neuron, generating Lewy bodies. Mutations in a number of other genes are associated with PD, including LRRK₂. All of these genes have been studied, but unfortunately none of these genetic mutations are able to fully reproduce Parkinson's disease in mice. This would indicate that there are a multitude of factors that contribute to the genesis of the disease.

α -synuclein plays an important role in the synaptic physiology of dopaminergic neurons: mice lacking aSyn show a strong alteration in the release of dopamine, as the supply of dopamine within the pool of vesicles ready for synaptic release has decreased. On the other hand, an overexpression of aSyn determines a lower exocytosis of dopaminergic neurons in culture, which release alongside dopamine, glutamate [60]. Furthermore, the insertion of a truncated form and an overexpression of aSyn into the nigrostriatal system of transgenic mice reduces vesicle density and dopamine release [61] resulting in motor damage.

Although the identification of specific genetic defects in familial cases of the disease offers important clues to the pathogenesis, most cases of PD are idiopathic and lack a recognizable genetic cause, some causes currently recognized seem to be due to environmental pollution, pesticides and nutrition.

Another hypothesis about pathogenesis in PD is the role of calcium channels, in fact these neurons are autonomous pacemakers [12], [20], [58], [62], [63], the spikes in these neurons maximizes Ca²⁺ entry [64].

The pacemaker activity is characterized by slow fluctuations in the intracellular concentration of Ca²⁺ [20], [62], [65], [66]. In particular, Cav_{1.3} channels are particularly involved in this phenomenon because activate at relatively hyperpolarized membrane potentials [67]. These Ca²⁺ fluctuations therefore produce an increased risk of degeneration in patients with PD [68]; this correlation has also been found in transgenic mouse models [69]. Ca²⁺ promotes aSyn aggregation [70] because the Ca²⁺-dependent

protease calpain cleaves off the carboxyl-terminus of aSyn, promoting the aggregation [70].

Different evidence show that isradipine, the selective blocker of L-type calcium channels, confers strong protection in SNc DA neurons. To test the importance of L-type channels, slices or isolated neurons were pre-treated with isradipine and exposed to preformed α -synuclein fibrils (PFF), or to the toxic effects of environmental factors known to cause PD. In these experiments, isradipine confers strong protection in SNc DA neurons, indicating that Ca^{2+} flow through L-type channels contributes significantly to neuronal cell death. The importance of the role of L-type calcium channel is also supported by the fact that the neighbouring ventral tegmental midbrain DA neurons, which do not express the $\text{Cav}_{1.3}$ channels, are less susceptible to cell death in PD [71]–[73].

Isradipine has already been used extensively in the clinic as an antihypertensive to treat hypertension and other cardiovascular conditions. The proposed role of Ca^{2+} channels in neurodegeneration opens up the possibility of reusing isradipine for the treatment of Parkinson's disease. A phase III clinical trial (NCT02168842; www.clinicaltrials.gov) [67], [74] has recently been completed to investigate the neuroprotective potential of isradipine in patients with early stage PD. Unfortunately, the results did not show a significant slowdown in the development of the disease, but there are several points still to be clarified also regarding the administration protocol used. However, this opens the way for important and promising studies on the relationship between the various isoforms of calcium channels (not only L-type) and dopaminergic neurons [73].

5.0 Physiological and pathological properties of aSyn

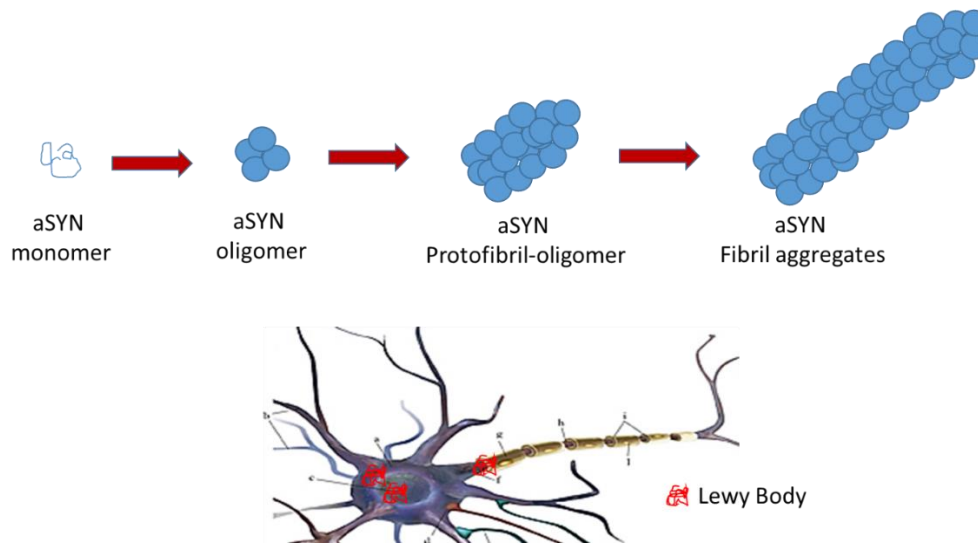


Figure 5 Different aSyn structure: monomeric, oligomeric, protofibrillar and fibrillar aggregates

α -Synuclein (aSyn) is an abundant and physiological protein localized in presynaptic terminals. This protein is well known for its close relationship with Parkinson's disease and other Parkinson-like neurodegenerative diseases. Paradoxically, much more is known about the role that this protein has when it begins to accumulate abnormally in the synaptic terminals, degenerating into more complex and neurotoxic structures such as oligomers and fibrils, but its physiological role is still under study. Both physiological and pathological aspects are the source of intense studies and research.

aSyn is encoded by the SNCA gene; it is composed of 140 amino acid residues with a molecular weight of approximately 15kDa [75], [76]. This protein exists in a balance between one soluble and one membrane-bound state; its secondary structure changes depending on of the state.

Cytosolic aSyn is soluble, unstructured and behaves like an originally unfolded protein [75], [77]–[79]. This binds to lipid membranes as artificial liposomes, lipid droplets and lipid rafts. By binding to lipids it adopts an α -helix structure [80]. Binding of the protein to lipid membranes requires groups such as phosphatidylserine or phosphatidylinositol, suggesting an interaction of the membrane with lysines present on opposite sides of the α -helix.

During the development of cultured neurons, the aSyn is initially localized in the soma of the immature neuron and during development it also concentrates in the presynaptic terminals during synapse formation.

The localization of this protein in the synapse may be due to its preference for synaptic vesicle membranes and/or for binding to the SNARE vesicular protein, the synaptobrevin-2 [78]. Numerous studies have reported that aSyn can also be localized in other locations such as mitochondria, endoplasmic reticulum and others; however the significance of these localizations is not yet clear and is a matter of debate in several studies [80][81].

Physiological aSyn appears to be involved in numerous activities such as:

- Transport and packaging of lipids and membrane biogenesis: The binding of aSyn to phospholipids and its similarity to apolipoproteins suggests its role in the transport of lipids. aSyn is a specific inhibitor of phospholipases D₁ and D₂ in vitro and in vivo [82]–[84], suggesting it may be involved in the cleavage of lipids of membrane and in the biogenesis of the latter. Furthermore, it has been suggested that aSyn is able to detect lipid packing defects and affect their packaging [85], [86] indicating that it may be able to actively remodel them.
- Molecular "chaperone" activity: The biochemical structure of aSyn provides a function as a molecular chaperone capable of binding to other intracellular proteins. The aSyn in fact shares the structural and functional homology with a specific family of molecular chaperones [87]. Second, through its domain C-terminal, aSyn suppresses the aggregation of thermally denatured proteins [88]–[92] and the overexpression of aSyn protects dopaminergic neurons from oxidative stress and apoptosis [93], [94].
- Vesicle trafficking: Numerous evidences from studies conducted on different animal models show that aSyn is associated with defects in vesicle trafficking.
- Synthesis and transport of dopamine: aSyn inhibits the synthesis of dopamine by inhibiting the expression and activity of TH [95]–[99].
- Release of neurotransmitters and synaptic plasticity: its presynaptic localization, its interaction with synaptic vesicles [100], [101] and synaptobrevin-2 [102], its accompanying activity of the SNARE complex [102] suggest that this protein plays

a role in neurotransmitter release and synaptic plasticity, although its precise function remains unclear. Within the presynaptic terminal the aSyn is mobile and disperses from the synaptic vesicles upon stimulation [103]. It also organizes itself into multimers in the synapses, which group synaptic vesicles, thus limiting their motility [104] and probably attenuating exo/endocytosis. Multimerization is triggered by membrane binding and mediates the accompanying activity of the SNARE complex [105]. The effect of aSyn on neurotransmitter release is probably not mediated by direct influence on the delivery machine, but through a regulation of vesicle pools within the presynaptic terminal.

Several studies have shown that aSyn can spread from neuron to neuron. This mechanism appears to derive from prion²-like propagation, with evidence deriving from both in vitro and in vivo models. The release of aSyn appears to occur through unconventional pathways of exocytosis. Some evidence indicates that aSyn can be released with exosomes (luminal vesicles of multi-vesicular bodies, MVBOs). This process is supposed to be calcium dependent [106], [107], providing a neuronal activity-dependent mechanism for aSyn exocytosis and suggesting spread along synaptically connected neurons.

Extracellular aSyn can be endocytosed by neurons and microglia [108], [109], although endocytosis-independent uptake has also been reported [110]. Recombinant aSyn fibrils can also be endocytosed by neurons and lead to aggregates similar to those detected in Lewy body disease in cells expressing endogenous levels of aSyn [110]. Exocytosis and uptake of aSyn may be an important mechanism for the progression and amplification of degenerative changes in synucleinopathies from certain cells to surrounding tissue, or they may also have a biological function not yet known.

Recently, it has been shown that aSyn is able to oligomerize in multimers after binding to membranes [78],[104].

² altered forms of the prion protein (PrP) which is normally present in various organs of our body, principally in the brain. In pathology, PrP changes its shape, becoming a prion, that is, an infectious protein capable of inducing normal PrP to assume the pathological form.

The aggregation process of several monomers of aSyn produce oligomers, that can assume different forms: spherical, chain-like annular or tubular [111], [112]. Recent evidence indicates that extracellular aSyn oligomeric aggregates, that precede fibril formation, may be the most neurotoxic species [113] and in the most of the case can be found extracellularly. For several years, it was thought that most of the toxicity by aSyn was due to intracellular deposits of fibril aggregates, and that mainly these were the causes of all synucleopathies including Parkinson's disease. Today this view has changed somewhat, recent evidence shows that these oligomers increase intracellular calcium levels [113], [114]. This high amount of intracellular calcium can lead to subsequent cell death.

Regarding the effects of fibril formation, several experimental studies have support the theory that fibrillar aSyn can induce normal aSyn to form pathogenic inclusions. Using cell lines overexpressing fibrillar aSyn generated by recombinant aSyn induces the formation of insoluble, phosphorylated and ubiquitinated aggregates [115]. Exposure of neurons expressing endogenous levels of aSyn to fibrils causes the formation of inclusions of aSyn that morphologically and biochemically resemble neurites and Lewy bodies [116]. The striatum was injected with aSyn fibrils, which produced a Lewy-like pathology in dopaminergic neurons of the *substantia nigra pars compacta*, resulting in loss of dopaminergic neurons and motor behaviour phenotypes similar to PD [117], [118].

Inclusions of α -synuclein are also produced in other brain regions relevant to Parkinson's disease, such as the cortex and amygdala. The formation of these inclusions in such different areas of the brain causes a significant loss in synaptic connections, this would explain why Parkinson's patients are characterized by a very broad spectrum of symptoms, ranging from motor problems to cognitive ones.

It has been observed that exposure of neurons from aSyn knockout mice to aSyn fibrils does not produce intracellular inclusions and does not alter neuronal connectivity. Therefore, it can be inferred that the corruption of endogenous aSyn to form insoluble fibrillar aggregates is responsible for neuronal dysfunction.

Studies demonstrating that peripheral fibril injection induces Parkinson's disease phenotypes specifically support that aggregated aSyn can travel along related neuronal pathway [119]–[122].

Ultimately the last two decades have been fundamental for the acquisition of knowledge on the function and role of aSyn, partly due to the development of in vitro and in vivo models which, with their limitations, as they do not fully reproduce PD, however, they can be considered similar to pathological processes in humans. We know that aSyn is important for the normal function and integrity of synapses and in the aging of the nervous system. The different conformations that aSyn can assume, i.e. monomer, oligomer and fibrils, have a fundamental and different role in synucleopathies, given its multiple interactions in different subcellular compartments, as well as its numerous post-translational modifications, which generate a spectrum of negative effects for the cell that can exacerbate and eventually culminate in cell death.

Overexpression of aSyn triggers redistribution of SNARE proteins, impairs proper vesicle trafficking and recycling, and large aSyn oligomers inhibit SNARE-mediated vesicle fusion in vitro [123]. Furthermore, misfolded aSyn, in the form of oligomers and aggregates, is believed to be particularly neurotoxic and able to propagate from neuron to neuron [116], [124]–[126].

We also know something more about its physiological function, especially in bioenergetic control or vesicle transport, both factors that outline the importance of this protein.

Despite these advances, the role of aSyn in the early events of the disease process, including the development and differentiation events of dopaminergic neurons, the causes of the selective vulnerability of the SNc dopaminergic neurons, remains to be determined. This could make it possible to discover the first biomarkers and even to advance therapeutic strategies to modify the natural course of the disease.

Chapter 2

Materials and Methods

1.0 Culture of midbrain dopaminergic neurons

The methods for the primary culture of mesencephalic dopamine neurons from substantia nigra (SN) was adapted from Pruzak et al. [127]. TH-GFP mice were kept heterozygous via breeding TH-GFP mice with C57BL/6J mice. All animals were housed under a 12 h light/dark cycle in an environmentally controlled room with food and water ad libitum. All experiments were conducted in accordance with the European Community's Council Directive 2010/63/UE and approved by the Italian Ministry of Health and the Local Organism responsible for animal welfare at the University of Turin (Authorization DGSAF 0011710-P-26/07/2017).

For the preparation of dopaminergic primary cell cultures, the *substantia nigra* portion was surgically isolated from the brain of E14-E18 embryos, taking the ventral midbrain area [128], [129]. The tissue fragments were digested with a papain solution and plated on dishes pre-treated with polylysine D at a density of 400 cells / mm² (approximately 40000 cells/dishes). Neurobasal (Gibco) implemented with B₂₇ (Gibco) and 2.5% dialysate FBS was used as the culture medium. Subsequently, to improve the yield, some changes were made to the protocol: a co-culture with cells from the *Striatum area* and the addition to the culture of 5 μM of antimitotic fluoro-deoxyuridine (FDU) starting from 4 DIV, reducing the uncontrolled growth of the glia and thus increasing survival and quality of dopaminergic neurons, favouring their dendritic development. FDU kills proliferating cells (mainly glial cells at E14-E18) by interfering with DNA synthesis[130], [131].

The addition of growth factors, such as NT₃, BDNF, NGF, has also been tried, obtaining satisfactory results in particular with the administration of 10 ng/mL of BDNF.

The culture is done only with embryos that appear to be fluorescent under the microscope, as can be seen from Figure 1. Statistically, about 50/60% of mice are found to be labelled with the fluorescent protein.

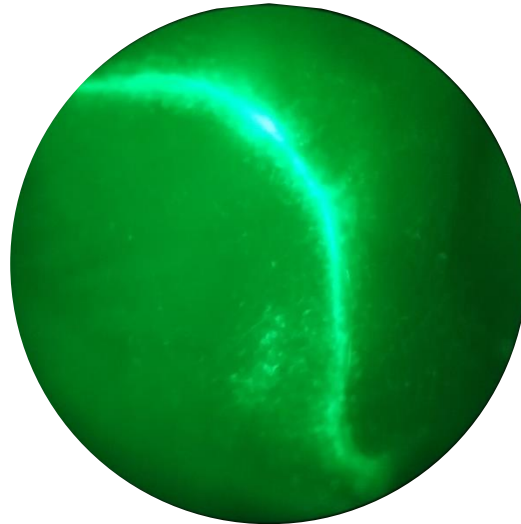


Figure 1. Dopaminergic midbrain neurons of embryonic TH-GFP mouse

The dissection of *substantia nigra* and *striatum* is performed by sagittal separation of the different areas of the brain, the meninges are removed from the hemisphere and the brainstem.

The mesencephalic region including the *substantia nigra* is dissected from a rostral and caudal section. The *striatum*, on the other hand, is located within the cerebral hemisphere. The caudal and dorsal part in the midbrain area is removed. The remaining portion of the midbrain contains the *substantia nigra* [132].

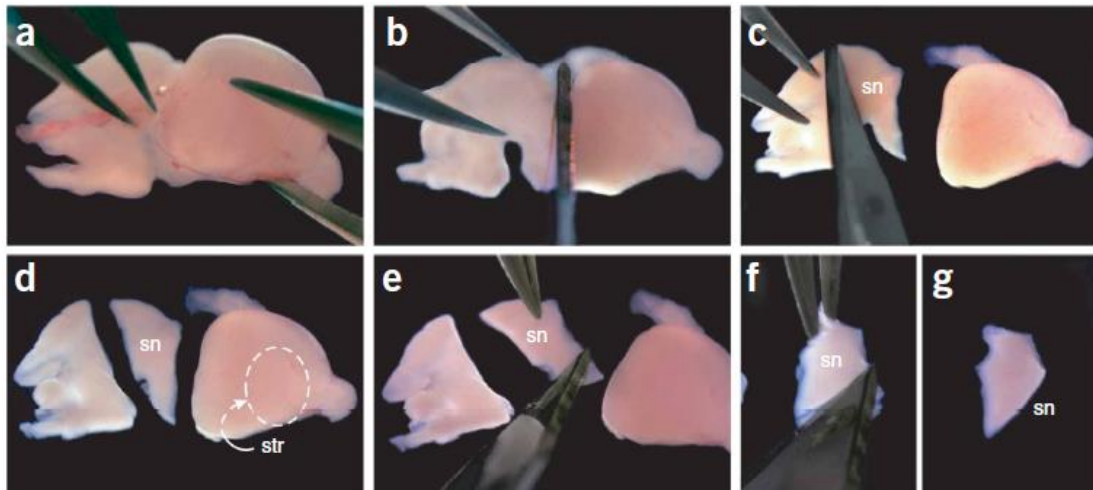


Figure 2 “Dissection of substantia nigra and striatum from embryonic E16.5 brains. (a) After sagittal separation of the brain halves, meninges are removed from the hemisphere and the brain stem. (b–d) The mesencephalic region containing the substantia nigra (sn) is dissected by a rostral and caudal section. The striatum is located on the inside of the brain hemisphere as indicated (broken lines in d). (e) The caudal part of the mesencephalic preparation is removed, (f) as well as the dorsal part. (g) The remaining preparation of the mesencephalon contains the substantia nigra (sn).” Cited from Fath et al. 2008, nature protocols [132].

At this point the digestion phase begins; the digestion buffer is composed by: HBSS (Hank’s balanced salt solution, without CaCl₂ and MgCl₂), enriched with 0.18% glucose, 1% BSA, 60% papain (*Worthington, Lakewood, NJ, United States*), 20% Dnase (*SigmaAldrich*) and it was stored at 4 °C.

Neurons were plated at final densities of 2.000 cells mm⁻² on conventional MEAs or μG-SCD-MEAs, 40.000 cells mm⁻² on dishes for patch-clamp measurements.

Cultured neurons were used at different DIV (days in vitro), depending on the experiment. MEAs, μG-SCD-MEAs and dishes were coated with poly-L-Lysine (0.1 mg ml⁻¹) as substrate adhesion. Cells were incubated at 37 °C in a 5% CO₂ atmosphere, with Neuro basal Medium containing 1% pen-strep, 1% ultra-glutamine, 2% B-27 plus and 2.5% FBSd; pH 7.4.

2.0 Techniques: Patch clamp, MultiElectrode Arrays (MEA), μ G-SCD MEAs

2.1 Patch clamp: voltage clamp, current clamp, capacitance

Patch-clamp experiments were performed using patchmaster software (HEKA Elektronik GmbH – a division of Harvard Bioscience). All the experiments were performed at room temperature (22–24 °C).

Voltage-clamp recordings

The voltage-clamp configuration allows to study voltage-gated ion channels by controlling the membrane potential. The recordings were made in whole-cell configuration, the extracellular solution containing (in mM): 135 TEA, 2 CaCl₂, 2 MgCl₂, 10 HEPES, 10 glucose (pH 7.4). Tetrodotoxin (0.3 μ M) (Tocris Cookson Ltd, Bristol, UK) was added to block voltage dependent Na⁺ channels and spontaneous action potentials propagation. GABAergic and glutamatergic currents were respectively isolated by PicROTOXIN (100 μ M), APV (50 μ M) and DNQX (20 μ M). The standard internal solution contained (in mM): 90 CsCl, 20 TEACl, 10 EGTA, 10 glucose, 1 MgCl, 4 ATP, 0.5 GTP and 15 phosphocreatine (pH 7.4).

Traces were sampled at 10 kHz and filtered using a low-pass Bessel filter set at 2 kHz. Borosilicate glass pipettes (Kimble Chase life science, Vineland, NJ, USA) with a resistance of 7-8 M Ω were used. Uncompensated capacitive currents were reduced by subtracting the averaged currents in response to P/4 hyperpolarizing pulses. Ca²⁺ currents were evoked by applying a single depolarization step (50 ms duration), from a holding of -70 mV to 0 mV. Fast capacitive transients due to the depolarizing pulse were minimized online by the patch-clamp analog compensation. Series resistance was compensated by 80% and monitored during the experiment [132].

Current-clamp recordings

The current-clamp configuration detects transmembrane voltage change resulting from ion channel activity. This technique allows to control the amount of current injected into the cell, thereby controlling the transmembrane potential.

The pipette internal solution contained in mM: 135 gluconic acid (potassium salt: K-gluconate), 10 HEPES, 0.5 EGTA, 2 MgCl₂, 5 NaCl, 2 ATP-Tris and 0.4 Tris-GTP, pH 7.4. The extracellular solution is tyrode standard solution contained in mM: 2 CaCl₂, 10 HEPES, 130 NaCl, 4 KCl, 2 MgCl₂, 10 glucose adjusted to pH 7.4. All experiments were performed at a temperature of 22–24°C. Data analysis was performed using Clampfit software.

Capacitance

The cell membrane is formed by a double layer of phospholipids which form a particularly effective barrier to charged molecules. This barrier is a dynamic substrate in which other constituents of the membrane are embedded (receptors, ion channels, cytoskeletal anchors, ion pumps, enzymes, etc). The flow of ions across the plasma membrane is facilitated by specialised proteins (ion channels, transport, pump, etc.). The membrane is generally defined as an insulator between two conductors, the intra-cellular and extra-cellular medium, charged with ions, and can be compared to a capacitor with flat and parallel faces. However, this electrical isolation is not perfect: there are ion channels, transporters and more that form the membrane resistance.

In electronic terms, the moving charge is expressed in current, i.e. the charge per unit of time:

$$I = \frac{dQ}{dt}$$

Where I is the current in ampere (A) and dQ/dt is the change in charge (coulomb, C) over time.

The cell membrane, the intracellular and extracellular media, form a capacitor, in terms of electronics. The cell membrane consists of the more negative intracellular side of the extracellular side, both sides exert an electromagnetic field through the membrane, which attracts charged particles, negative ions (anions). The outer side will be positively charged

and accumulate close to the membrane, while positive ions (cations) will accumulate on the outside. The ions accumulated along the two sides are characterized by a quantity of stored charge which can be calculated as:

$$Q = E_m C$$

where Q is the charge, E_m is the potential difference across the membrane and C is the membrane capacitance expressed in Farad. The physical dimensions of the membrane are important in determining the capacitance: the more membrane is large, the more charge can be accumulating, therefore the capacitance is proportional to membrane surface area.

Membrane capacitance increases can be used to detect exocytosis because when secretory vesicles undergo fusion with the plasma membrane during exocytosis the membrane surface area increase. The capacitance per unit area of membrane is referred to as the specific capacitance (C_m), C_m was estimated to be $1 \mu\text{F}/\text{cm}^2$ [133]–[135]. Therefore, these changes in the membrane surface area can be monitored by measuring the cell capacitance (Figure 3). Exocytosis of secretory granules results in an increase of the cell surface area that is compensated by membrane retrieval processes (e.g., endocytosis) that consequently reduce the cell surface area. Because of the low-noise and high temporal resolution, this method enables fast quantitative measurements of changes in membrane capacitance [135]–[138].

The pipette internal solution contained in mM: 90 CsCl, 20 TEACl, 10 EGTA, 10 glucose, 1 MgCl, 4 ATP, 0.5 GTP and 15 phosphocreatine pH 7.4. The extracellular solution contained in mM: 4 TEA, 2 CaCl₂, 2 MgCl₂, 10 HEPES, 10 glucose, pH 7.4.

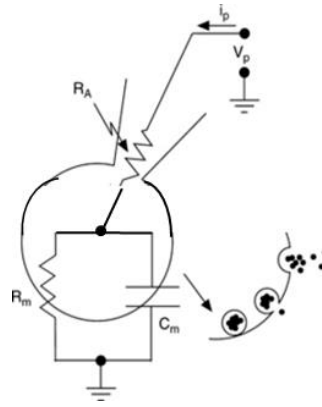


Figure 3 Vesicle fusion with cell membrane

In the whole-cell voltage-clamp mode, I measured the capacitance using a lock-in amplifier. The protocol provides that membrane potential is modified in a sinusoidal manner, there is a phase shift of 90° between the resistive and the capacitive current components [136]. The formula that describes it is:

$$I(t) = G_m V + C_m \left(\frac{dV}{dt} \right)$$

Where V is the command voltage, G_m is the membrane conductance, and C_m is the cell capacitance. When a sinusoidal voltage command, $V = V_0 \sin \omega t$ is applied:

$$I(t) = G_m V_0 \sin \omega t + C_m V_0 \sin \omega t$$

In the phase plan, G_m and C_m are orthogonal to each other. Usually, to perform this protocol is necessary lock-in amplifiers, that are implemented only in the software HEKA Pulse and Patchmaster.

2.2 Microelectrode arrays (MEA): recordings

The MEA - Microelectrode arrays (Multichannel Systems, MCS, Reutlingen Germany) consisted of 60 TiN/SiN planar round electrodes ($30 \mu\text{m}$ diameter; $200 \mu\text{m}$ center-to-

center inter-electrode distance). The MEA is characterized by 8x8 recording electrodes included the ground electrode. After 1200x amplification, signals were sampled at 10 kHz and acquired through the data acquisition card and MC-Rack software (MCS). The matrix on which the electrodes rest is made of glass, a chemically inert and biocompatible material, which makes these devices reusable. The disadvantages of glass are undoubtedly linked to its fragility and to the fact that after several autoclave washes it tends to become opaque.

The MEA is inserted inside an incubator with a controlled temperature (37°C) and a controlled atmosphere (i.e., gas flow of 5% CO₂ and 95% O₂).

The auxiliary or counter electrode is a fixed electrode (number 15, defined REF in Figure 4), structurally larger than the other electrodes. The auxiliary electrode establishes the electrical potential against which the other potentials can be measured. The auxiliary electrode often has a larger surface area than the working electrode to ensure that the reactions occurring on the working electrode are not limited by the surface area via the auxiliary electrode [139]–[142].

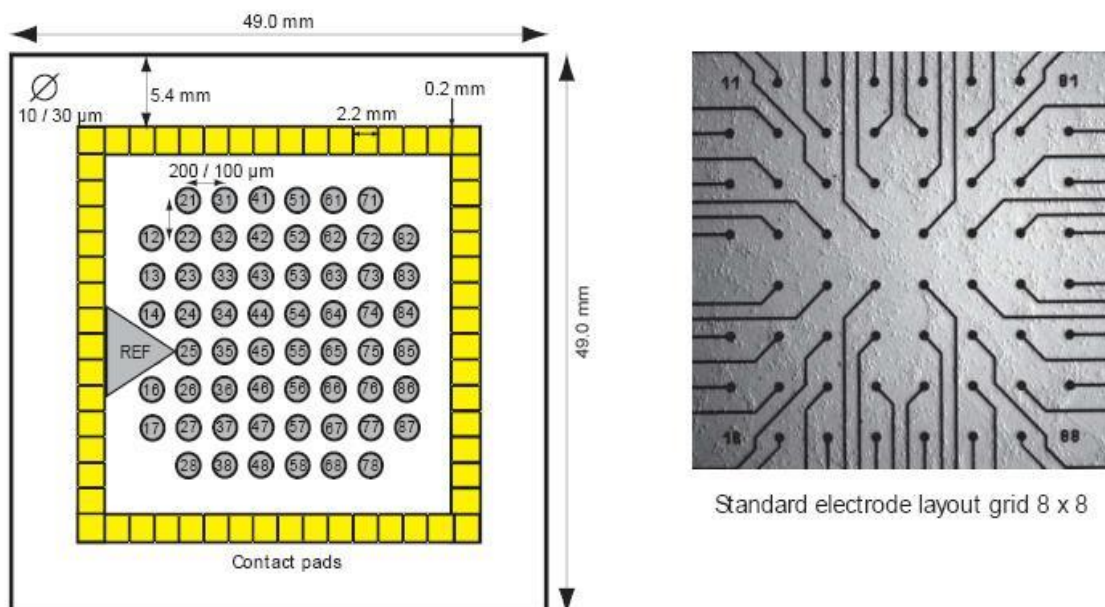


Figure 4 Multichannel System – Standard Microelectrode Arrays (MEAs)

The MEA is connected to an amplifier by means of a conductive track and a series of gold pins, each unit in titanium nitride (NiT) detects the extracellular signals produced from neurons; these signals can arrive either from a single cell or from a sum of signals coming from several cells, or even from different cellular parts such as soma and axons in the case of neurons. Above the electrodes and metal tracks there is a polyamide layer, with insulating function, above which there is the culture chamber delimited by a glass cylinder (internal diameter 19 mm, external diameter 24 mm, height 6 mm) with a capacity of 1 mL.

Each MEA is covered with an ethylene-propylene membrane, the latter reducing evaporation of the culture medium, still allowing a gaseous exchange with the environment and maintaining the conditions of sterility necessary for repeated recordings over time.

To conduct the experiments, a MEA 1060-Inv-BC amplifier filter supplied with the device was used, the latter amplifies and filters the acquired signal before it is transferred to the analog / digital converter. The MEA is placed in the preamplifier which contains a suppression circuit (MEA 1060-BC-PA); when closing the amplifier, the contact pins fixed on its cover are pressed on the pads on the MEA. Contact between this results in a favourable signal-to-noise ratio.

The filter and gain specifications are set by the operator. To record high frequency electrical signals, it is necessary to set a bandwidth between 300 Hz and 3 kHz; for those at low frequency an interval between 1 and 300 Hz is required. The gain is set to a value between 100 and 5000; the amplifier will multiply the signal by the value set before the signal is acquired via cable and then processed in digital format.

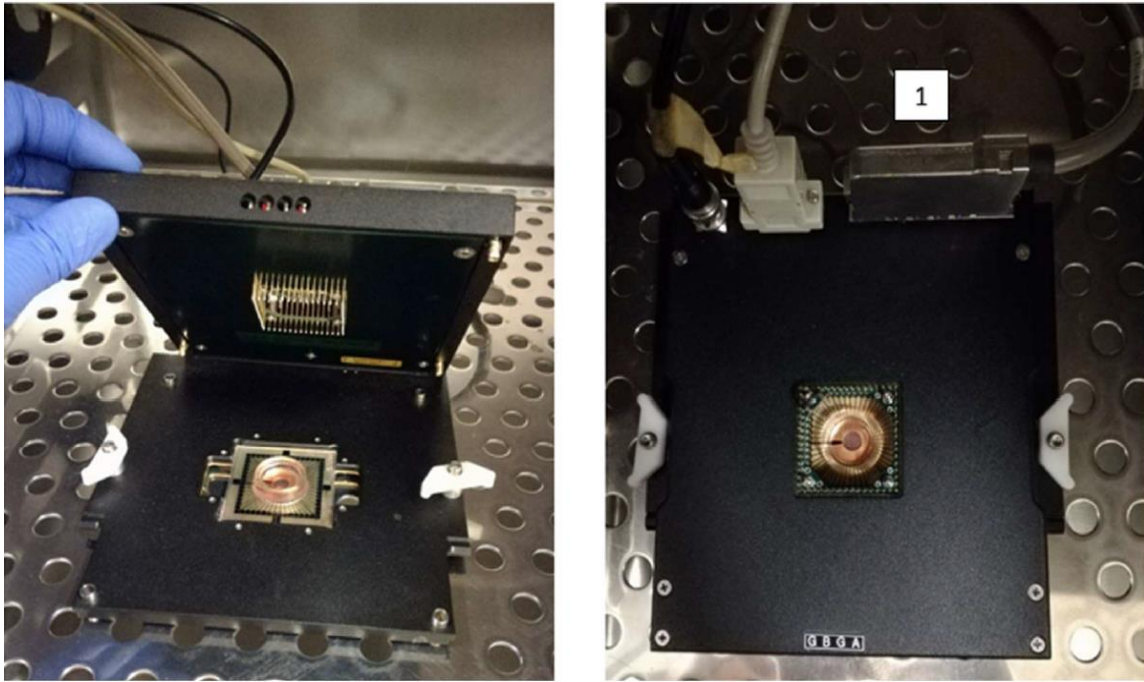


Figure 5 On the left, the amplifier (used for the experiments) with a view on the pins that contact the pads on the MEA. Right, amplifier with view of the amplifier filter and ADC (1).

MEA devices are a powerful tool for studying time-dependent potential interactions among neurons [9], [143]. Unlike conventional electrophysiology (e.g. patch-clamp technique), the multielectrode-based approach is certainly a non-invasive technique, as cells are grown over the multilayer of electrodes. The main advantage of MEA is the possibility to perform repeated measurements on the same culture over time.

2.3 Micro-Electrode Array: analysis

The electrical activity of the cells can be characterized by single action potentials (spikes) or by rapid sequences of action potentials (synchronous bursts) [143].

After amplification and filtration, the signal is converted in real time from analog to digital by means of an ADC (MC_Card), or an analog / digital card. It is possible to obtain sampling rates up to 50 kHz / channel.

Once the data have been acquired, they are analyzed using a multichannel system acquisition and analysis software (MC_Rack). Through this software it is possible to set specific thresholds for each channel in order to eliminate noise from the tracks.

Once the signal has been digitized, the final analysis is carried out using Neuroexplorer software (Nex Technologies, Littleton, MA, USA). Through Neuroexplorer the burst analysis and the study of cross-correlation have been developed.

The burst analysis allows to extract the parameters related to the spontaneous firing of neurons, including the average frequency, the number of signals, the number of bursts and the related parameters related to the burst analysis (duration of the burst and percentage of spikes in the burst). The cross-correlation analysis, on the other hand, allows information to be obtained concerning the electrical synchronization of neurons through a probability index Y_{max} ($0 < Y_{max} < 1$).

Once the analysis setting has been chosen, the following criteria are set:

Burst analysis

Burst was detected using the Poisson-surprise method. The surprise method distinguishes bursting periods from basal firing. The method assumes that the spike trains are distributed in a Poissonian way. The Poisson Surprise method in a period (T) containing n spikes calculates the value:

$$S = -\log P$$

$$P = \exp(-\lambda T) \sum_{n=N}^{\infty} \frac{(\lambda T)^n}{n!}$$

Where λ is the average firing rate, T is the period of length and N is the number of spikes. This equation defines the probability that N spikes are randomly distributed in a period T [144], [145].

Cross correlation analysis

Synchronization was analyzed using the same software in cross-correlation histogram mode (± 500 ms, bin size 1 ms), smoothed with a boxcar 3 filter. Pairs of neurons were considered synchronous if there was a clear peak exceeding the 99% confidence limit [146]. For greater statistical completeness we have not limited to choosing a single reference electrode, but we have divided the quadrant of the electrodes into four parts and for each single zone of each MEA we have chosen from one to two reference electrodes. This choice frees the analysis from the selective choice of the operator.

We used different inferential static tests depending on whether the analyzed sample was normally distributed or not. We used parametric type tests (t-test, ANOVA) or non-parametric type tests (Kruskal-Wallis), via the Origin Pro software.

Auto correlation analysis

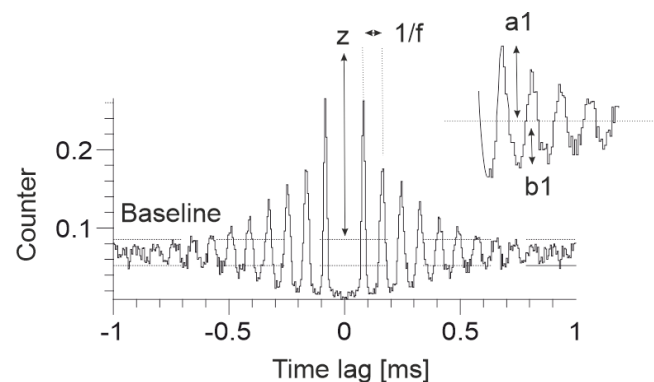


Figure 6 autocorrelogram detailing the parameters used in the peak algorithm. Adapted from [147].

The peaks and valleys were determined using the following mathematical criteria:

The method that will be described was defined in 1995 by Sugihara et al [147]. The first step is the individuation of the baseline, after which the algorithm searches the peaks and valleys, these are recognized if their heights and depths exceeded the average base level \pm SD of the fluctuation, or if the difference between one peak and the next valley exceeded the double the SD of the spontaneous fluctuation. The first peak was defined as the highest bin within a time interval that is defined by the operator, similarly the first valley

was defined as the shortest bin within the same interval. If the n th peak and valley were recognized, the next peak and valley were searched within an interval time of:

$$t_n + t_{(peak)} \pm \frac{t_{peak}}{2}$$

Where t_n is the time lag of the n^{th} peak or valley and $t_{(peak)}$ is the time lag of the first peak. The oscillation frequency was defined as the reciprocal of the time lag of the first peak. The rhythm index (RI) that defined the number of peak that exceed to the baseline was defined by the following formula:

$$RI = \frac{a_1}{z} + \frac{b_1}{z} + \dots + \frac{a_i}{z} + \frac{b_i}{z}$$

In which a_i ($i = 1, 2, \dots, n$) is the difference the height of the i^{th} peak and baseline level in the autocorrelogram, b_i ($i = 1, 2, \dots, n$) is the difference the depth of the i^{th} peak and baseline level, and z is the difference between the height of the zero-time bin and the baseline level (*Figure 6*).

3.0 Amperometric detection of quantal dopamine release by carbon fibers and μ G-SCD-MEAs

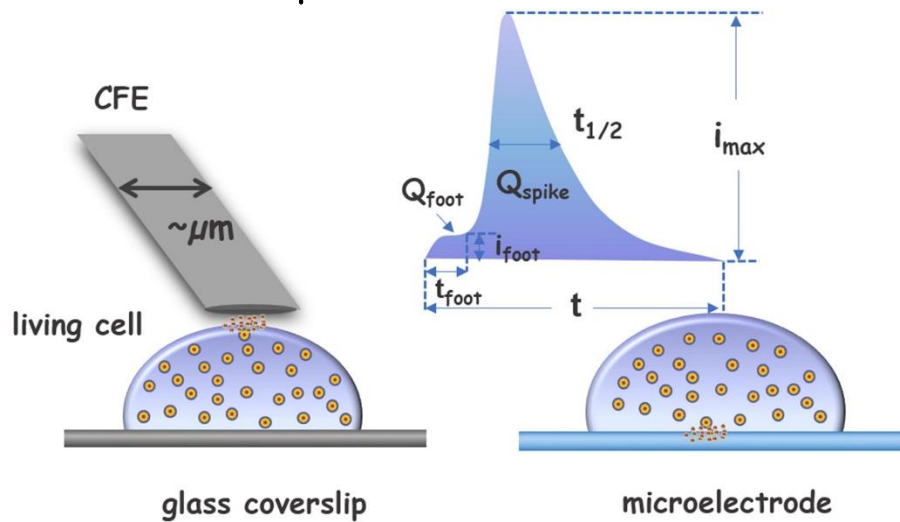


Figure 7 Schematic illustration of the electrochemical detection of vesicular exocytosis performed at the apical pole (by CFE, left image) or at the basal pole (by microelectrode, right image). Note that the planar microelectrode is used both as substrate for cell adhesion and to detect oxidation signals. In both cases, single vesicle secretion is recorded as an individual current spike. The signal represents the amperometric spike. Adapted from Liu et al., [148].

Historically, the amperometric detection of exocytosis on a single cell is obtained with a carbon fiber microelectrode (CFE) by Wightman et al., in the 1990s [149]. Catecholamines are the main recorded electroactive reporters used for the electrochemical test of cell secretions by exocytosis. These can be detected at femto to zeptomole levels with time resolutions from microseconds to milliseconds. Single cell amperometer has become a large and widely used tool for studying exocytosis. The amperometric detection of cellular exocytosis has been carried out for years with a single microelectrode, providing average information over the entire electrode surface. Recently this technique has been extended by designing various micro-electrode arrays (MEAs) to collect electrochemical information related to specific exocytotic areas on the surface of the single cell, speed up cell measurement, make the measurement easier. To perform traditional amperometric test, a constant potential is applied to the microelectrode and the resulting current is monitored with time lapse.

Integration of current spike area gives the total charge transferred Q , which is related to the number of moles of biomolecules released “ N ”. According to Faraday's law:

$$N = \frac{Q}{nF}$$

“n” is the number of electrons removed from each molecule and $F = 96,485 \text{ C mol}^{-1}$ [149],[52], [150].

3.1 $\mu\text{G-SCD}$ MEAs: micro graphitic single crystal diamond MEAs (*Picollo et al.*, *Scientific reports DOI: 10.1038/srep20682*)

The diamond prototypes were developed during a long lasting collaboration with the Physics Department of Torino University (Dr. Picollo). Purpose of this research was to overcome various critical issues typical of the standard amperometric technique with CFE (carbon electrode fiber), in fact the diamond prototype characterized by: mechanical and chemical stability over long periods measurement, substrate transparency, biocompatibility, parallel multielectrode recordings and the possibility of directly culturing living cells on the substrate.

The $\mu\text{G-SCD}$ MEAs were realized using optical-grade single-crystal artificial diamond substrates by means of an advanced MeV ion beam lithography technique. This diamond-based MEAs were realized in high-purity monocrystalline CVD (Chemical Vapour Deposition) diamond substrates produced by ElementSix™ (UK). The substrates are $4.5 \times 4.5 \times 0.5 \text{ mm}^3$ in size, cut along the (100) crystalline direction and optically polished on the two opposite large faces. The presence of low impurity concentrations ensures a good transparency of the substrates in the visible spectrum, up to the near UV.

The samples were implanted at room temperature with a 1.2 MeV He^+ ion beam, it was carried out at the AN2000 accelerator facility of the INFN Legnaro National Laboratories. The implantation of MeV ions induces structural damage in matter mainly at end of the penetration range of the ions, where the cross section for nuclear collisions is strongly enhanced. The high damage density induced by ion implantation promotes the conversion of the diamond lattice into an amorphous phase within a layer which is located $\sim 2 \mu\text{m}$ below the sample surface. The implantation fluence, $F = 1.5 \times 10^{17} \text{ cm}^{-2}$, was chosen to

overcome a critical damage density (usually referred to as “graphitization threshold”) in correspondence of the Bragg peak and to determine the formation of a ~ 250 nm thick and ~ 2 μm deep fully amorphized layer below the sample surface [151],[151].

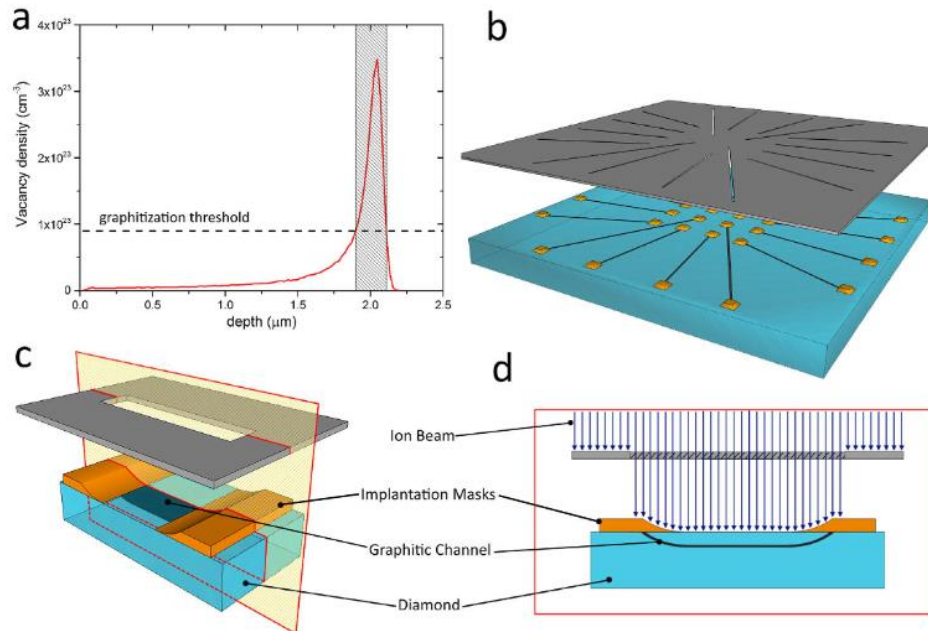


Figure 8 – Adapted from Picollo et al., Scientific reports DOI: 10.1038/srep20682. Deep ion beam lithography of synthetic diamond. (a) Vacancy density profile induced by 1.2 MeV He+ ions implanted in diamond at a fluence of $1.5 \times 10^{17} \text{ cm}^{-2}$. The horizontal line indicates the graphitization threshold, while the patterned rectangle highlights the thickness of the graphitic layer formed upon thermal annealing. Schematics (not to scale) of the fabrication a sub-superficial graphitic channel: three-dimensional view of the masked diamond (b), zoom of three-dimensional (c) and cross-sectional (d) view of a single channel with emerging end-points. The lateral features of the electrode are defined by the aperture in the non-contact mask (in grey), while its depth profile is defined by the contact variable-thickness metallic mask (in yellow) [151].

The three-dimensional geometry of the implanted structures was defined by the combination of two masking systems, as shown in Figure 8. The first system consists of an array of variable-thickness copper masks directly deposited over the sample surface which modulate the penetration depth of the ions, thus ensuring the connection of the sub-superficial amorphized structures with the sample surface at their endpoints [152]–[154]. The second system consists of a free-standing mask realized in a 15 μm thick aluminium foil microfabricated with high-power laser ablation. This mask is thick enough to fully stop the broad MeV ion beam, thus allowing the definition of the lateral geometry of the

amorphized regions. The two masking systems were suitably aligned to simultaneously define in each sample 16 amorphous-carbon micro-channels with emerging end-points. After the implantation, a high temperature thermal annealing, 950 °C for 2 hours in high vacuum, was performed to induce the permanent conversion of the amorphized regions to a graphite-like phase.

As a consequence, 16 graphitic micro-channels (width: ~ 20 μm , length: 1.4–1.9 mm, thickness: ~ 250 nm) were obtained at a depth of ~ 2 μm in each substrate, with surface-emerging endpoints, as schematically shown for a single channel in Figure 8 c,d.

The device consists of 16 sub-superficial graphitic micro-channels converging into a central region where their endpoints (i.e. the sensing electrodes) are exposed to the sample surface. As a consequence of the geometrical elongation of its thickness as it emerges in contact with surface [154], each ~ 250 nm thick channel terminates with a ~ $20 \times 3.5 \mu\text{m}^2$ sensing electrode at the sample surface, and the 16 electrodes are arranged on a 4×4 square grid with 200 μm spacing. At the substrate periphery, the other emerging endpoints of the micro-channels provide electrical contacts for bonding to a dedicated chip carrier.

The chip carrier was specifically designed to perform in vitro measurements on cells directly cultured on the micro-fabricated diamond substrate and was therefore equipped with a 1 ml perfusion chamber [151].

3.2 Acquisition electronic chain

The chip carrier was directly plugged into the front-end electronics (designed by Dr. Pasquarelli, Ulm university) and controlled by an acquisition software developed in LabView™ environment [155], [156].

The front-end electronics consists of 16 low noise trans-impedance amplifiers having an input bias current of ~ 2 pA and a gain, set by feedback-resistors, of 100 M Ω . The amplified signals were filtered at 4 kHz with 4th Bessel low-pass filters and were subsequently acquired at a sampling rate of 25 kHz per channel. The filtered signals are then acquired by a 16-bit analog/digital converter working over an input range of ± 10 V. A buffered 16-bit digital/analog converter (DAQ, the National Instruments) provides the bias voltage for

the catecholamine oxidation, over the common quasi-reference Ag/AgCl electrode immersed into the working solution. The noise level was evaluated in spike-free trace segments and then averaged over the 16 electrodes, leading to a mean amplitude of 5.5 ± 0.7 pA, with a mean signal-to-noise ratio (S/N) of ~ 3 [157],[158].

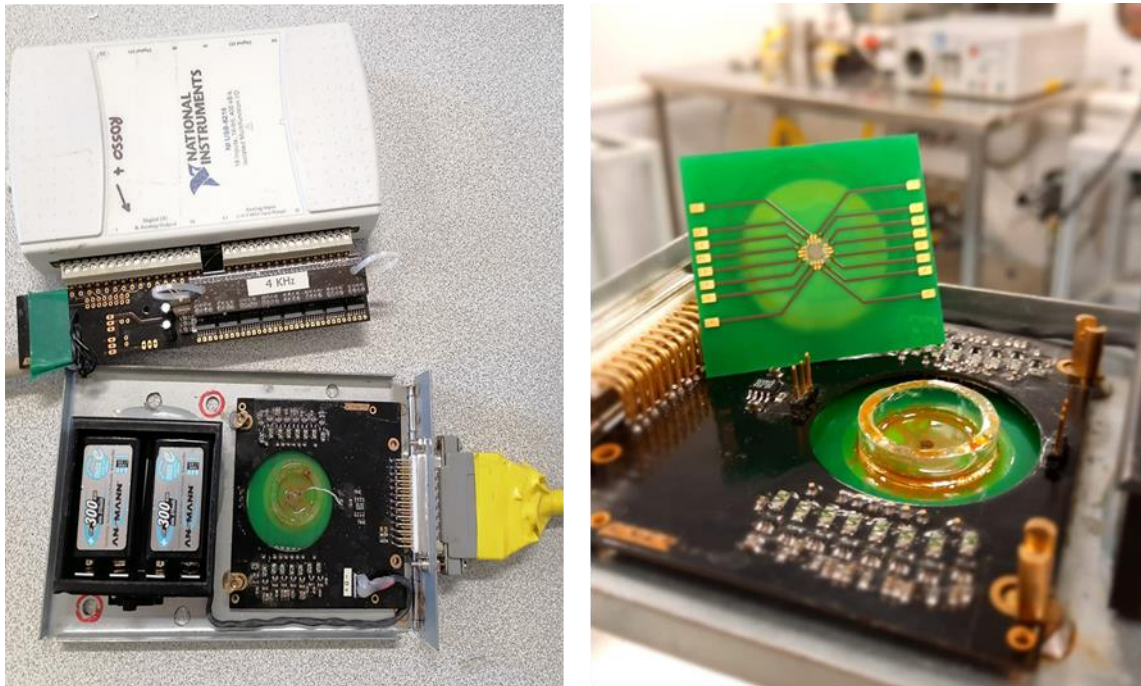


Figure 9 Left: Electronic board with a diamond prototype inserted, connected to the ADC (white NI board) through a 6th order Bessel filter. Right: magnification of electronic board with a diamond prototype.

3.3 Electrical characterization (Tomagra et al., Sensors, Lecture Notes in Electrical Engineering 539, doi.org/10.1007/978-3-030-04324-7_17)

The graphitic microchannels of both devices were electrically characterized before performing the cell sensing.

I-V characteristics of the graphitic electrodes were measured to identify their conduction properties. Figure 10 shows linear trends indicating that the electrodes have an ohmic conduction with resistances comprised between 5 k Ω and 9 k Ω , which correspond to a resistivity of $\rho \sim 1.3$ m Ω *cm, once the geometrical parameters are suitably taken into

account. This value is in very satisfactory agreement with that of nanocrystalline graphite ($\rho \sim 1.3 \text{ m}\Omega\cdot\text{cm}$) [154], [158], [159].

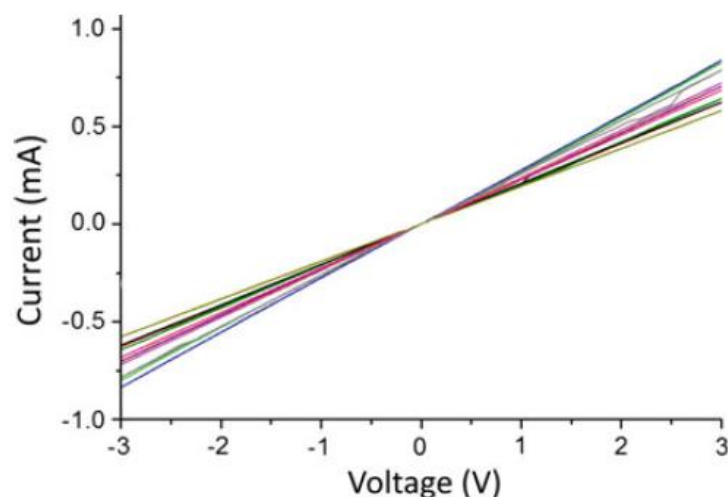


Figure 10 Current-voltage characteristics of 16 graphitic electrodes [158].

In Electrochemical Impedance Spectroscopy measurements (EIS), a sinusoidal voltage of 10mV and variable frequency is applied, with the help of a potentiostat, between the working and the counter electrode and monitored by means of a reference electrode (3-electrode cell), thus measuring the total complex impedance of the circuit. EIS measurements were performed using a water-based electrolyte (PBS, phosphate buffer saline). The AC signal frequency varied between 0.1 Hz and 100 kHz with seven discrete points per decade, while the DC potential was kept constant at 0 mV. Figure 10 a, b reports the data of a representative channel. The module and phase of the impedance $|Z|$ as a function of the modulation frequent (*Bode plot*) were fitted using the equivalent circuit

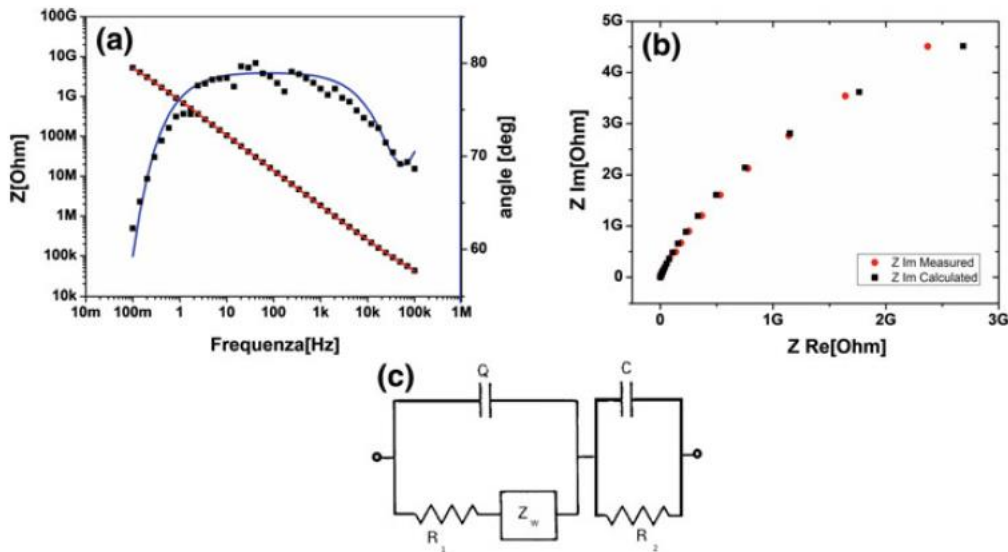


Figure 11 a Bode plot of a representative channel. The black squares represent the measured values, while the solid lines represent the fit considering the equivalent circuit reported in panel (c). b Nyquist plot. The red circles represent the measured values, while the black squares represent the values calculated using the fit results. c Equivalent circuit used to fit the experimental data. The first circuit mesh corresponds to a double layer imperfect capacitor Q , placed in parallel with the resistance due to charge transfer and the impedance due to the diffusion (the Warburg element Z_w). In addition to these elements, a second RC circuit (to the right) is considered to account for the bulk of the electrode [158].

reported in Figure 11c. Best-fit parameters were used to calculate the imaginary part of the impedance as function of the real part of the impedance and were compared with the experimental data, as shown in Figure 11b, indicating good agreement between model and experimental data [158].

Cyclic voltammetry (see Figure 12) was performed to evaluate the sensitivity of $\mu\text{G-SCD-MEA}$ electrodes to detect dopamine. A physiological saline solution (*Tyrode solution*) containing (in mM) 128 NaCl, 2 MgCl_2 , 10 glucose, 10 HEPES, 10 CaCl_2 and 4 KCl (pH 7.4), and a Tyrode solution containing dopamine at different concentrations (25 and 100 μM), were employed in these tests. A triangular voltage waveform, ranging from -0.5 and $+1.1$ V, and with 20 mVs^{-1} scan rate was applied to the graphitic electrodes.

The solution was grounded with a quasi-reference Ag/AgCl electrode. No redox activity was observed using the *Tyrode solution* in the anodic interval of the hydrolysis window,

i.e. up to a polarization voltage of +0.9 V. Under these conditions, a leakage current of less than 10 pA was measured at +0.6 V.

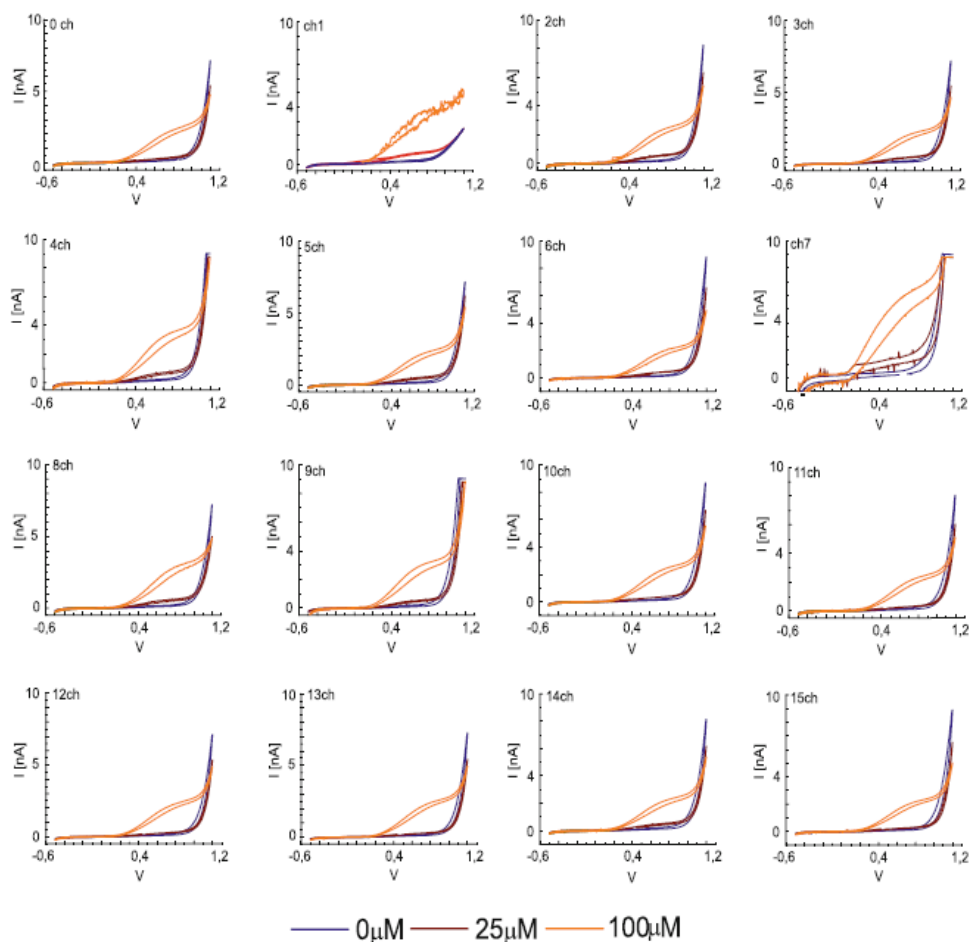


Figure 12 Steady-state cyclic voltammograms of tyrode in control ($0 \mu\text{M}$) and with dopamine solution at different concentration ($25, 100 \mu\text{M}$) [158].

The width of the electrochemical window of the graphitic microelectrodes allows the detection of the oxidation peak of dopamine, located between + 0.5 V and + 0.8 V, as shown in Figure 12. On the basis of these results, the optimal bias voltage for the subsequent amperometric measurement was set to + 0.8 V, i.e. in correspondence of the maximum value of the ratio between the voltammetric signals of dopamine oxidation and water hydrolysis [158].

Chapter 3

Firing properties of cultured midbrain dopaminergic neurons

In my experimental model, dopaminergic neurons are obtained by enzymatic dissociation from the *substantia nigra* (SN) (see materials and methods) even though, we cannot exclude a contamination by the adjacent *ventral tegmental area* (VTA), the *globus pallidus* and *subthalamic nucleus*. The SN in turn is subdivided into the *substantia nigra pars compacta* (SN_c) mainly consisting of dopaminergic neurons modulated by GABAergic neurons and *substantia nigra pars reticulata* (SN_r), consisting of GABAergic neurons. Moreover, different dopaminergic neurons belonging to the SN are characterized by different electrophysiological properties, as described in the *chapter 1* [160]–[162]. The *tegmental area* is mainly composed of dopaminergic neurons synaptically connected to each other, but also with glutamatergic and GABAergic neurons [163]–[165]. A subpopulation of glutamatergic neurons has been described within the VTA, representing a glutamatergic modulatory pathway on dopaminergic neurons [166].

Because of this heterogeneity, I initially monitored the electrical activity of the whole network over time, and then I quantified the role of inhibitory and excitatory components to isolate the contribution of dopaminergic neurons.

1.0 The firing mode of midbrain neurons switches from isolated spikes to burst-driven activity along with the network development (Tomagra et al., in preparation)

In a first series of experiments I focused on monitoring the spontaneous firing of cultured mesencephalic neurons. The measurements were made using the MEA (Multi-Electrode Array). As previously described (see *chapter 2: Materials and Methods*), this experimental approach allows to simultaneously record the electrical activity from 60 electrodes and to

carry out repeated measurements over time, from the same cell preparation, because of sterility conditions are preserved. The recordings were made inside an incubator, under standard temperature (37 °C) and CO₂ (5%) conditions. The electrical activity of mesencephalic neurons was studied by keeping the cells in their culture medium (see Materials and Methods) and was monitored during the first three weeks of their development, respectively at 7, 9, 11, 14, 16, 18 and 21 DIV (days in vitro).

In figure 1A, 7 representative traces, detected from the same electrode over time, are shown: these represent the spontaneous activity of the network evolving from 7 DIV until 21 DIV. At 7 and 9 DIV the firing was mainly characterized by single spikes, generated with low frequency: respectively 2.27 ± 0.11 Hz and 2.84 ± 0.14 Hz ($p > 0.05$). At 11 DIV the firing rate significantly increased to 4.07 ± 0.15 Hz ($p < 0.05$). Otherwise, from 14 DIV to 21 DIV, a further slight increase was observed, which however was not statistically different with respect to the one measured for 14 DIV neurons, as shown in the histogram in Figure 1B. I also observed an increase in the number of active electrodes, a phenomenon clearly linked to the development and maturation of the network. This is shown in figure 1C: the number of active electrode increased from 50% (7 DIV) to 72% (14 DIV, $p < 0.05$), whereas remained unaltered in the range 14-21 DIV ($N_{MEA} = 15$). Thus, since 14 DIV is a critical stage for network maturation, I considered the network mature at 14 DIV.

For what concerns the distribution of the firing rates at 14 DIV, values are broadly scattered from 0.1 to 40 Hz (Figure 1D). By setting a threshold at 4.5 Hz [8], I found that 55% of neurons were spontaneously firing at low frequency (1.59 ± 0.05 Hz), whereas 45% fired at 10.2 ± 0.2 Hz [11]. As mentioned in the introduction, this expected variability of the firing rates is due to the variability of dopaminergic and non-dopaminergic neurons in the network [11], [160]. In Figure 1E, the distributions of the firing frequency values are showed in the range 9-21 DIV.

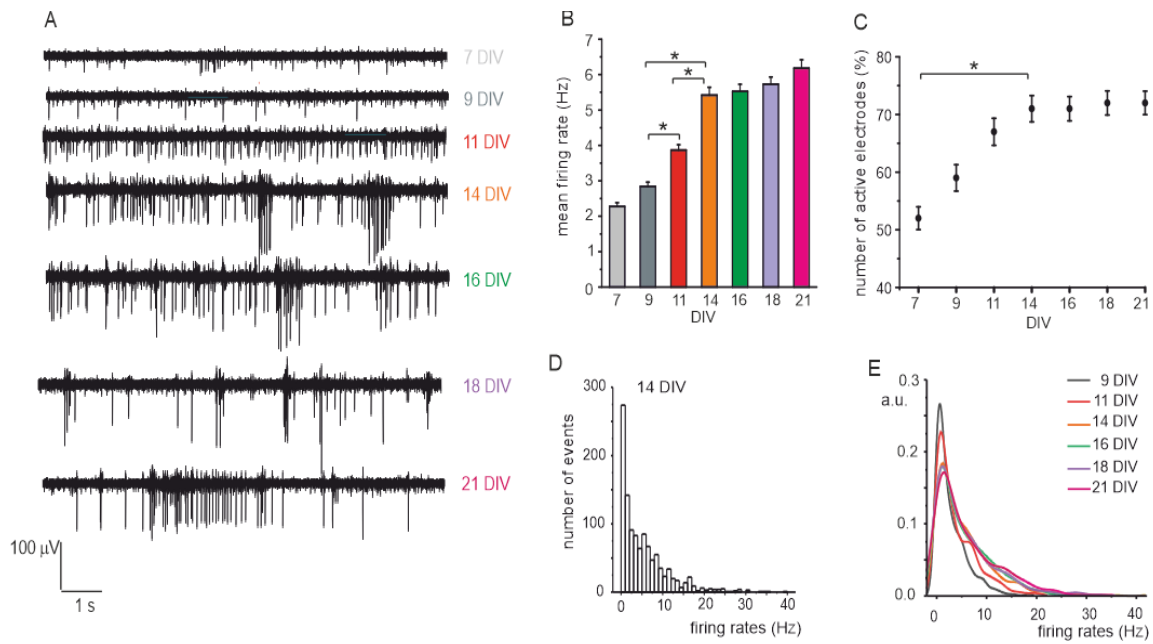


Figure 1 A: Seven representative traces from 7 to 21 DIV. B: Histograms of mean firing rate from 7 to 21 DIV. C: % of active electrodes from 7 to 21 DIV. D: firing rate distribution at 14 DIV. E: distributions of the firing frequency values in the range 9-21 DIV.

After measuring the firing rate, I also compared, among the young (7-9 DIV) and the mature neurons (>14 DIV), the waveform and peak amplitude of the extracellular action potentials. I limited this analysis only to biphasic waveform signals, characterized by a pronounced negative peak followed by a positive peak (antipeak).

Two representative examples of peak amplitudes at 7DIV and 14 DIV (from the same electrode) are shown in figure 2. On average, the negative peak, for 7-9 DIV neurons, had a mean amplitude of $-30.0 \pm 1.4 \mu\text{V}$ and was followed by a smaller antipeak ($11.9 \pm 0.5 \mu\text{V}$) [167]. In elder neurons (14-21 DIV), the amplitude of the antipeak was still distributed around a unique value ($21.7 \pm 0.8 \mu\text{V}$), while the distribution of negative peaks shows three different peaks distribution, centered at $-49.0 \pm 2.4 \mu\text{V}$, $-155 \pm 27 \mu\text{V}$ and $-218 \pm 20 \mu\text{V}$, respectively (Figure 2). Different hypotheses have been put forward to explain this phenomenon: (a) as reported in recent studies [168], [169] on high density MEA (HD-MEAs) as the network matures, neuronal interconnections increase, depending on the area of the neuron (soma axons or dendrites) located above the electrode varies the amplitude of the recorded signal; (b) another possibility is that there is a remodelling in the distribution of ion conductance's during the development of the network; (c) last but

not least, the presence of the burst that before the 14 DIV is not well developed, this in fact is characterized by a first larger amplitude peak and the following ones that decrease in amplitude.

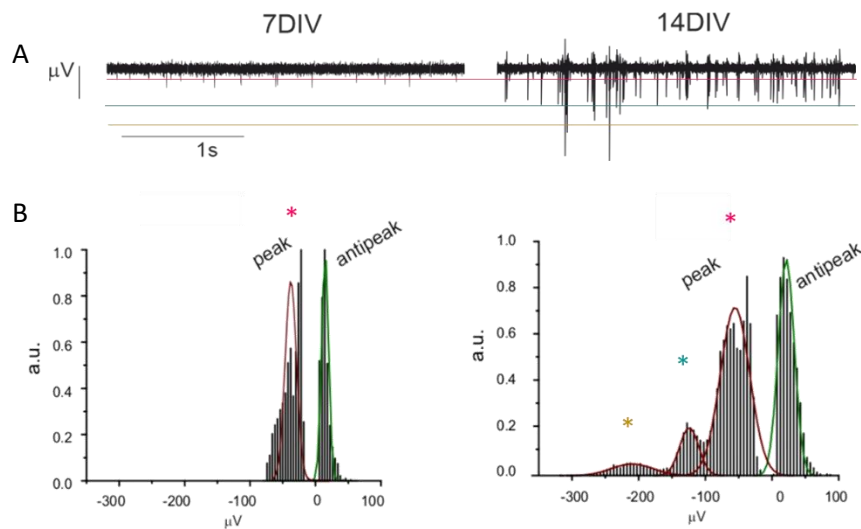


Figure 2 A representative traces at 7 and 14 DIV from the same electrode, B: peak amplitude distributions ($N_{MEA} = 15$).

Thus, until 9 days in culture, only isolated peaks are observed (Figure 2), while after 14 DIV, the occurrence of burst begins and progressively increases with the development of the network. A burst is described as a set of action potentials generated in rapid succession and followed by a period of relative quiescence [170]. In dopaminergic neurons, burst generation can be associated to NMDA receptor activation and GABA-mediated disinhibition [171]. Figure 3A shows three representative recordings, acquired consecutively from the same electrode at 11, 14 and 21 DIV, respectively. The average progressive increase in the number of bursts is shown in the histogram in Figure 3D.

A quantitative detection of burst activity can be performed by analyzing the interspike interval (ISI) distribution. As reported by Chen et al. [172], it is possible to define the type of firing, if characterized by single spikes (sporadic) or bursts, by analyzing the ISI. I analyzed the number of cases for each MEA of sporadic and burst firing over time from 7 to 21 DIV (Figure 3C). As shown in Figure 3C, the ISI distribution may drastically vary among sporadic spike generation and burst-driven activity [173]. Sporadic firing has a broad heterogeneous ISI distribution, whereas burst firing pattern displays a single-peak distribution (Figure 3B). I used this method for measuring the number of electrodes that

were detecting burst activity or sporadic spike firing ($N_{MEA} = 15$, Figure 3C). It is possible to observe that at 14 DIV there is a trend inversion, characterized by an increase in the burst firing respect to the sporadic single-spike firing mode. Number of bursts progressively increased from 7 to 21 DIV, together with the number of spikes / bursts (Figure 3D), whereas burst duration does not exhibit significant variations.

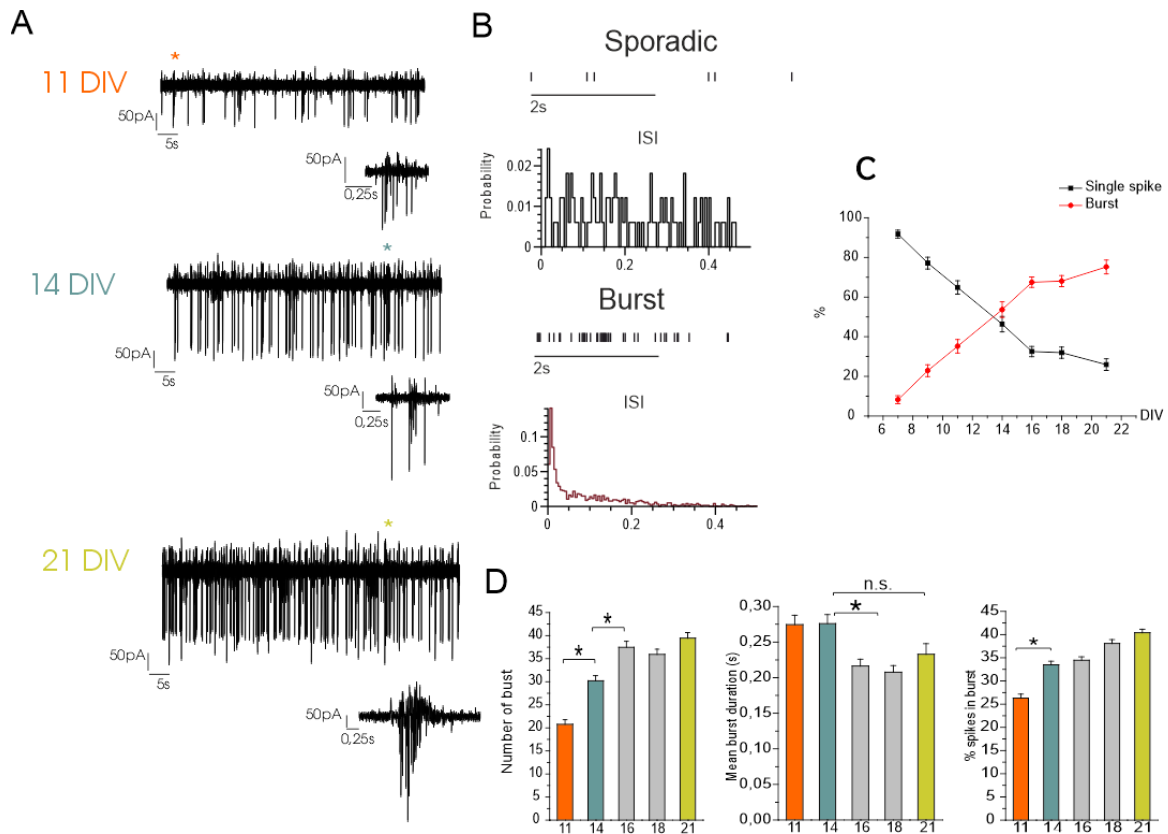


Figure 3 A: Representative traces at 11, 14, 21 DIV acquired from the same electrode. Examples of bursts are indicated by the black asterisks, while the red asterisk indicates the one shown in the enlargement. B: Interspike interval distribution in sporadic (black trace) and burst (red trace) activity. C: percentage of number of electrodes that were detecting burst activity or sporadic spike firing. D: Burst analysis histograms: number of burst, mean burst duration, % spikes in burst.

2.0 Modulation of the firing rate and the synchronism by GABAergic and glutamatergic input

In a successive series of experiments, I studied, through the use of selective blockers, the role of glutamatergic and GABAergic tone in the regulation of the network spontaneous activity and the network synchronism. It is reported that in dopaminergic neurons, the generation of bursts is associated with the activation of NMDA receptors mediated by the disinhibition of the GABAergic tone [174].

To this purpose, mature neurons (14 DIV) were exposed to picrotoxin (100 μ M), APV (50 μ M) and DNQX (20 μ M). Drugs have been acutely applied to sequentially and selectively block GABA_A, NMDA and AMPA/kainate receptors and thus reveal the involvement of the specific neurotransmitters.

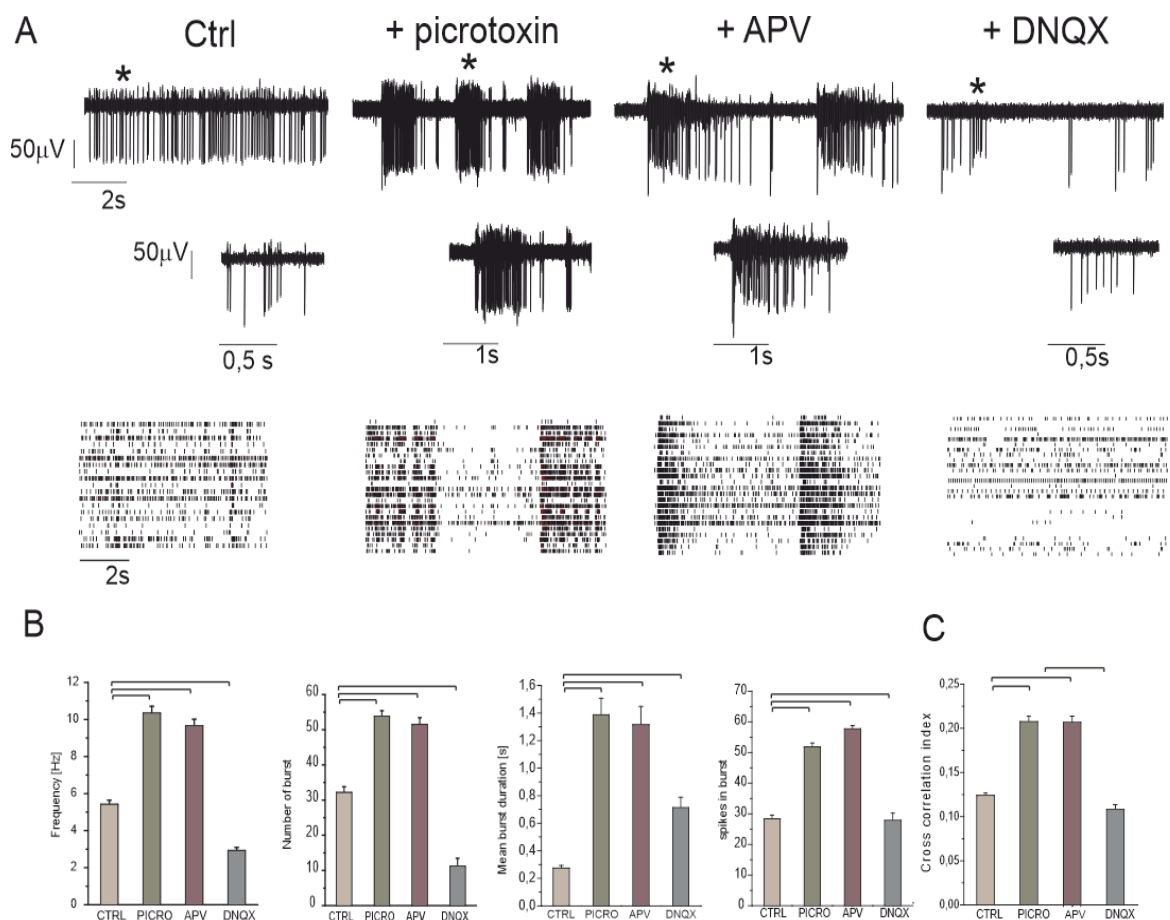


Figure 4 A: representative traces in sequence of the recordings made in control condition at 14DIV, after administration of picrotoxin, APV and DNQX, and relative magnification of

a burst. Under each recording there is the relative raster plot. B: histograms representing the mean firing rate, the mean number of bursts, the mean burst duration, the % spikes in bursts and (C) the cross correlation index.

Administration of picrotoxin caused a significant increase of the firing rate, from 5.4 ± 0.2 Hz to 10.3 ± 0.4 Hz ($p < 0.05$, Figure 3A, B). Similarly, picrotoxin caused a comparable increase of the number of bursts, the duration of the burst and the percentage of peaks during the burst. These data are in good agreement with the records, which show that the GABA-mediated inhibition of nigral dopaminergic neurons *in vivo* arises from the collateral axons of *pars reticulata* projection neurons [174]. The subsequent administration of APV did not produce a significant change in firing, only a decreasing trend can be observed compared to the previous administration with picrotoxin (9.7 ± 0.4 Hz). On the contrary, the addition of DNQX drastically reduced the firing frequency to 2.9 ± 0.2 Hz ($p < 0.05$), as well as the burst parameters, confirming the role of glutamate receptors in the burst activity [175]–[177]. Recent evidence suggests that, in addition to glutamatergic excitatory inputs from the *subthalamic nucleus*, excitatory cholinergic and glutamatergic inputs can arrive from the PPN (*pedunculopontine nucleus*) [178]; furthermore, glutamatergic neurons were also recently discovered in the VTA [179]. This reduction in mean discharge rate respect to control conditions suggests that a basal glutamate tone is driving the network [179].

3.0 Synchronization of midbrain neurons

The functional connection within neuronal networks *in vitro* can be analyzed by measuring the synchronism of the network [180]. Synchronization is quantified by cross-correlation histograms (CCH) [146], [181].

Cross-correlation compares two-time series of signals and objectively find how they couple over time, and in particular where the best match occurs. The cross-correlation can therefore reveal the periodicity in the data. In the case of the MEA, a reference electrode is identified with respect to all the other electrodes that are defined as targets, the more synchronized the two signals, the greater the cross-correlation peak.

The time-lag refers to how much the signals are offset, two ideally synchronous signals are spiked to 0, in general there is always a time delay, so that the sign of the time-lag determines which signal is displaced with respect to the other. Note that as the delay increases, the number of possible matches decreases because the signals "hang" at the ends and do not overlap. The value of the delay with the highest correlation coefficient represents the best fit between the two sets of signals. The sampling interval delay time provides the length of time one signal precedes or follows the other [182]–[184].

I observed that, under control conditions, immature midbrain neurons show low synchronism. This was quantified by measuring the maximum CCH peak probability (0.05%). On the contrary, this value increased up to 0.13% and 0.24%, respectively for 14 and 21 DIV neurons. This is in accordance with the development of the network over time, not only increases the frequency and the burst parameters, but also the synchronism of the network as expected [185]. The addition of picrotoxin (14 DIV) dramatically enhances the CCH peak (0.21%), indicating improved synchronization and suggesting that the gabaergic input exerts a negative control on the network synchronization. Thus, GABA_A receptors influence both the initiation of the burst and the timing of the burst. The subsequent addition of APV has no significant effect, while a drastic reduction of the CCH peak is observed in the presence of DNQX (0.11 %), indicating that synchronous activation in the mature network depended on AMPA / kainate receptors.

Another information about the network synchronism can be inferred by measuring the position of the CCH peak probability respect the time lag 0. When the CCH peak is centered at 0 ms, no delay offset exists between the spike trains revealed by a pair of electrodes, which have been randomly selected respectively as *reference* and *target* electrode [169], [186]. On the contrary, when the CCH peak is shifted from 0 ms, this indicates that activation of one electrode is delayed (or anticipated) respect to the other one. Under control conditions (14 DIV, without GABAergic and glutamatergic receptor antagonists), the mean CCH peak was centered around 1.16 ± 0.31 ms. Three representative CCH (control condition) are shown in Figure 5A. CCH peak values are described by a gaussian distribution, whose mean value is 1.13 ± 0.31 ms (Figure 5C). In this condition it is possible to define that neither neuron drives the other, probably because the network is in equilibrium between the excitatory and the inhibitory input.

On the other hand, as a consequence of the addition of picrotoxin, the CCH maximum peak probability was enhanced (Figure 5B), but also exhibited a significant (positive or negative) time lag. On average, the positive shift was 26 ± 1 ms and indicates that the activation of the reference electrode respectively precedes the activation of the target electrode, while the opposite occurs for the negative shift -27 ± 2 ms. As described by Opalka et al. [168], if the peak is shifted to the left it means that the reference neuron fires slower than the target neuron, on the contrary, if shifted to the right, the reference neuron fires faster than the target neuron. This suggests that one of the two signals (inhibitory / excitatory) prevails over the other and is therefore conditioned by it. Therefore, if the reference neuron, for example, is excitatory while the target neuron is inhibitory, it will activate faster than other, and conversely. This defines the importance of a correct balance in a neuronal network between inhibition and excitation.

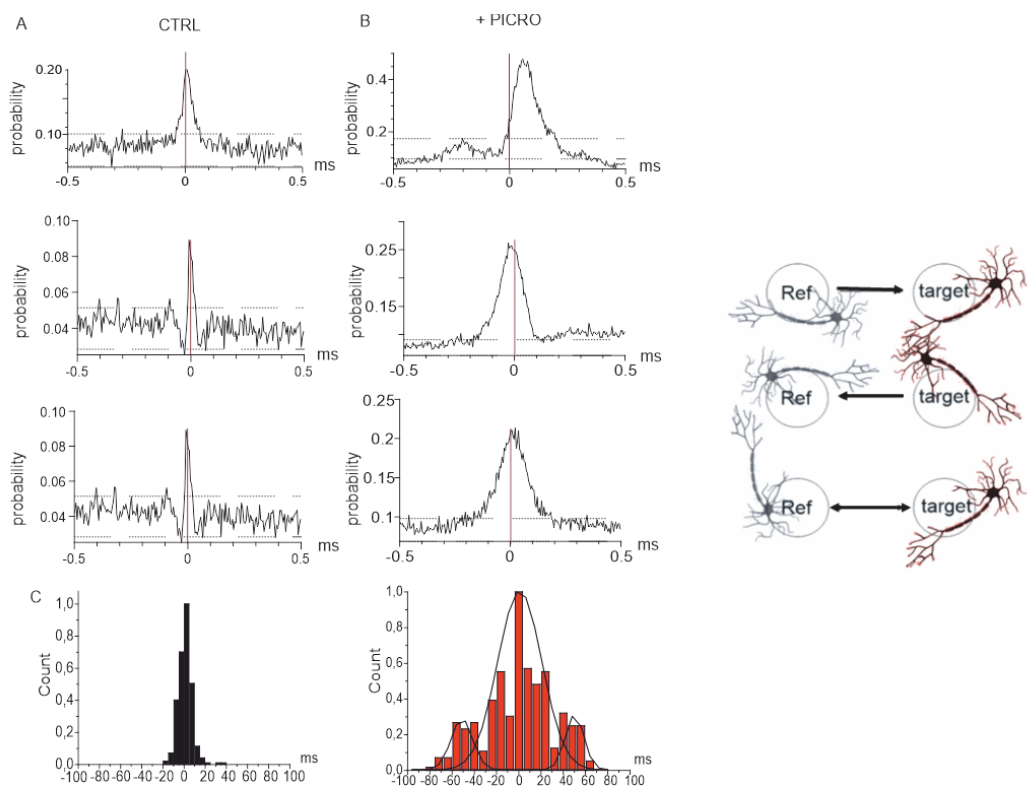


Figure 5 Cross correlogram at 14 DIV in control condition (A) and after picrotoxin administration (B). C: Distribution of the time lag (ms).

Another important conclusion that can be drawn from these results is related to the fact that, after the administration of glutamatergic and GABAergic antagonists, a residual spontaneous activity persists and the network is not completely silenced, suggesting a

role of dopaminergic neurons. This is different from what observed in cultured hippocampal neurons [187], which are completely silenced by the addition of glutamatergic antagonists.

For this reason, next step was to investigate the role of dopaminergic neurons within the network.

4.0 The pacemaking activity of cultured midbrain dopaminergic neurons

The addition of GABAergic and glutamatergic antagonists allowed us to quantify the contribution of dopaminergic neurons in the overall firing of the network. Since a peculiarity of these neurons is related to their pacemaking activity, this has been quantified by measuring the existence of multiple equally spaced peaks in the autocorrelograms [11]. Autocorrelation defines the degree of cross-correlation of the signal with itself. This means that the signal at instant t is compared with the value of the signal at instant $t + \Delta t$ to verify how much it correlates with the progress of time. If the autocorrelation between two values of t is proved, as one of the two varies, the other will also vary. So autocorrelation is nothing more than the cross-correlation of the signal with itself [188].

I separated neuronal populations by quantifying the firing frequency and the number of symmetric peaks of autocorrelogram that exceed the 99% confidence level, according to the procedure described in [146]. The peaks of the autocorrelogram are an intrinsic property of the degree of synchrony of the neuron, depending on the number of peaks and valleys present it is possible to define the different neuronal populations of your model (see materials and methods).

In order to distinguish among the different firing of dopaminergic neurons, I followed the protocol described by Berretta et al. [11] on SN slices. Interfacing SN slices with the same multi-electrode arrays (MEA) that I used, Berretta and colleagues demonstrated that most of SN dopaminergic neurons (50.21%) had a low discharge frequency (1-3 Hz) and a stable pacemaker-like pattern, while others (44.84%) were sporadic, but are characterized of a low frequency. The remaining population (4.95%) included neurons with higher regular activation in frequency (5-10 Hz). This allowed therefore defines three populations: the

low rate (LR), including the pacemaker (LR_p) the not-pacemaker ones (LR_{n-p}), and the high rate (HR). Thus, I decided to study whether such a parallelism observed on the slice model could be applied even on dissociated dopaminergic neurons [11].

I found that in 21% of cases neurons were characterized by high firing rates (HR_p) (9.2 ± 0.5 Hz) and were accompanied by more than four consecutive peaks in the autocorrelogram, thus revealing regular activity [11]. The autocorrelation probability measured on the first of the repetitive peaks was 18.21 ± 1.12 % and CV 0.62 ± 0.04 .

Another set of pacemaking neurons exhibited low frequency values (low-rate pacemaking neurons, LR_p), with 2.9 ± 0.1 Hz firing rate, and more than three consecutive peaks in the autocorrelogram. These were contributing to 8% of the total population, the autocorrelation probability measured on the first of the repetitive peaks was 21.36 ± 0.73 % and their mean CV was 0.67 ± 0.07 .

Finally, low rate not pacemaking neurons were firing at 0.76 ± 0.05 Hz and showed one consecutive peak in the autocorrelogram, with a first peak spike autocorrelation probability 7.47 ± 0.43 % and CV was 0.92 ± 0.03 .

These data are in perfect agreement with what reported by Berretta et al. for the same experiments performed on *substantia nigra* slices.

All these results further confirm that cultured dopaminergic neurons represent a reliable model and exhibit functional properties which are comparable to those observed in slices.

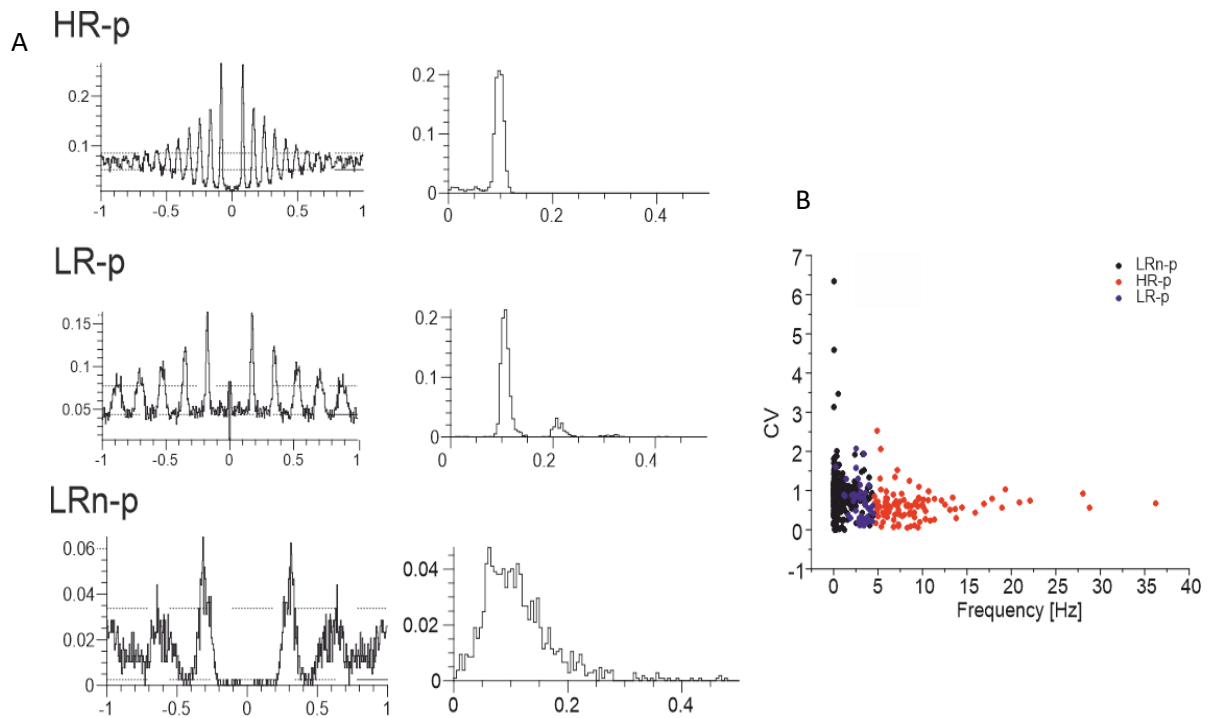


Figure 6. HR-p (top), LR-p (middle) and LRn-p (bottom) neurones. A. The spike time autocorrelograms are represented, while on the right the inter-spike interval histograms are represented. Horizontal dotted lines in the autocorrelograms indicate 99% confidence limits [25]. B Scatter plots of the basal firing rate vs. coefficient of variation (CV), showing fairly distinct clusters, corresponding to the three different populations.

After the characterization of the network of dopaminergic neurons of the midbrain in dissociated culture, I studied the effects that exogenous α -synuclein oligomers may exert on the firing activity. I performed these experiment by combining MEA and patch-clamp recordings, the latter in current-clamp mode.

Chapter 4

Time- and dose-dependent alteration of the firing rate by exogenous α -synuclein

α -synuclein (aSyn) is a presynaptic protein involved in the processes of exocytosis and endocytosis [80], [189], [190]. Despite its consolidated physiological role, α -synuclein (aSyn) is still a subject of study. Under physiological conditions it is a soluble protein, but for reasons still unclear, insoluble protein aggregates can be created, with altered structure (protein misfolding), known as Lewy bodies, involved in the neuronal degeneration that characterizes Parkinson's disease. The mechanism driving the change from the normal conformation to the pathological one that generates aggregates is still not clear, but one hypothesis is that it may be attributable to an alteration of specific genes that code for aSyn or to errors in the appropriate mechanism to the metabolism of altered proteins [191]–[193].

It is also believed that aSyn accumulated on the extracellular side can be internalized in neurons through non-selective endocytosis or receptor-mediated endocytosis [194], propagating toxicity from one cell to another (spreading).

Recent evidence indicate that extracellular aSyn oligomeric aggregates, that precede fibril formation, may be the most neurotoxic species [195], [196]. The *in vitro* application of aSyn oligomers mimicked the synaptic effects observed *in vivo* in Parkinson's disease models [197].

For all these reasons, the goal of these experiments is to investigate, through the use of MEAs and conventional electrophysiology, the effects of aSyn oligomers accumulated on the extracellular side. I studied the effect of exogenous aSyn at different concentrations on mesencephalic neurons by measuring the activity of the network in acute, after 24 hours and after 48 hours. The measurements were initially carried out at 14 DIV, since as

described in chapter 3, the network can be considered mature. But once the concentration was defined, I also studied the effect of aSyn on an immature network. Since the measurements have been carried out through the MEA, and this approach provides information on the whole network, next I evaluated the specific effect that aSyn has on dopaminergic neurons using the patch-clamp technique, by identifying TH-GFP positive (dopaminergic) neurons.

1.0 Effect of aSyn at different concentrations in a mature network (14 DIV)

In a first series of experiments, I tested the effects of extracellular aSyn on the spontaneous firing, by varying the exposure time and the concentration of applied aSyn (Figure 1). These trials have been performed using MEAs.

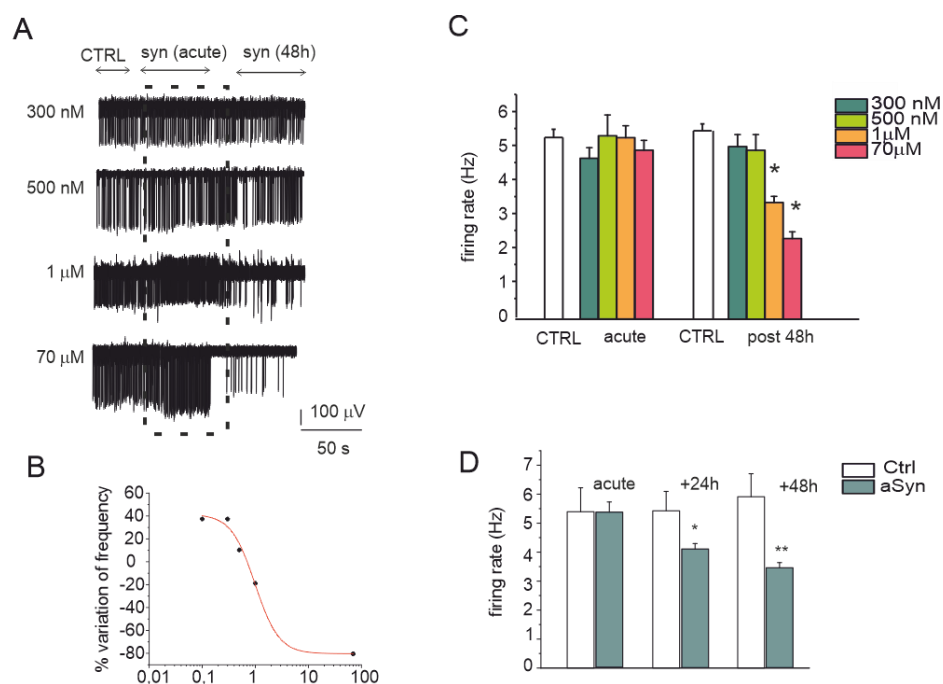


Figure 1 A Dose- and time-dependence effect of aSyn. Representative traces are shown at different concentrations (300 nM, 500 nM, 1 μM, 70 μM): in control condition, in acute and after 48 h exposure. B Dose-response curve showing % variation of the firing rate versus increasing aSyn concentrations. C Mean firing rate in control condition, acute and after 48h at 4 different concentrations. D time-dependence of frequency reduction as a

function of the exposure time (acute exposure, 24 hours and 28 hours for 48h at 1 μ M concentration).

Firing rate was monitored in control condition, immediately after aSyn exposure (acute), after 24 and 48 hours. aSyn-treated cells were always compared with a control sample at the same DIV. I performed a dose-response test at different concentrations (0.1, 0.3, 0.5, 1 and 70 μ M). As it can be seen from figure 1, in the presence of 300 and 500 nM aSyn, both in acute and after incubation for 48h, the firing frequency is not significantly changed compared to the control condition ($p > 0.05$). At concentrations of 1 μ M and 70 μ M, in acute, no significant differences are observed, but after incubation for 48 h the firing frequency is significantly reduced by 35% (1 μ M) and 55% (70 μ M) respect the control condition ($p < 0.05$).

Thus, we decided to use 1 μ M for future experiments. In more details, at 1 μ M, the firing rate decreased from 5.43 ± 0.67 Hz to 4.10 ± 0.19 Hz after 24 hours ($p < 0.05$) and 5.91 ± 0.79 Hz to 3.44 ± 0.18 Hz after 48 hours ($p < 0.001$, Figure 1D). After 48h I observed a significant decrease in firing, for this reason I carried out tests to verify if the effect was actually due to the formation of aSyn oligomers.

To validate the presence of aSyn oligomers, in collaboration with Dr. Federico Cesano (Department of Chemistry, Torino University), we have performed some trials using the AFM (atomic force) microscope. As shown in Figure 2, after 48h of incubation at 37 °C, using a concentration of 1 μ M, we found that the height and width of the oligomers were in the range of few micrometres. These data are comparable with those reported in the literature [198]–[200], thus confirming the formation of the oligomer structures in our experimental conditions.

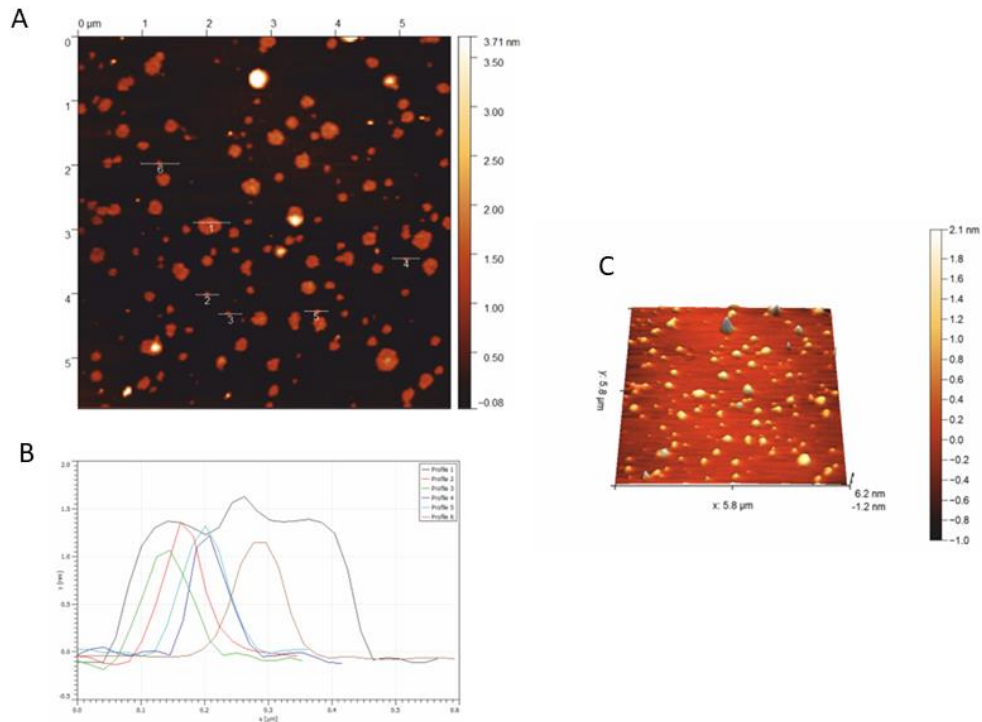


Figure 2 AFM measurement, A: 2-dimensions oligomeric profile; B: High (y) and weight(x) of different oligomeric form defined in the picture A with number from 1 to 5; C: 3-dimention oligomeric from profile.

Next, I investigated whether aSyn oligomers, besides causing a reduction of the spontaneous firing frequency, could also induce an altered firing mode. I found that the reduction of the firing frequency after aSyn 48 h exposure was associated to a reduced number of bursts, which decreased from 24 ± 1 to 15 ± 1 , and to an increased burst duration and number of spikes/bursts (Figure 3A-B). Change of the burst activity was also by comparing the ISI (interspike interval) in control and after aSyn exposure. As can be seen in Figure 3C, after 48 h exposure, the mean number of neurons exhibiting burst decreases while under control conditions the network is more burstly and not sporadic, in ordinate it was counted for each channel of each MEA ($N_{\text{MEA}} = 10$) when the channel has a typically sporadic ISI and when instead it is typically burstly (as shown in figure 3A, chapter 3).

I also observed that the cross correlogram after 48h is significantly different compared to the control condition measurement: the cross correlogram peak decreases from $0.137 \pm$

0.004 to 0.101 ± 0.004 (Figure 3B, $p < 0.05$). This data indicates that another effect of synuclein is an impairment of the network synchronism.

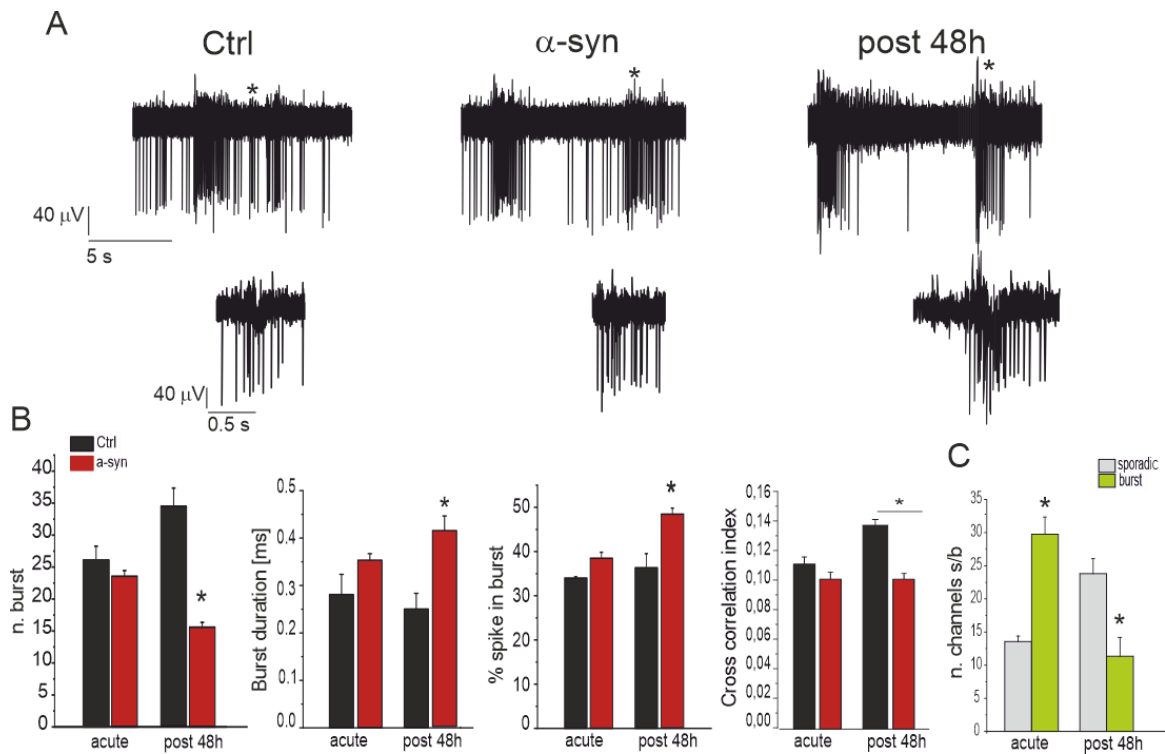


Figure 3 A representative trace in control condition, in acute and after aSyn exposure for 48h, with a corresponding enlargement of a representative burst. B The burst parameters in acute and after exposure for 48h: number of burst, mean burst duration, % spikes in burst and cross correlation index. C Mean percentage of electrodes exhibiting burst activity, measured counting for each channel of each MEA ($N_{MEA} = 10$) when the channel has a typically sporadic ISI and when it is typically burstly (as shown in figure 3A, chapter 3) (in control condition at 14DIV and after 48h exposure to aSyn for sporadic firing is represented in grey, the burst firing in green).

2.0 aSyn is uneffective on young neurons (9 DIV)

Since, through the use of MEAs, we can monitor the evolution of the neuronal network [201], [202], I decided to study whether the effect exerted by aSyn on a mature network (previous paragraph) is analogous to the effect exerted on an immature network. For this

reason, I performed the same experiments on a young (9 DIV) neurons, which are characterized by few bursts and mostly absent synchronism.

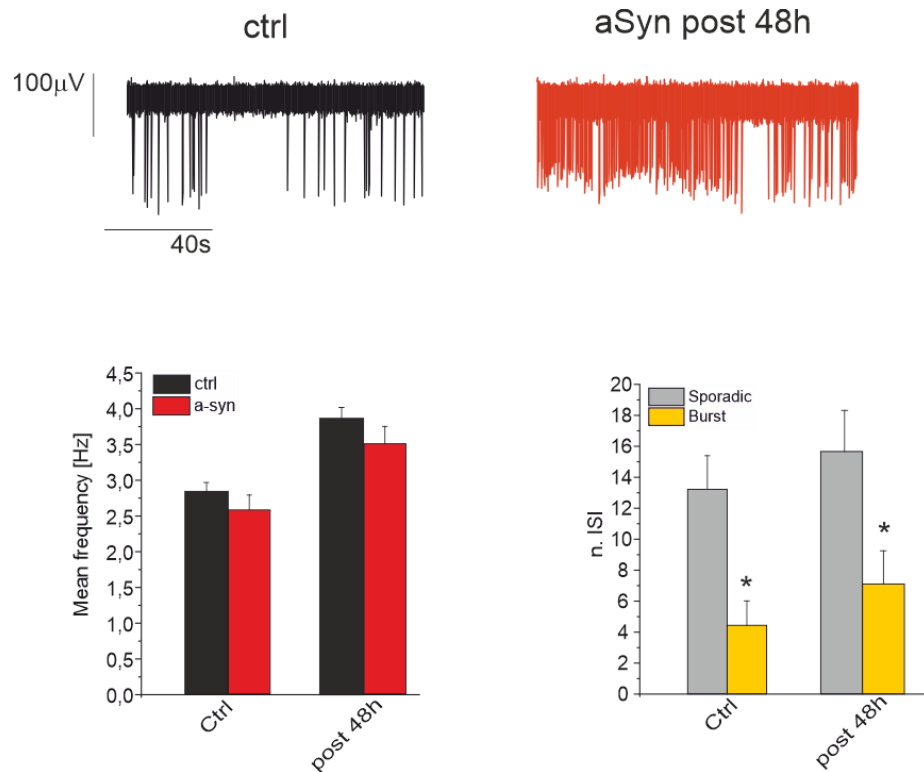


Figure 4 Top. Representative traces in control condition (9 DIV) and after 48h exposure to aSyn. Below. Mean frequency histogram and ISI histogram in control condition and after aSyn incubation for 48h.

As expected, acute exposure to aSyn, did not significantly altered the firing frequency, even for immature neurons, as observed for mature neurons. Same conclusions can be drawn even after 48 hours' exposure: aSyn was still ineffective on young neurons, whereas drastically impaired the firing frequency of mature neurons. More experiments will be needed to better understand this phenomenon.

3.0 aSyn-reduction of the firing rate is reversed by MVIIC

After studying the effect of aSyn on the whole network, I focused on studying the effect exerted by aSyn on dopaminergic neurons. These measurements were carried out using the patch-clamp technique, in order to limit this trials to GFP-stained dopaminergic neurons.

To this purpose, I blocked both the inhibitory and excitatory synapses (by applying picrotoxin (100 μ M), APV (50 μ M) and DNQX (20 μ M)). Recordings were conducted on mature cells, exposed for 48 h to 1 μ M aSyn.

I measured the cell activity in *current-clamp* mode. Even in these conditions, dopaminergic neurons are spontaneously firing, similarly to what observed from the MEA trials (see figure 1). Without applying any stimulating pulse, as can be seen in figure 5, and as already emerged from the tests at the MEA, in the presence of aSyn the frequency is significantly reduced, varying from 3.1 ± 0.3 Hz to 1.7 ± 0.1 Hz (N= 10, $p < 0.05$).

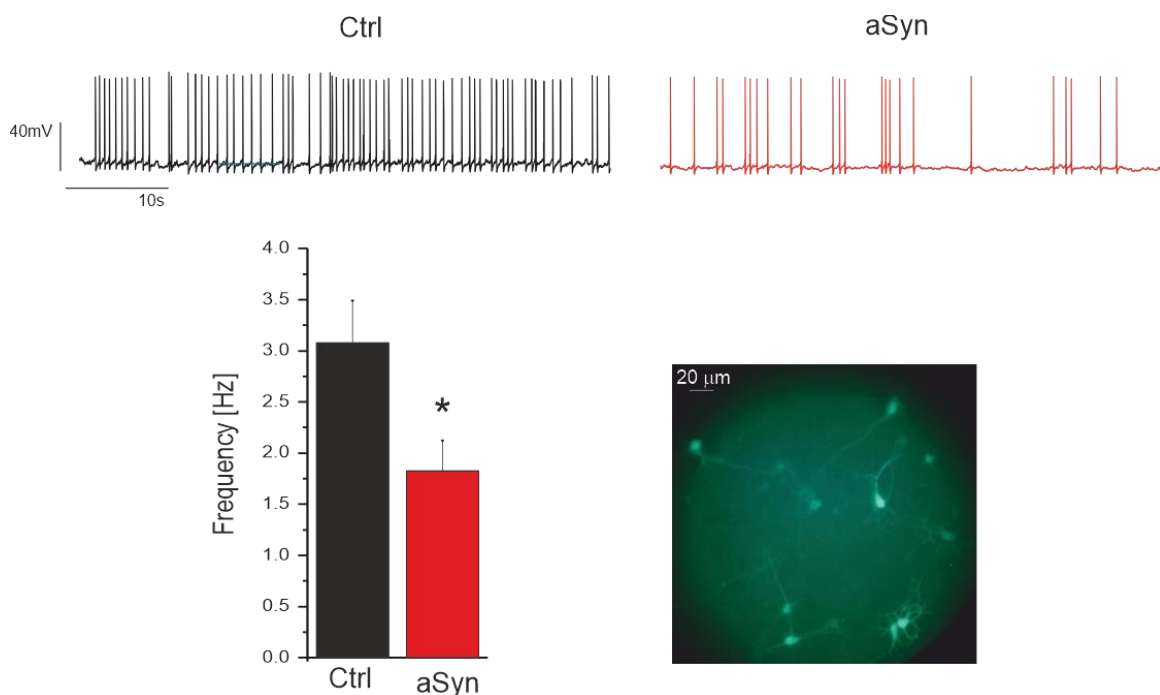


Figure 5 Top, representative trace in control condition (black) and after 48h aSyn (1 μ M exposure) (red). Below (left) histogram of the mean firing frequency and (right) images of TH-GFP midbrain dopaminergic neurons.

Thus, this experiments confirms that exogenous aSyn oligomers, impair both the spontaneous activity of dopaminergic neurons (current clamp experiments) and the spontaneous activity of the whole network (MEA). Future trials will be necessary to

understand whether the inhibition of the dopaminergic tone is also associated to altered firing of GABAergic and glutamatergic neurons.

In a successive set of experiments, I studied the effects of aSyn oligomers on dopaminergic neurons stimulated by current pulses of increasing amplitude.

In spontaneous firing conditions (0 pA injected), as already observed in the previous experiment, the firing frequency is drastically lowered by aSyn.

In the pulsed protocol, pulses increasing current amplitude were applied (20 pA steps). The results observed are exactly the opposite of the expected ones:

- without aSyn (control condition), the frequency increases proportionally to the applied current pulse. The average frequency is 2.73 ± 0.56 Hz (0 pA), 3.98 ± 1.23 Hz (+ 20 pA), 5.47 ± 1.62 Hz (+ 40 pA), 5.23 ± 1.37 Hz (+ 60 pA);
- after aSyn exposure, 20 pA pulses were sufficient to produce a dramatic increase of the firing rate, whereas under control conditions the same step caused only a moderate increase. This different behaviour among control and aSyn-treated neurons persists for current pulses > 20 pA: 7.39 ± 1.15 Hz (+ 20 pA), 9.79 ± 1.77 Hz (+ 40 pA) and 8.21 ± 1.48 Hz (+ 60 pA).

So, it is possible to conclude (figure 6) that in a pulsed protocol aSyn significantly increases the firing frequency at each pulse, but adapts much earlier than the control condition. Infact by applying stimuli of increasing intensity from 20 to 40 pA, the firing frequency doubled compared to that observed in the control condition. Preliminary data suggest different adaptation of the firing frequency: the firing rate decreases by 40 ± 5 % control and by 70 ± 3 % after aSyn incubation. Though, further experiments are needed to confirm these findings. Another interesting parameter is the derivative of the voltage over time (dV/dt), which represents the rising phase, or the speed with which the action potential is generated. This parameter is closely related to the role of Nav and Cav channels. After incubation with aSyn, the rising phase is significantly higher than in control (control condition: 102.01 ± 14.62 mV/ms, aSyn: 151.30 ± 10.85 mV/ms, $p < 0.05$). This may suggest that a different recruitment of Nav and Cav involved in the rising phase of the AP. More studies will be needed to better understand this effect.

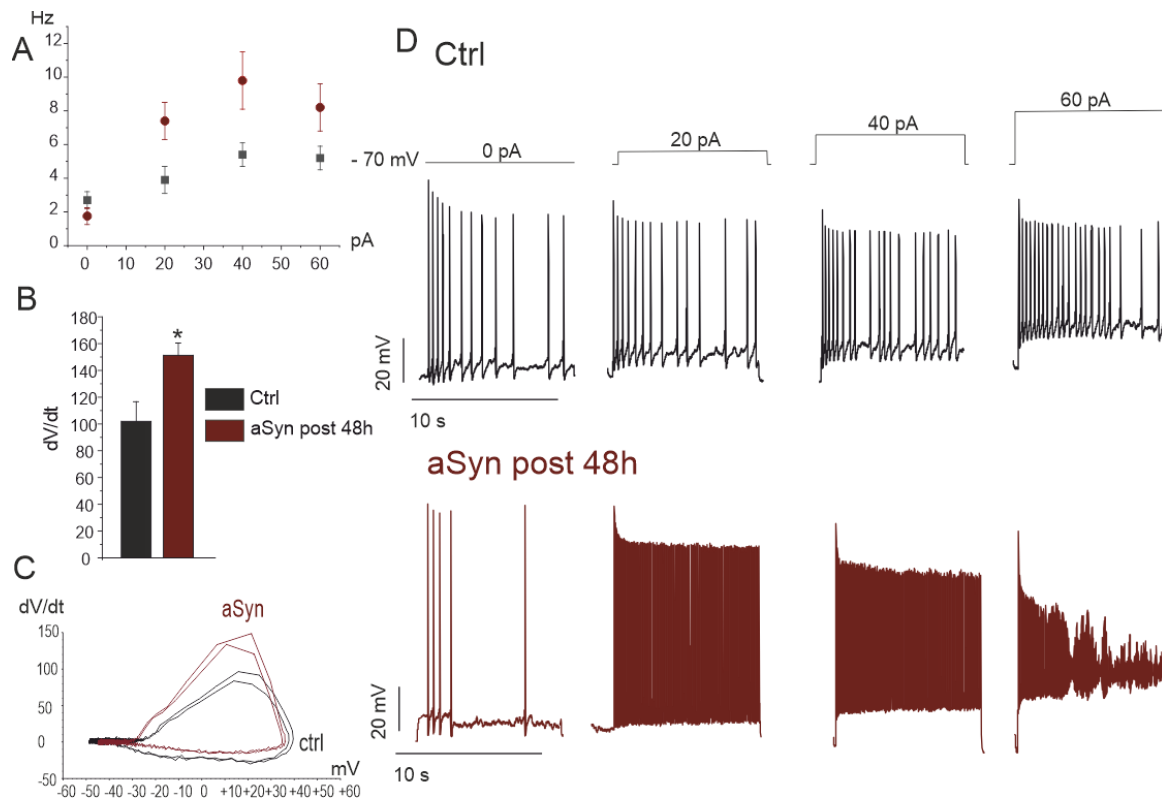


Figure 6 A: Frequency variation vs pulse (0 pA, +20 pA, +40 pA, +60 pA); B: Barr plot of derivative of voltage over time in control condition (black) and after aSyn post 48h (red); C: phase plane plot in control condition (black) and after aSyn post 48h (red); D: representative pulse trace in control condition (black) and after aSyn incubation (red).

4.0 MVIIC restores the firing rate

Cav_{2.2} are targeted to presynaptic nerve terminals where they open in response to incoming action potential [203], [204]. The ensuing entry of calcium ions then triggers the fusion of synaptic vesicles, culminating in the release of neurotransmitters into the synaptic cleft [205].

Recent evidence [206]–[208] suggests that aSyn selectively activates Cav_{2.2} channels, and this activation correlates with increased neurotransmitter release. In particular, it has been observed that *in vivo* microdialysis of aSyn into the striatum, leads a tonic increase of dopamine, this is attributable to aSyn accumulation in the synaptic cleft [206].

I therefore carried out some tests using chronic MVIIC (2 μM), to block Cav_{2.1} and Cav_{2.2} channels. As can be observed in Figure 8, significant difference appears in the firing rate between the control condition and with MVIIC (control condition: 3.07 ± 0.10, MVIIC: 2.83 ± 0.21, p > 0.05). These data confirm that Cav_{2.1} and Cav_{2.2} do not contribute to the spontaneous firing of DA neurons.

Then, I repeated the experiment by incubating with aSyn for 48h, and by administering chronic MVIIC after aSyn incubation. In these conditions, I found that by MVIIC reversed the aSyn-induced effects on the firing rate. The basal firing rate increased the values comparable with those of the control condition (aSyn post 48h + MVIIC: 4.98 ± 0.95 Hz). From these trials, we can therefore conclude the blocking effect of MVIIC could represent a mechanism for restoring the firing activity.

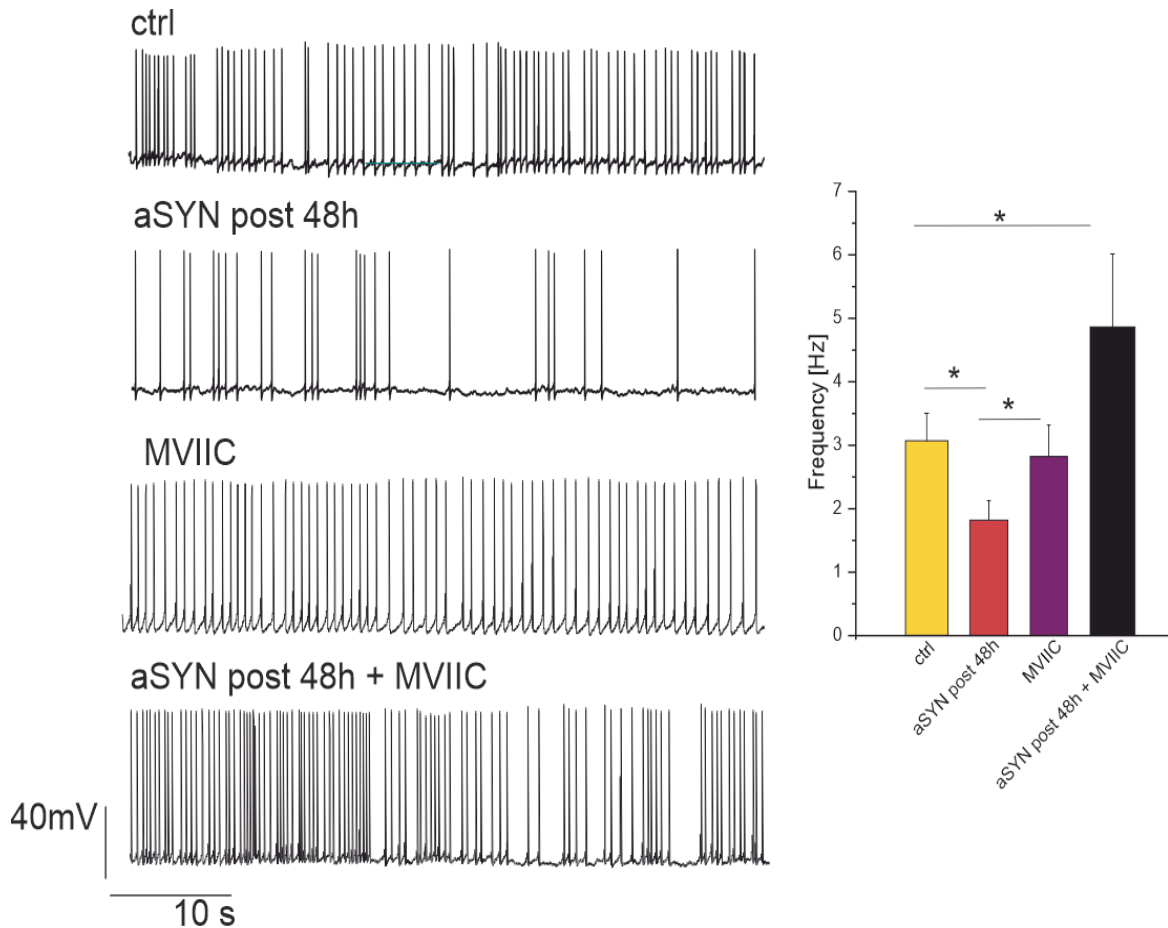


Figure 7 Left: Representative traces and the corresponding histogram of the firing frequency in control condition, aSYN post 48h, MVIIC and aSYN post 48h + MVIIC. Right: relative bar plot histogram.

Chapter 5

Role of calcium channels in sustaining the firing and the Ca^{2+} dependent secretion of midbrain dopaminergic neurons (by means of conventional electrophysiology)

After characterizing through the use of MEA the firing patterns of midbrain neuronal networks, I investigated the electrophysiological properties of single dopaminergic neurons and, in particular, I focused on the contribution of calcium channels in sustaining the spontaneous firing and in regulating the Ca^{2+} -dependent exocytosis.

For these experiments, I used the patch-clamp technique, both in the current-clamp configuration, to measure the action potential firing, and, in the voltage-clamp configuration, to detect the contribution of ion channels and to measure the membrane capacitance increases (ΔC_m).

- *Cav_{1.3}*

It is well known that L-type Ca^{2+} channels, in particular isoform *Cav_{1.3}*, contributes to the autonomous activation of dopaminergic neurons of the *substantia nigra pars compacta* [205], [209]. Besides having a role in the spontaneous firing, it was demonstrated that the activity of *Cav_{1.3}* channels supports the release of dopamine [210], [211]. Infact, DA release is crucial for voluntary movement and it is strictly Ca^{2+} - and electrical activity-dependent. Indeed, the continuous supply of dopamine to the different brain areas, e.g. striatum is guaranteed by an autonomous pacemaking mechanism, which occurs in the absence of normally synaptic input, but it is orchestrated thank to the action of different ion channels. The presence of voltage-dependent L-type Ca^{2+} channels allow calcium entry

with an oscillatory pathway and contribute to the membrane potential threshold [19], [20], [211], [212]. Recent evidence shows that DA itself, upon release, acts in a negative feedback vicious circle in which binding to D₂-receptors inhibits DA neurons electrical activity and further DA release, but both Ca²⁺ influx and receptor desensitization limit this action [28], [136], [211]. Some in vivo studies showed neuroprotection by the systemic administration of dihydropyridine (DHP) L-type channel blockers in 6-OHDA and MPTP animal models of PD thus further supporting a role of LTCCs as potential neuroprotective drug target [213].

In addition to L-type, other types of Cav expressed in SN DA neurons, such as Cav_{2.3} (R-type) [214]–[216] may also contribute to pacemaking activity and to Ca²⁺-induced metabolic stress in SN DA neurons.

- *Cav_{2.3}*

Cav_{2.3} is abundantly expressed in mature SN dopaminergic neurons and contributes to activity-related Ca²⁺ oscillations. Benkert et al. [14], indicated that Cav_{2.3} contributes significantly to Ca²⁺ fluxes and Ca²⁺ currents upon pacemaking in the somata of SN dopaminergic neurons. Currently, it remains also unclear to which extent Cav-mediated Ca²⁺ oscillations [212], [217] in dopaminergic neurons are coupled and amplified by Ca²⁺-induced Ca²⁺ release from intracellular Ca²⁺ stores [218].

However, a lot of evidence support the idea that Ca²⁺ and DA are two critical components in the PD disease, but the complexity of DA metabolism that includes an autoregulatory nature of DA secretion and its relationship with Ca²⁺ channels is still an obscure issue. The development of novel neuroprotective strategies for the treatment of early PD requires the understanding of the cellular mechanisms responsible for the high vulnerability of SN DA neurons. Among these mechanisms elevated metabolic stress appears to play a central role, these neurons must handle a constant intracellular Ca²⁺-load resulting from dendritic and somatic Ca²⁺-oscillations triggered during their continuous electrical activity [219], [220].

In this chapter I have investigated through the patch clamp technique (in current-clamp mode and by means of membrane capacitance increases) the role of Cav_{1.3} and Cav_{2.3} on the firing and secretion of midbrain dopaminergic neurons. All of the experiments discussed below were done after blocking both inhibitory and excitatory synapses.

1.0 Role of Cav_{1.3} in sustaining the spontaneous firing activity of midbrain dopaminergic neurons.

I performed these experiments to validate the role of Cav_{1.3} channels in dopaminergic neurons. To this purpose, I have used the selective blocker isradipine at a concentration of 3 μ M [220], [221]. As it is possible to observe in figure 1, after isradipine administration, the firing rate is significantly reduced from 2.03 ± 0.67 Hz (control, n = 8) to 0.36 ± 0.09 Hz (isradipine, n = 8) ($p < 0.05$, paired Student's t-test). Isradipine does not only reduces the firing rate, but also significantly modifies the AP waveform. In particular, I found a reduced mean AP half-width (control: 7.1 ± 0.1 ms, isradipine: 4.9 ± 0.3 ms, $p < 0.05$, paired Student's t-test), and a more hyperpolarized resting membrane potential ($V_{resting}$) (control: -41.6 ± 1.8 mV, isradipine: -44.3 ± 3.2 ms, $p < 0.05$, paired Student's t-test).

Thus, from these experiments I can conclude that, in culture dopaminergic neurons, isradipine significantly decreases the spontaneous firing frequency, and that this reduction is associated with a more sustained hyperpolarization, confirming the fundamental role of L-type calcium channels in our experimental model. My data confirm most of the experimental evidence that have been performed on SN slices [213], [222]–[224].

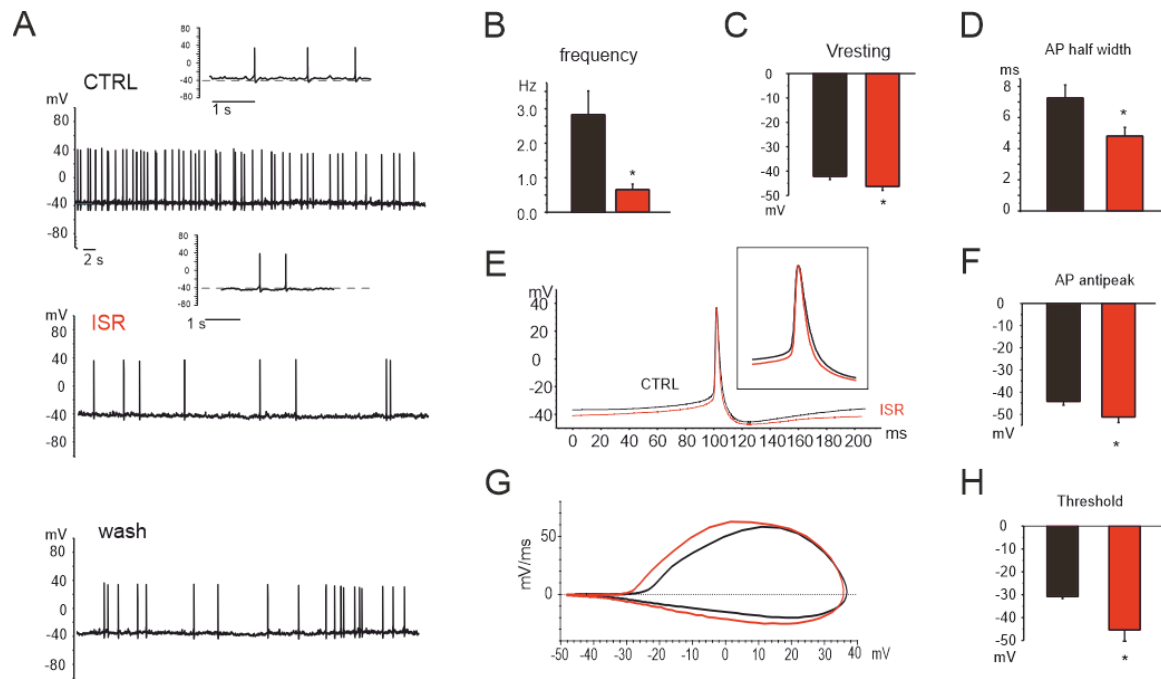


Figure 1. Isradipine effects on pacemaking of cultured mouse midbrain DA neurons. A. Representative recordings of spontaneous firing activity of cultured midbrain dopaminergic neurons before, during and after the application (wash-out) of 3 μM isradipine. B: Firing frequency [Hz], C: Vresting, D: AP antipeak [mV], F: AP half width [ms] and H: threshold [mV] before (control) and during the application of 3 μM isradipine. Statistical significance was determined using paired Student's t-test.: * $p < 0.05$. E-G: Phase-plane plot analysis (time derivative of voltage (dV/dt) vs. voltage (V)) before (control) and during the application of 3 μM isradipine. Inset: overlay of one single AP before (control) and during the application of 3 μM isradipine.

2.0 Role of Cav_{2.3} sustaining the firing activity of midbrain dopaminergic neurons: SNX-482 inhibits Ca²⁺ current (I_{Ca}) and reduces spontaneous AP firing (Siller et al. e-life 2021, peer review e-Life)

Recently it has been shown that in SN DA neurons Cav_{2.3} channels contribute to action potential (AP)-induced somatic Ca²⁺-oscillations. This continuous Ca²⁺ load can potentially contribute to the high vulnerability of these neurons in PD [14]. To investigate the role of Cav_{2.3} on firing frequency and AP shape in spontaneously firing neurons, I have used the selective blocker SNX-482. We employed SNX-482 at a low concentration (100 nM) to inhibit Cav_{2.3} current components (IC₅₀=30 nM) but spare L-type channels (IC₅₀>1 μM , [14], [245]).

In Figure 2 A,B it is possible to observe that, in current-clamp recordings, the spontaneous firing frequency is significantly reduced, from 4.1 ± 0.8 Hz (control, n=10) to 1.1 ± 0.2 Hz (SNX-482, n=10, $p = 0.0036$, paired Student's t-test). Another effect is the decreased

regularity of pacemaking: this was evaluated by measuring the coefficient of variation (CV) of the mean interspike interval. The CV increased from 0.25 ± 0.06 (control) to 0.78 ± 0.13 (SNX-482, $p = 0.0032$, paired Student's t-test; figure 2B). Slowing down of the firing was associated with hyperpolarization of the most negative voltage reached during the after hyperpolarization immediately after the spike (AHP peak), which decreased from -43.2 ± 1.3 mV (control) to -47.0 ± 1.2 mV (SNX-482, $p = 0.0005$, paired Student's t-test; figure 2B).

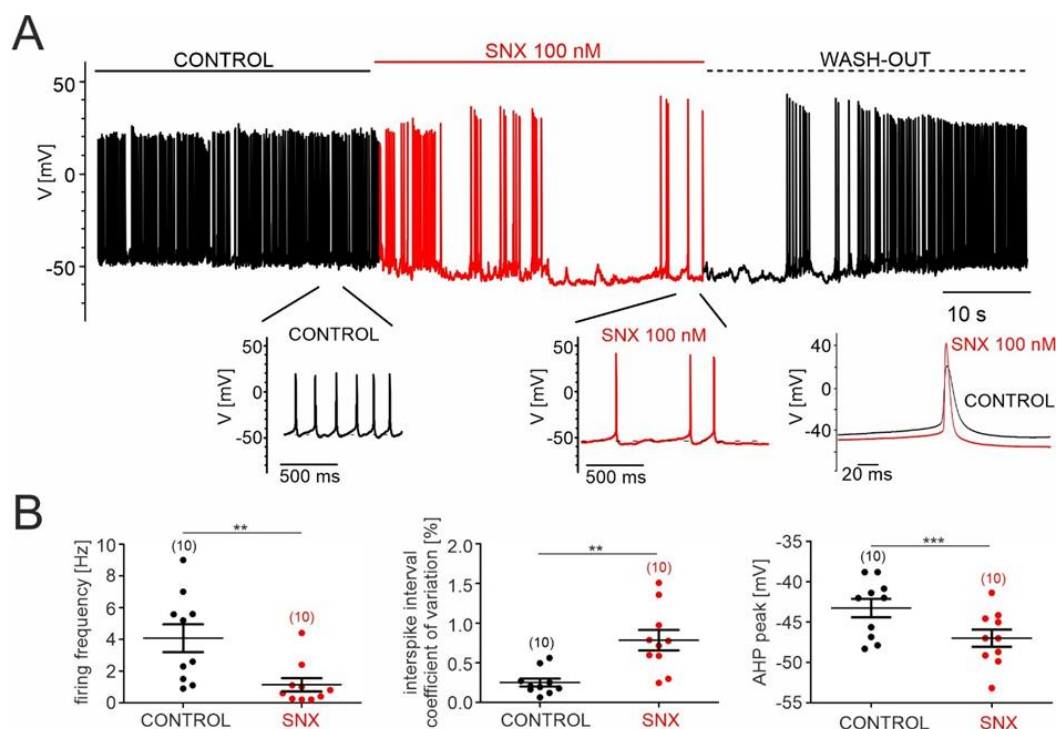


Figure 2. SNX-482 effects on pacemaking of cultured mouse midbrain DA neurons. A. Representative recording of spontaneous firing activity of cultured midbrain dopaminergic neurons before, during and after the application (wash-out) of 100 nM SNX-482. Inset (bottom right): overlay of one single AP before (control) and during the application of 100 nM SNX-482. B. Firing frequency [Hz], coefficient of variation of the interspike interval [%], and AHP peak [mV] before (control) and during the application of 100 nM SNX-482. Statistical significance was determined using paired Student's t-test.: *** $p < 0.001$; ** $p < 0.01$; * $p < 0.05$.

Other changes in the AP waveform, which are related with the slowing of AP frequency or result from inhibition of Cav_{2.3} channels, were also noted: a reduced mean AP half-width (control: 5.1 ± 0.3 ms, SNX-482: 4.2 ± 0.3 ms, p = 0.005, paired Student's t-test), and a trend towards increased maximum time-derivative of voltage (control: 45.3 ± 4.9 mV/ms, SNX-482: 74.3 ± 13.5 mV/ms p = 0.0625, paired Student's t-test, estimated from the phase-plane plot of Figure 3C). The latter is likely due to the recruitment of more voltage-gated Na⁺-channels during the AP onset from the more hyperpolarized interspike membrane potential [9].

It is possible to note that isradipine reduces the firing rate by 82%, while SNX-482 by 70%, and that both drugs produce a significant hyperpolarization. Thus we can deduce that the Cav_{1.3} channel is certainly more involved in the firing of these neurons, even though a significant contribution of Cav_{2.3} channels cannot be ruled out.

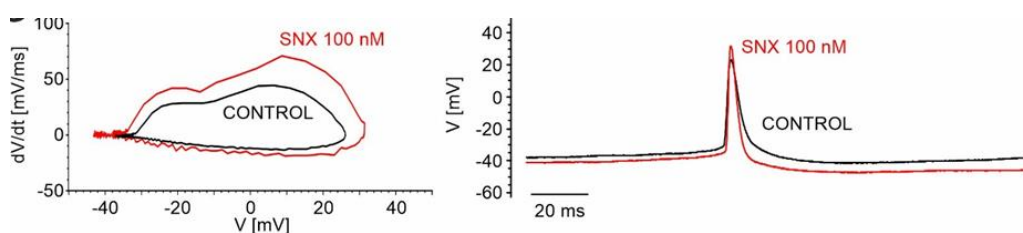


Figure 3C. Left panel: Phase-plane plot analysis (time derivative of voltage (dV/dt) vs. voltage (V)) before (control) and during the application of 100 nM SNX-482. Right panel: corresponding AP trace in control and in the presence of SNX-482.

I also isolated SNX-482-sensitive Cav_{2.3} currents in cultured DA midbrain neurons under the voltage-clamp experiments. Ca²⁺-currents were elicited by consecutive depolarizing 50 ms square pulses to 0 mV from a holding potential of -70 mV every 10 s. Once stable recordings were obtained in the presence of isradipine (see representative experiments in Figure 4A, B), 100 nM of SNX-482 were applied. Addition of 100 nM SNX-482 significantly reduced non-L-type currents by 41 ± 4 % (paired Student's t-test; p<0.001) (figure 4C) corresponding to an absolute decrease of current amplitude from 529 ± 57 pA to 313 ± 33 pA (n = 20, p<0.01, paired Students t-test) (figure 4D). All residual I_{Ca} components were blocked by adding 500 μM Cd²⁺ to the bath solution (figure 4A, B).

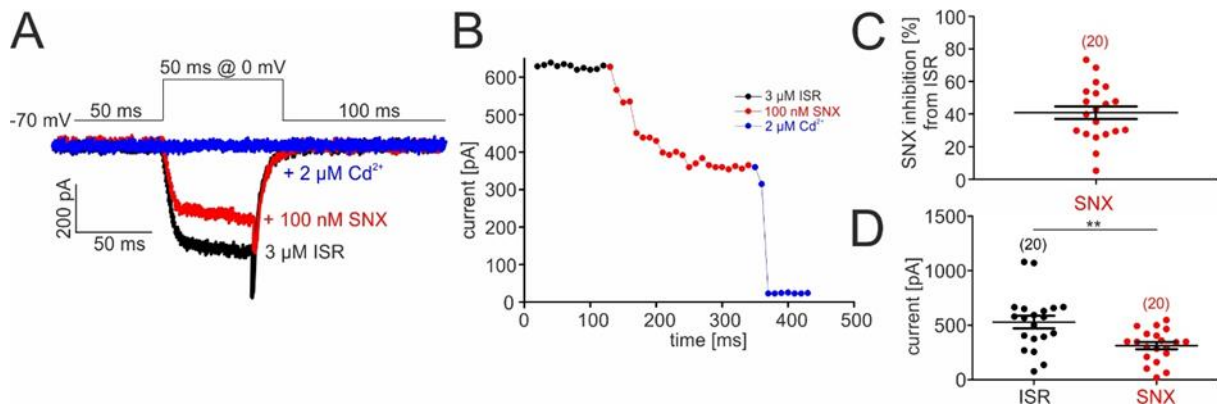


Figure 4. SNX-482 inhibition of non-L-type I_{Ca} in cultured midbrain DA neurons. A. Representative traces illustrating the inhibition of non-L-type I_{Ca} by 100 nM SNX-482 (red). Cells were initially perfused with a bath solution containing 3 μ M ISRADIPINE (ISR, black). Full block was obtained using 500 μ M Cd^{2+} (blue). Square pulses (50 ms) were applied to 0 mV from a holding potential -70 mV (top) B. Current amplitude values plotted as a function of time. After stabilization of I_{Ca} with ISR (black circles), 100 nM SNX-482 was applied. The remaining currents was blocked by 500 μ M Cd^{2+} C. SNX-482 inhibition expressed as % of control I_{Ca} after LTCC block using 3 μ M ISR. D. Mean current amplitude at the end of ISR application and at the end of SNX-482 application. Statistical significance was determined using paired Student's t-test: *** $p < 0.001$; ** $p < 0.01$; * $p < 0.05$.

Nevertheless, our experiments clearly demonstrate that $Cav_{2.3}$ channels contribute to total Ca^{2+} -current and can support pacemaking in cultured mouse DA neurons. This finding requires that $Cav_{2.3}$ channels must be continuously available throughout the average interspike membrane potentials of these cells (between -70 to -40 mV).

3.0 Ca^{2+} channels contribution to the Ca^{2+} -dependent secretion in midbrain DA neurons.

After characterizing the role of $Cav_{1.3}$ and $Cav_{2.3}$ channels in firing, I investigated their role on the Ca^{2+} -dependent secretion [225], [226]. The measurements were performed by means of the patch-clamp technique, which allows to measure the capacitance increases following depolarization-evoked Ca^{2+} influx. The membrane capacitance, which reflects the surface area of the plasma membrane, increases during an exocytotic process by fusion of secretory granules with the plasma membrane [136] (see chapter 2). Exocytosis was estimated by the membrane-capacitance increment (ΔC) evoked by the depolarizing step according to the Lindau-Neher technique [138] implemented as the "sine + dc" feature of the PATCHMASTER lock-in module. A sinusoidal wave function (1 kHz, ± 25 mV amplitude) was superimposed on the holding potential, for more information see material and methods (chapter 2).

I measured respectively the effect of isradipine (3 μ M, Cav_{1.3} blocker), SNX-482 (100 nM, Cav_{2.3} blocker) and MVIIC (2 μ M, Cav_{2.1} and Cav_{2.2} blocker) on the quantity of charge and the capacitance increase. Results are shown in Figure 5. The greatest contribution to the overall quantity of charge is given by the Cav_{1.3}, even though also Cav_{2.3}, Cav_{2.1} and Cav_{2.2} contribute as well. For what concerns the depolarization-evoked secretion, ΔC , this changes from 91.47 ± 36.01 fF in control condition to 18.40 ± 7.66 fF with *isradipine*, 46.53 ± 7.36 fF with SNX and 39.80 ± 6.28 fF with MVIIC. Thus, using selective blockers for the Cav_{1.3}, Cav_{2.3}, Cav_{2.1} and Cav_{2.2}, I observed that the Cav_{1.3} maximally contribute to secretion, but the Cav_{2.3}, Cav_{2.1} and Cav_{2.2} also appear to play a significant role. Quantity of Ca²⁺ charge and corresponding secretion (ΔC) increases proportionally each other.

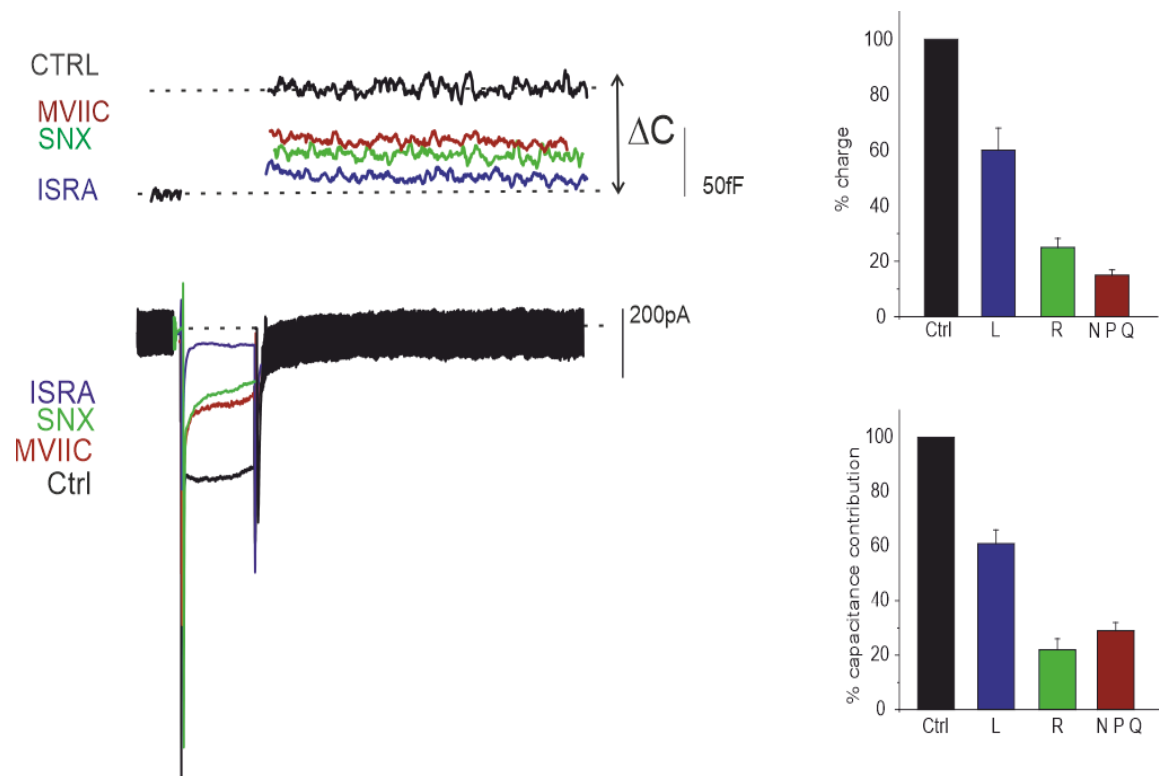


Figure 5 (Left) depolarization-evoked membrane capacitance increases in control condition and in the presence of isradipine, SNX and MVIIC and (below) the corresponding depolarization-evoked Ca²⁺ current traces. (Right) Percentage variations of the mean quantal charge and membrane capacitance increase in the different experimental conditions.

Now, I focused on L-DOPA effects on firing and subsequently on the study of the relative dopaminergic receptors. Also in this case the measurement was carried out using the patch-clamp technique which allows a specific measurement on a single dopaminergic cell, and with conventional MEAs and μ G-SCD-MEA. The measurement with conventional

MEAs was carried out in order to confirm the correct functioning also at the potentiometric level of the diamond prototypes.

Chapter 6

New approaches for investigating multisite detection of DA release and cell firing (diamond-based multiarray prototypes)

1.0 L-DOPA potentiates the stimulus-dependent exocytosis and down-regulates the spontaneous firing activity

In the previous chapter I showed the importance that the calcium channels Cav_{1.3} and Cav_{2.3} have both in firing and secretion, defining the possible neuroprotective role that their antagonists (isradipine and SNX-482) may have in Parkinson's disease. In this chapter I focused on the role of L-DOPA and relative dopaminergic receptors.

My goal is to characterize the role of L-DOPA both in the firing and in the secretion, using different techniques. Currently these two mechanisms are studied separately, as there is no single device that simultaneously allows recording both firing and secretion. In this chapter I demonstrate that cellular sensors based on embedded graphitic micro-channels in diamond substrates (μ G-SCD-MEAs) can be successfully applied for the investigation of both types of cellular signal mechanisms. The final goal is realizing a single device that it will allow to record both in amperometry and potentiometry simultaneously. For this purpose, in these years I have been working in collaboration with: the physics department (UNITO) and the electronics department of Uhm, on the development of a device that allows to perform amperometric and potentiometric measurements at the same time.

To validate the μ G-SCD-MEAs in the secretion I started using a simple neurosecretion model: the PC12 dopaminergic cell model. Having defined the correct functioning of the sensor, I replicated the measurement using the dopaminergic neurons of the midbrain. In the same way I validated the diamond prototype for potentiometry by carrying out

parallel measurements between the two devices and confirming a uniformity in the results both from conventional MEAs and from μ G-SCD-MEAs.

The strong interest of L-DOPA arises because, unlike dopamine, crosses the blood-brain barrier. Once it reaches the dopaminergic neurons it is internalized and converted into dopamine, for this reason L-DOPA plays a fundamental role in Parkinson's disease therapy. L-DOPA in fact thanks to an amino acid transport system, is able to enter the SNC and once here it is metabolized into dopamine, using the enzyme DOPA decarboxylase. The clinical assumption of the use of L-DOPA starts from the observation of a dopamine deficiency in the substantia nigra, and since the administration of this is not useful, L-DOPA is used to restore dopamine levels in this area.

Though, L-DOPA does not represent a valid pharmacological alternative. Complications of a motor and non-motor nature occur in the evolution of the disease. Reduced response to levodopa (or L-DOPA) exposes the motor neuronal circuit to complications. It has been observed, in fact, that after about 5 years of treatment with L-DOPA, motor fluctuations (on-off phenomenon) and dyskinesias (involuntary movements other than tremors) arise. Late motor complications are included in the term "*long-term levodopa treatment syndrome*" and, as we have seen, depend on the duration of exposure and the daily dosage of L-DOPA [227]–[229].

The pathogenesis of the disease has not yet been delineated with certainty. Several hypotheses have been advanced:

- hypersensitivity of dopamine receptors (in particular dopaminergic D₂ receptors) due to the long-term blocking of the neuroleptic drug. This generates an exaggerated response to endogenous dopamine at the level of the extrapyramidal circuits (most accredited hypothesis). To control this effect, *benserazide* (decarboxylase inhibitor) is also administered together with L-DOPA;
- Neuronal damage from the pro-oxidant effect of these drugs (the intake of antioxidants such as vitamins or melatonin seems to decrease the possibility of developing the syndrome);
- Damage to the GABAergic pathways (this derives from the observation that benzodiazepines relieve symptoms) [230], [231].

From all these observations it is easy to understand that L-DOPA and dopaminergic receptors play a very important role in Parkinson's disease and understanding its physiology could be of great help in defining much more targeted therapies.

Not only that, L-DOPA plays a dual role in firing and secretion, which has not yet been fully gutted and understood. It was observed that L-DOPA decreased the firing frequency in the zona of *substantia nigra pars compacta* and *ventral tegmental areas* [9], [11], [28], while, on the contrary, increased the quantal size [232]. The concomitance of these two opposite effects has not yet been fully clarified.

Another important task in this characterization is the relationship of L-DOPA and DA receptor; dopamine receptors are G-protein coupled metabotropic receptors, these are divided into two groups: D₁-like and D₂-like [28], [233], [234]. These two groups have different actions when activated by DA. The activation of D₁-like receptors leads to the activation of adenylate cyclase, as they are coupled to stimulatory G_s proteins. The activity of adenylate cyclase involves the synthesis of the second messenger cAMP. On the contrary, D₂-like receptors are coupled to inhibitory G_i proteins. The activation of these receptors by dopamine and other agonists leads to the inhibition of adenylate cyclase and therefore to a decrease in the second messenger cAMP [235], [236].

2.0 The μ G-SCD-MEAs: compact and versatile device that allows the measurement of secretion from 16 electrodes

The historical technique conventionally used for the measurement of secretion is the carbon electrode [237]–[241]. This technique, however, has several disadvantages: it requires a fixed setup with an amplifier, it allows the measurement of one cell at a time, it is rather complex and expensive. In this context it was decided to develop a multi-electrode that would allow for compact and portable electronics and a less expensive, more versatile chip that would allow the simultaneous measurement of several cells from different electrodes. In collaboration with UNITO physic department we have therefore developed a diamond matrix device (μ G-SCD-MEAs). Diamond was chosen as it is transparent, biocompatible and chemically inert material, in which it is possible to create

conductive graphite tracks that allow the measurement of oxidizable molecules (for more information see chapter 2).

3.0 Dopamine detection in the PC12 dopaminergic cells by means of μ G-SCD-MEAs (Tomagra et al., *Biophysical chemistry* 2019 [157])

To validate the performance of μ G-SCD-MEAs prototypes, initially I used the dopaminergic PC12 cell line. The major advantage of performing real-time measurement using multi-arrays is to simultaneously measure the secretion from multiple cells. In these experiments μ G-SCD-MEAs have been used in the amperometric configuration (see material and methods) for monitoring DA release from many cells simultaneously.

PC12 cells are conventionally used as model for neurosecretion [242]. PC12 vesicles store dopamine and also limited amount of norepinephrine; this characteristic makes PC12 one of the best models to study the effects of L-DOPA on secretion using and testing μ G-SCD-MEAs [157].

In Figure 1A it is possible to observe a typical recording of amperometric spikes using the μ G-SCD-MEA. The secretory activity of several PC12 cells was stimulated by external KCl (30 mM) and recorded by 13 out of the 16 electrodes, allowing to collect a significant number of events in few recordings (i.e. $n \cong 1500$ events/device/trial).

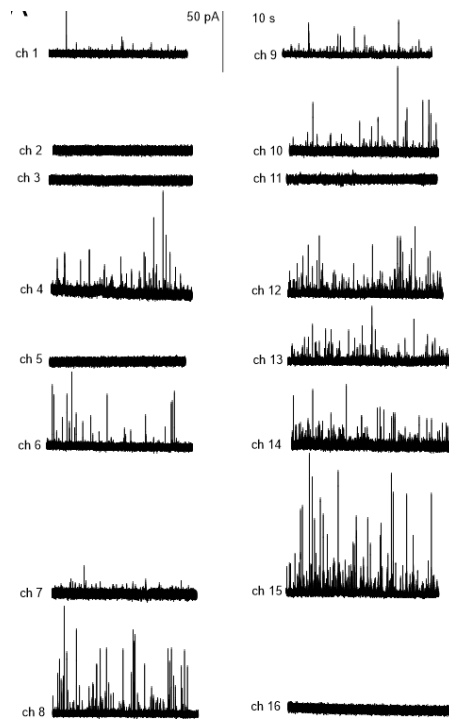


Figure 1. Amperometric recordings from 16 different electrodes.

After recording under control conditions (external stimulation with 30 mM KCl), PC12 cells are incubated for 1h with L-DOPA (20 μ M), to increase the dopamine content [243]. The effect of the treatment with L-DOPA is shown for a representative electrode in Figure 2B. I found that the frequency of amperometric spikes generation is not affected by L-DOPA [232] (0.60 ± 0.16 Hz in control condition and 0.56 ± 0.12 Hz after L-DOPA incubation, $p > 0.1$), and that the Ca^{2+} channel blocker CdCl_2 (500 μ M), completely suppressed the exocytotic response. On the contrary, L-DOPA caused a significant increase in the number of secreted molecules (250% with respect to control, $p < 0.05$). The mean values of the spike charge (Q) increased from 0.143 ± 0.002 pC (control) to 0.320 ± 0.010 pC (L-DOPA) ($p < 0.05$). Similarly, concerning the kinetic spike parameters, that the $t_{1/2}$ is increased by over 120% with respect to control condition, i.e. from 2.79 ± 0.03 ms to 6.01 ± 0.18 ms ($p < .05$). These findings are in good agreement with those reported by Pothos et al. [232]. In the cited work, 1 h incubation with 50 μ M of L-DOPA potentiated by 250% the quantal release; in our case, we have incubated PC12 cells for 1 h at 20 μ M and we have obtained an increment of 120%.

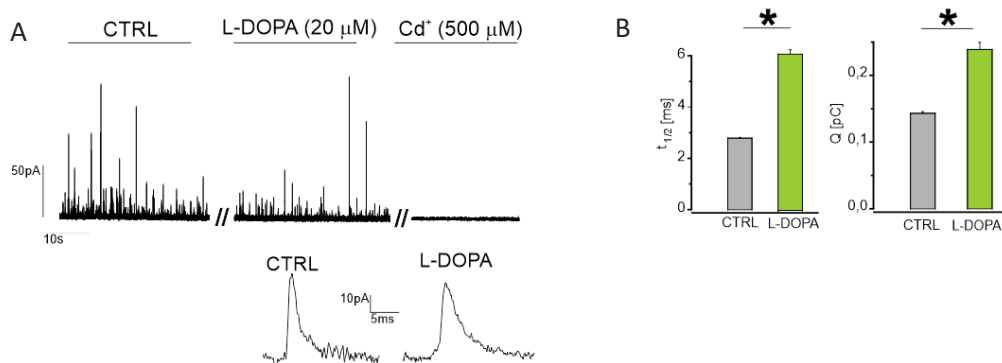


Figure 2 A. A representative trace in control condition, after incubation with L-DOPA for 30 min and in the presence of CdCl₂ (500 μM). Inset: magnification of two amperometric spikes, in control conditions and following L-DOPA incubation. B. Histograms of half-height width and relative charge in control and after incubation with L-DOPA.

The reason for this change in the shape of the spikes is rather complex, nonetheless some hypotheses can be advanced. Sombers et al. [244] hypothesized that L-DOPA favours multiple pre-fusion events (i.e. fusion between two or more vesicles before exocytosis). Alternatively, Colliver et al. [245] from TEM images observed that after incubation with L-DOPA there is a significant increase in the diameter and volume of the vesicles, these pharmacological studies demonstrated that this increase is mediated by the vesicular monoamine transporter (VMAT).

If we plot the histogram of the vesicular content (Q or molecules), what we get is an asymmetric (non-Gaussian) distribution. The most feasible explanation for this distribution is that the vesicles have a range of radii with a relatively uniform concentration of catecholamines [149]. Therefore, if the cube root of the vesicular content ($Q^{1/3}$ or $\text{mole}^{1/3}$) is used for the generation of the histograms, a normal (Gaussian) distribution is obtained.

For this reason, I plotted the distribution of the vesicles radii derives from molecule^{1/3} values using the Faraday law assuming spherical shape of the vesicles:

$$N = \frac{Q}{nF}$$

Where n is the number of electrons transferred in the redox reaction (n = 1 or 2 for oxidation of catecholamines), N is the number of neurotransmitter molecules detected, and F is the Faraday constant (96 485 C mol⁻¹). The total charge (Q) can be calculated by integrating the current versus time for each recorded amperometric peak [246].

The cube root of the quantal size before and after L-DOPA is normally distributed (Figure 3), as confirmed from the determination coefficient calculated from the fit ($R_{CTRL} = 0.99$; $R_{L-DOPA} = 0,96$). The entire population of quanta after L-DOPA treatment is significantly shifted to larger values with respect to control ($p < 0.05$, KS test = 0.79). The corresponding cumulative distribution is shown in Figure 3, where it is evident that the distribution with L-DOPA is shifted by 17% toward higher values with respect to control (peak $max_{CTRL} = 71.9 \pm 0.3$ pA, peak $max_{L-DOPA} = 84.2 \pm 0.7$ pA) [150], [247]. These results, using the μ G-SCD-MEA, confirm that incubating with L-DOPA increases the quantal size.

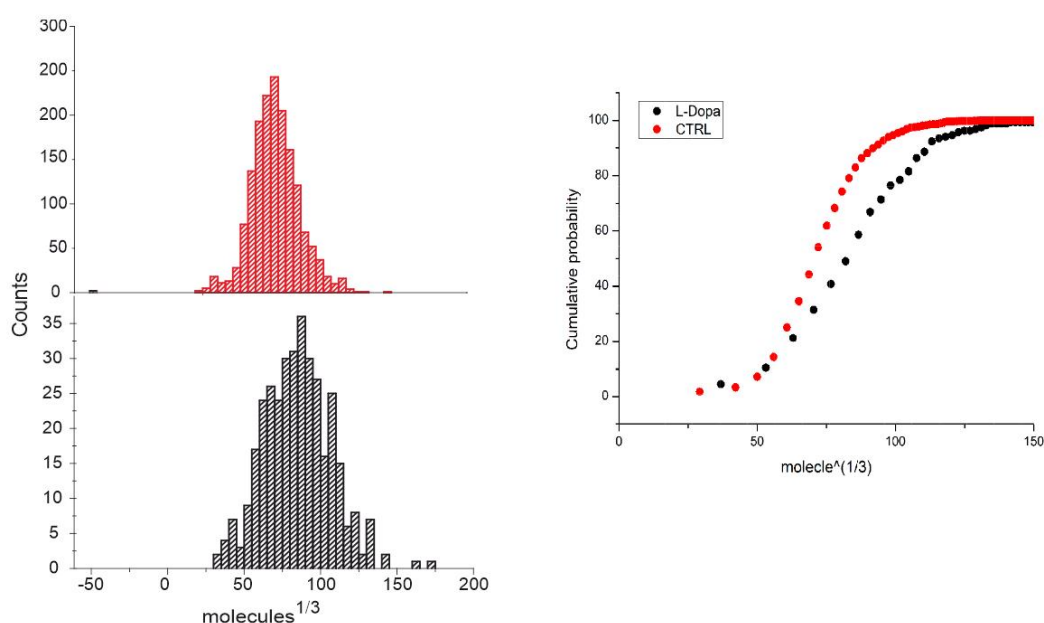


Figure 3 left: probability distribution of the $molecules^{1/3}$, in control (red) and with L-DOPA (black). The $molecules^{1/3}$ distribution with L-DOPA is shifted to the right, toward values greater than control. right: cumulative probability of the $molecule^{1/3}$, in control and after incubation with L-DOPA.

4.0 Detection of quantal DA release from dopaminergic neurons using μ G-SCD-MEAs (Tomagra et al., *Frontiers in Neuroscience* 2019 [9])

Having defined the correct functioning of the diamond prototypes using PC12 cells, I studied the effect of L-DOPA on the culture of dopaminergic neurons of the midbrain [9]. DA release from cultured midbrain neurons can either occur at the somato-dendritic or the axon-terminal level [57]. Quantal exocytotic events are detected after 10 DIV.

Unstimulated (i.e., spontaneous) release was barely detectable (5% of trials) and occurred at low frequency (0.11 ± 0.07 Hz) in 2 mM CaCl_2 (figure 4A).

Amperometric spikes were characterized by a mean maximum current amplitude (I_{max}) of 10.1 ± 1.0 pA and a half-time width ($t_{1/2}$) of 0.31 ± 0.01 ms ($n = 5$). After L-DOPA (20 μM) incubation (1h) it is possible to observe a significant increase in these parameters: I_{max} was 30 ± 1.9 pA and $t_{1/2}$ was 0.36 ± 0.02 ms ($n = 5$) ($p < 0.5$). Stimulation with KCl after L-DOPA administration does not modify any spike parameter, but significantly increases the frequency: 0.35 ± 0.14 Hz (L-DOPA) respect 0.90 ± 0.35 (L-DOPA+ KCl) Hz ($p < 0.05$).

Therefore, it is possible to state that both in the control condition and after incubating with L-DOPA, by stimulating with KCl the release frequency increases significantly (see Figure 4).

On the contrary, 500 μM CdCl_2 suppressed Ca^{2+} -dependent exocytosis through voltage-gated Ca^{2+} channels, as shown in figure 4. No events were detected when the recording electrodes were polarized to 0 mV to nullify dopamine detection.

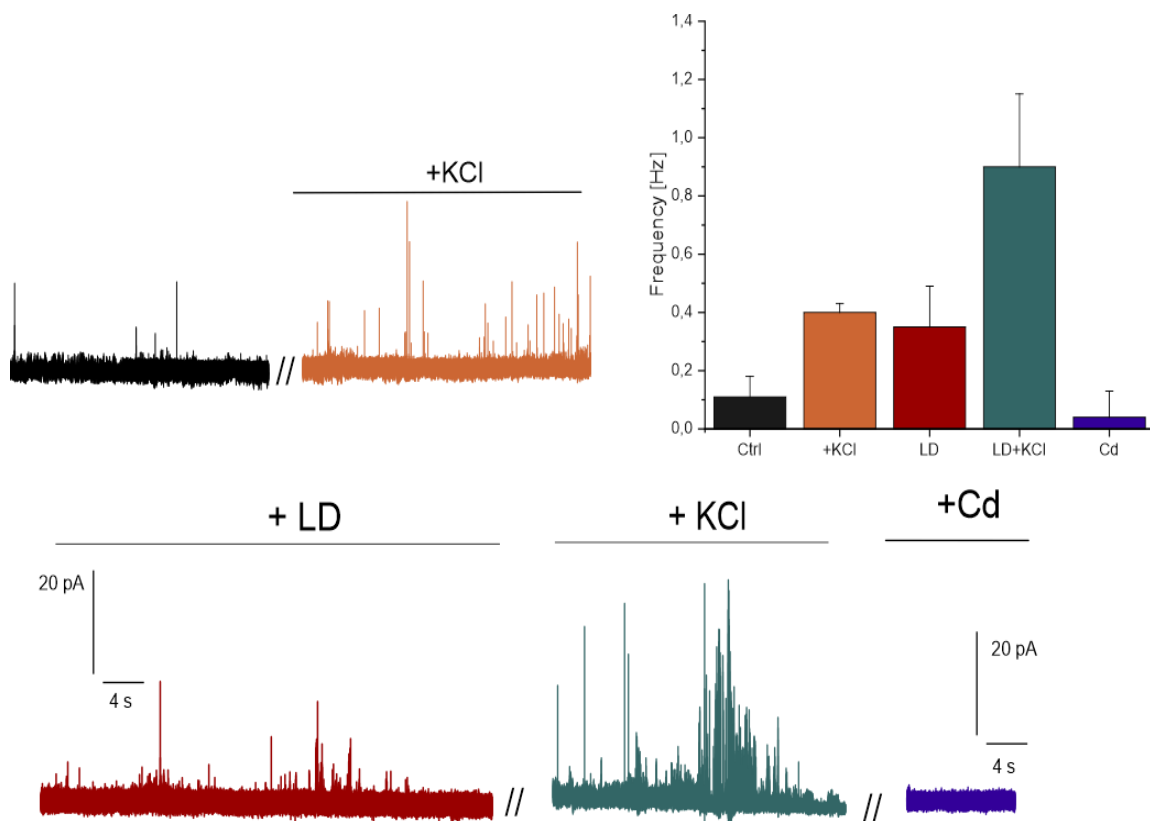


Figure 4 Detection of quantal dopamine release by $\mu\text{G-SCD-MEAs}$. Representative recordings from one channel of $\mu\text{G-SCD-MEAs}$ (4×4). DA release occurred spontaneously

in 2 mM CaCl₂; following stimulation with 30 mM KCl, the frequency of release increased without significantly altering spike parameters (see text for details). DA release occurred after LD incubation for 1h, following stimulation with 30 mM KCl the frequency increase significantly and it is suppressed with Cd. Relative histograms of frequency.

5.0 L-DOPA-induced modulation of firing dopaminergic neurons and role of D₂-autoreceptors (Tomagra et al., *Frontiers in Neuroscience* 2019)

In order to investigate the role of Dopamine in the regulation of DA neuron firing, I studied the modulation of dopaminergic neurons by perfusing L-DOPA and subsequently the modulation of the dopaminergic receptors D₂, using the relative antagonists sulpiride. For these measurements I combined classical electrophysiological approaches (current-clamp) together with multielectrode: conventional MEA (Multi Electrode Array) and μ G-SCD-MEAs. I used both conventional MEAs and μ G-SCD-MEAs to also validate the potentiometric measurement of these diamond prototypes. All these measurements made using conventional techniques and the diamond prototypes were done in order to achieve the double measurement simultaneously.

6.0 D₂-autoreceptor induced inhibition after L-DOPA administration in Current-Clamp Recordings

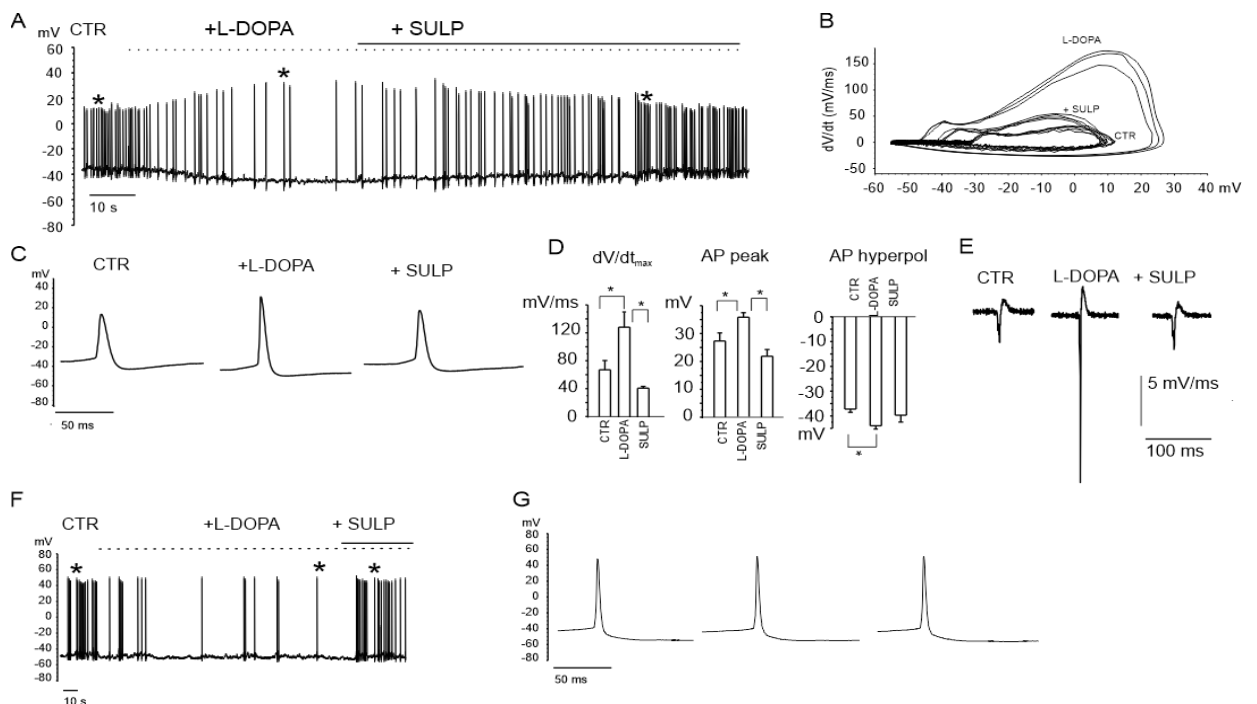


Figure 5. Current-clamp recordings exhibiting the features of L-DOPA induced modulation of neuronal firing. (A) Repetitive firing activity is inhibited by L-DOPA (20 μ M) and restored by blocking the D₂ autoreceptors. Firing inhibition is accompanied by a membrane hyperpolarization and increased peak amplitude. (B) Phase-plane plot analysis of the action potential shown in (A). (C) Signals identified by the asterisk in (A) are shown through an enlarge scale. (D) The following parameters have been calculated from the phase-plot analysis: maximum dV/dt versus V , action potential (AP) peak amplitude, AP hyperpolarization peak. Data are expressed as mean values. Statistical difference ($p < 0.05$) is indicated on the bar histogram. (E) Negative first derivative of signals reported in (C). (F) Example of firing inhibited by L-DOPA without significant alterations in the AP peak amplitude, shown in (G) on an enlarged scale. Image from [9].

The firing of nigral dopaminergic neurons is down-regulated by DA release through a D₂-autoreceptor mediated pathway [248], [249]. Preliminary experiments were performed in whole-cell current clamp configuration, by applying the L-DOPA (20 μ M). Recordings were selectively performed on 11 DIV dopaminergic neurons that were identified by means of GFP staining. Although the responses to applied L-DOPA varied, it caused a $70 \pm 4\%$ reduction of the firing frequency in 80% of cases ($n = 20$ cells, from 1.36 ± 0.02 to 0.41 ± 0.11 Hz; Figures 5 A, F). Maximum inhibition occurred within 2–5 min of L-DOPA perfusion, and was reversed some minutes after the application of the D₂ antagonist sulpiride (10 μ M). The repetitive firing frequency measured in the presence of the D₂ antagonist recovered to 1.2 ± 0.2 Hz, thus confirming the autocrine inhibition that is induced by released DA [250]. It is worth mentioning that the reduced firing frequency was associated, in 70% of the cases, to a membrane hyperpolarization of -7.8 ± 1.1 μ V and by a sharp increase in AP peak amplitude (from 27 ± 3 to 36 ± 2 μ V; $n = 14$, $p < 0.05$; Figures 5 C, D). All this was most likely induced by the DA mediated activation of a G-protein-coupled potassium channel (GIRK) [29]. Both effects were reversed after perfusion with sulpiride.

In the remaining 30% of neurons, the nearly threefold reduction of firing frequency occurred without causing either the significant hyperpolarization of the membrane potential, or alterations in the AP waveform (Figures 5 F, G). For this subset of neurons, in some cases sulpiride restored the control firing frequency, even though the recovery was not always complete. This variability reveals the probable existence of distinct modulatory pathways that may originate from different midbrain neuron subpopulations [251].

Phase plane plot analysis was performed in order to gain further insights into the APs properties and their modulation by L-DOPA [252], [253]. By plotting the time derivative of voltage versus time (dV/dt), parameters such as the AP threshold can be easily inferred from the voltage value at which dV/dt suddenly increases. The phase plane plots in Figure 5B are referred to the same APs that are indicated by the asterisks in Figure 5A. From the plot we found that: (i) the maximum derivative (dV/dt_{max}), which is associated with the maximum current density through voltage gated Nav channels, was drastically enhanced by L-DOPA (from 67 to 129 $mV\ ms^{-1}$, $p < 0.05$, Figure 5D), suggesting a sustained recruitment of Nav channels [254]; (ii) the AP hyperpolarization peak was significantly augmented by L-DOPA, from -37.2 ± 1.3 to -40 ± 2 mV ($p < 0.05$, Figure 5D); (iii) the AP threshold, measured from the phase-plane plot when an abrupt change in dV/dt was observed (at 4.5 ± 1.2 $mV\ ms^{-1}$ for control and 6.4 ± 0.9 $mV\ ms^{-1}$ for L-DOPA-treated neurons), decreased from -25.3 ± 1.8 to -31.9 ± 1.8 mV ($p < 0.05$), respectively. This again confirms a potentiated recruitment of Nav channels during L-DOPA treatment.

In order to compare the AP waveform recorded intracellularly with those recorded extracellularly, the negative first derivative of AP traces shown in Figure 5C is reported in Figure 5E.

They correspond to the AP shape recorded extracellularly by the MEAs [255] and identified as a biphasic AP waveform, it is characterized by a large negative peak and a small positive antipeak component can be distinguished. Finally, a range of different effects on neuronal activity were detected in the neurons that were not inhibited by L-DOPA (20% of neurons). L-DOPA accelerated repetitive firing by $80 \pm 20\%$ (17% of neurons), while it was ineffective in the remaining ones (3% of neurons).

7.0 Dopamine-induced modulation of neuronal firing observed through μ G-SCD-MEAs and conventional MEAs: role of D_2 receptor (Tomagra et al., *Frontiers in Neuroscience* 2019)

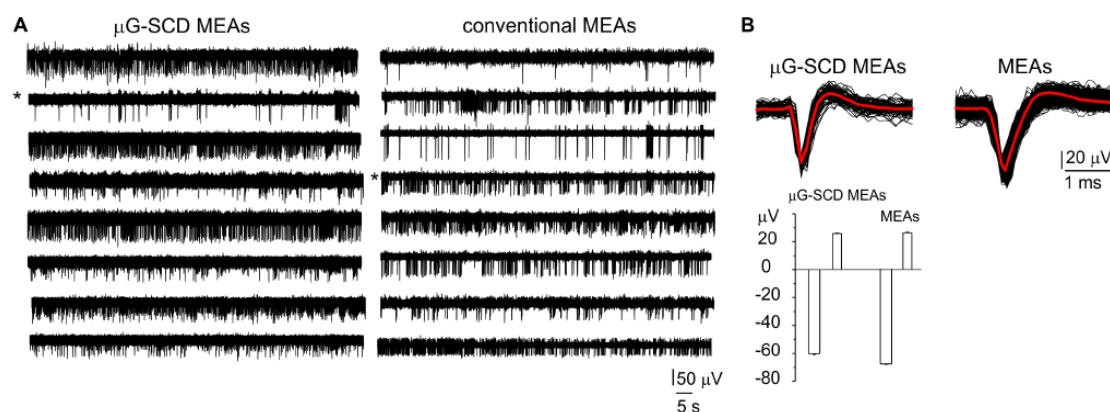


Figure 6. Potentiometric recordings from μ G-SCD-MEAs and MEAs. (A) Representative spontaneous firing activity of cultured midbrain neurons detected using μ G-SCD-MEAs (left) and conventional MEAs (right). (B) Top: representative extracellularly detected APs shown on an expanded time scale for both devices. The red trace is the averaged signal. Bottom: the bar histogram represents the mean peak amplitude (negative deflection) and antipeak amplitude (positive deflection) of the extracellularly recorded APs. Data refer to the traces indicated by the asterisks in (A).

With the aim of carrying out the same studies on the effect of L-DOPA in a neuronal network, recordings were performed in parallel using μ G-SCD-MEAs and conventional MEAs, for a more rigorous interpretation of acquired data.

Representative recordings of spontaneously firing midbrain neurons, measured using μ G-SCD-MEAs and conventional MEAs, are shown in Figure 6A. This spontaneous spiking activity occurred under physiological conditions (external solution contained 2 mM Ca^{2+}) and was suppressed by blocking the firing during the exogenous application of 300 nM TTX (data not shown). Unlike amperometric spikes, which exhibit monopolar waveforms, single APs (Figure 6B) were characterized by a fast downward deflection (negative peak), which corresponds to the AP rising phase, followed by an upward deflection (positive antipeak), which is associated to the AP repolarising phase [256], [257]. The mean amplitude of the negative peaks recorded by μ G-SCD-MEAs ($n = 10$) was $-50.2 \pm 3.6 \mu V$, with S/N of ~ 4 , while the mean signal amplitude was equal to $-54.0 \pm 4.7 \mu V$, with S/N of ~ 5 , for conventional MEAs ($n = 10$).

Here, the objective of this comparison was to validate the correct functioning of the diamond prototype with respect to conventional multi-electrode arrays.

These recordings are the first experimental evidence that μ G-SCD-MEAs are suitable for potentiometric recordings from primary cultures of cultured midbrain neurons.

At this point, I used μ G-SCD-MEAs to investigate the modulation of the firing activity by L-DOPA on a network of dopaminergic neurons and the relative effect of the antagonist D_2 (Figure 7).

Potentiometric recordings using μ G-SCD-MEAs were performed to simultaneously detect spikes arising from different neuronal populations and to investigate their responses to the applied drugs. With respect to patch-clamp experiments (see chapter 6, paragraph 6.0), performed on isolated and young neurons (10 DIV), these trials were designed to provide a rapid screening of the effects of L-DOPA on mature networks (14 DIV). After the firing properties under control conditions were monitored for a couple of minutes, the addition of L-DOPA to the culture medium revealed three different responses, confirming the existence of heterogeneous firing, as measured in SN slices [11]. In most cases (70% of neurons), the firing activity was significantly reduced by L-DOPA and the inhibitory effect required some minutes for completion [248]. As shown in a representative recording using μ G-SCD-MEAs, the firing frequency was reduced by 80% after 2–3 min, and the extracellular AP peak increased from -75 ± 1 to -87 ± 3 μ V, while sulpiride reversed both effects, suggesting that D_2 autoreceptors are involved (Figures 7A, C). On average L-DOPA decreased the spontaneous spiking activity from 1.1 to 0.3 Hz and increased the negative peak amplitude by 14% ($n = 5$ μ G-SCD-MEAs, $p < 0.05$), suggesting a prominent recruitment of Nav channels following L-DOPA hyperpolarization.

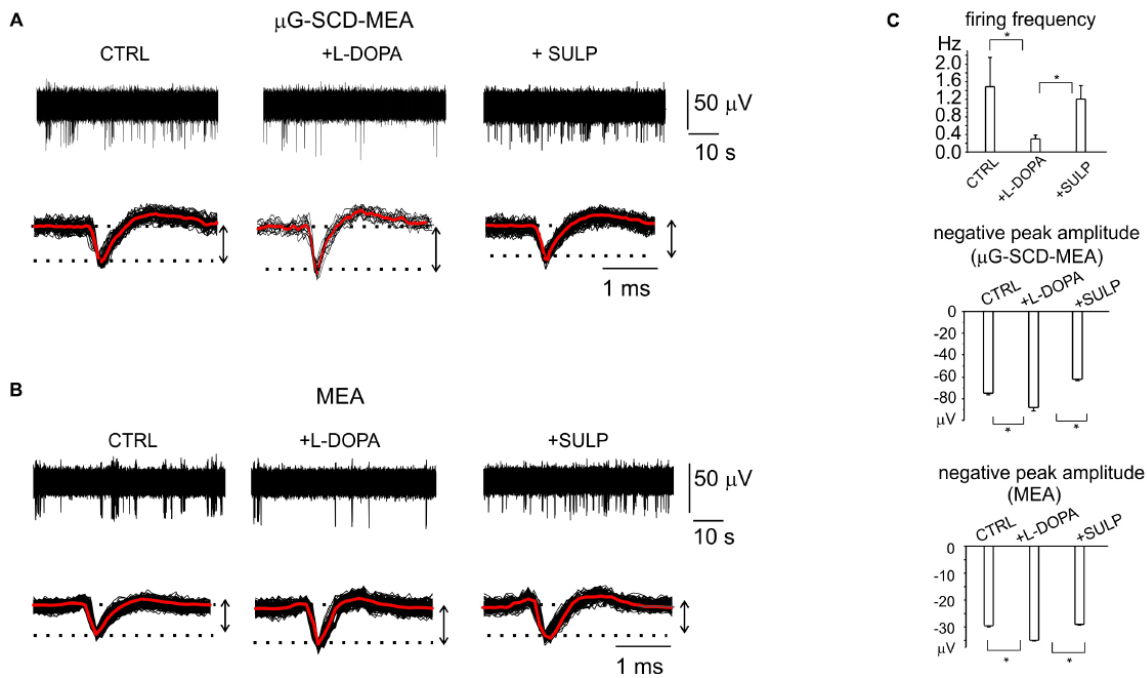


Figure 7 D₂-autoreceptor mediated down-regulation of neuronal firing activity measured by μ G-SCD-MEAs and MEAs. (A) Representative recordings from one channels of μ G-SCD-MEAs. Bottom: potentiometric signals from (A) are visualized on an enlarged scale (black traces). Averaged signals are shown in red. (B) Representative recording from one electrode belonging to a conventional MEA, showing the reduction of the firing frequency and its recovery induced by sulpiride Bottom: individual (black) and averaged signals (red). (C) Top: the bar histograms represent the mean firing frequency in the three conditions (control, with L-DOPA and with L-DOPA + sulpiride), measured by conventional MEAs. Centre, bottom: the bar histogram shows the mean values of the negative peak amplitude and related statistical significance ($p < 0.05$), for μ G-SCD-MEAs and MEAs, respectively.

In order to validate these experimental findings, I repeated the same experiments using conventional MEAs. Once again, the majority of neurons (64%), responded to L-DOPA by reducing the mean firing frequency, on average from 1.5 ± 0.7 to 0.29 ± 0.09 Hz $p < 0.05$, $n = 10$ MEAs; Figure 6B), while sulpiride restored the basal frequency to 1.1 ± 0.3 Hz (Figure 7B). In this subset of neurons, firing frequency reduction was also associated to a 20% increase in the negative peak amplitude, confirming the prominent role that D₂-autoreceptors play in L-DOPA induced inhibition.

Nevertheless, a relevant fraction of neurons in the mature networks (30 and 36%, respectively for μ G-SCD-MEAs and MEAs) also displayed a significant increase (up to six fold) in spontaneous frequency and a 30% reduction in the negative peak amplitude following exposure to L-DOPA. This is in good agreement with the heterogeneity of responses that we observed in dissociated neurons under current-clamp conditions. In the example shown in Figure 8A for μ G-SCD-MEAs, the negative peak amplitude

decreased from -44.1 ± 1.2 to -34.2 ± 1.1 mV, while the firing frequency increased from 0.5 to 2.9 Hz [258]. Similarly, the potentiation of firing activity by L-DOPA occurred with a mean threefold increase in firing frequency when using conventional MEAs, and was usually accompanied by a 28% decrease in the negative peak amplitude (Figure 8B).

L-DOPA reduced the spiking activity without affecting the AP shape in the remaining cases. Examples of this modulation are shown in Figure 8C. The unaltered amplitude of the negative AP peak, that have been revealed by μ G-SCD-MEAs and conventional MEAs (Figure 8D), confirms the findings obtained under patch-clamp conditions, in which 30% of neurons displayed a reduced firing frequency without alterations of the AP rising phase.

Concerning the opposing effect that was observed in a minority of neurons, in which L-DOPA increased the spiking activity (Figure 8), variable responses have also been described in *Substantia Nigra pars compacta* (SNc) neurons, using MEA recordings from midbrain slices [11]. In that case, neurons that fired at high rates (>5 Hz) were insensitive to DA, while low-firing neurons were either highly or weakly inhibited by DA. Furthermore, a fraction of low rate spiking neurons was insensitive to DA, or excited by DA, and a minority of neurons were potentiated by L-DOPA.

Under my experimental conditions, where midbrain neurons were cultured for weeks on the microarray, signals detection may occur from different DA subpopulations [35], [259], either from non-DA neurons or from DA neurons of the nearby ventral tegmental area. Indeed, the excitatory effects of L-DOPA on nigral dopaminergic neurons have been previously described, and were featured as an “early” and a “late” phase of excitation [250]. Finally, regarding the fraction of neurons that were inhibited by L-DOPA and did not undergo relevant membrane potential hyperpolarization, several pathways may be responsible for this modulation, based on the involvement of K^+ channels other than GIRK [260], or D1-mediated signalling cascades [261].

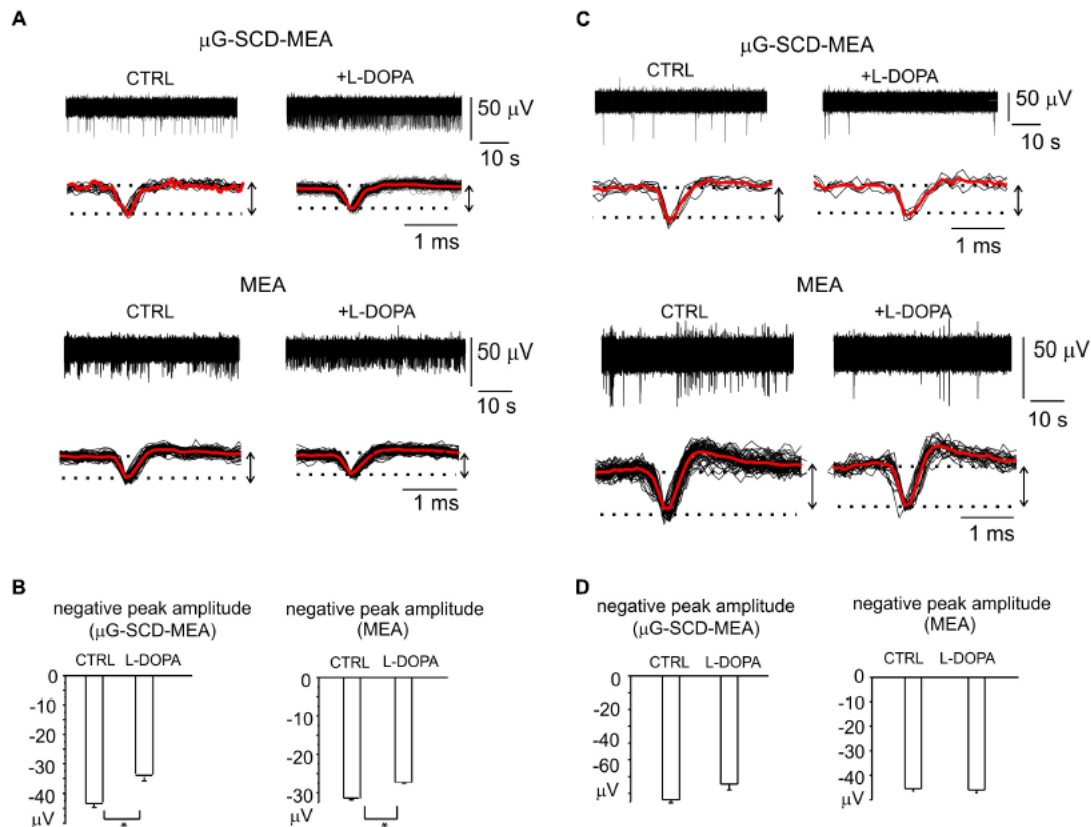


Figure 8. Heterogeneity of L-DOPA-induced responses on midbrain neurons viewed through μ G-SCD-MEAs and MEAs. (A) Representative recordings of L-DOPA-induced potentiation of neuronal firing, respectively acquired by μ G-SCD-MEAs (top) and MEAs (bottom). Under each recording, individual (black) and averaged signals (red) are shown on an expanded time scale. (B) L-DOPA induced potentiation is associated to the reduced amplitude of the AP peak, as shown in the bar histograms. (C) L-DOPA reduces the firing frequency without causing any significant alteration in the extracellularly recorded peak amplitude. Significant recordings detected by μ G-SCD-MEAs (top) and MEAs (bottom). (D) The bar histograms show the mean negative peak amplitude, which is not affected by L-DOPA, for both devices.

I started studying the causes of these side effects by perfusing, after L-DOPA administration, with SCH-23390, a selective antagonist of the dopaminergic D₁ receptor. These preliminary data show both in current clamp and with multi-electrode measurements, that after an increase in firing frequency with L-DOPA administration, a subsequently reduction in the firing rate after perfusion with the D₁ antagonist. Despite everything, the statistics of these data are still not sufficient to be able to draw adequate conclusions. More experiments will be needed in the future.

8.0 Simultaneous amperometric and potentiometric detection of neural signals

Recently micrographitized MEAs have been interfaced with dopaminergic neurons to detect, for the first time, amperometric and potentiometric signals from the same diamond device simultaneously. As shown in Figure 9, the simultaneous measurement of firing and secretion is detected by two electrodes.

As mentioned before, this results further demonstrate the extreme versatility of diamond probes.

The operating modality (amperometric versus potentiometric) was independently selected for each of the 16 electrodes by the operator. As shown in Figure 9, following stimulation with external KCl (30 mM), electrical spiking activity and quantal exocytotic release from midbrain dopaminergic neurons could be simultaneously detected by two electrodes of the array. In good agreement with values reported in the literature and previous trials using micrographitized diamond MEA uniquely as amperometric probes, detected amperometric spikes had 0.60 ± 0.05 ms half-time width and 35.5 ± 1.9 pA unitary amplitude ($n = 248$ spikes). Simultaneous detection of action potential from another electrode of the array revealed events with 35 ± 1 μ V peak amplitude ($n = 152$ events). These pionieristic results confirm the potentiality of micrographitized diamond MEAs as sensitive bio-probes for performing multiparametric detection of neuronal activity.

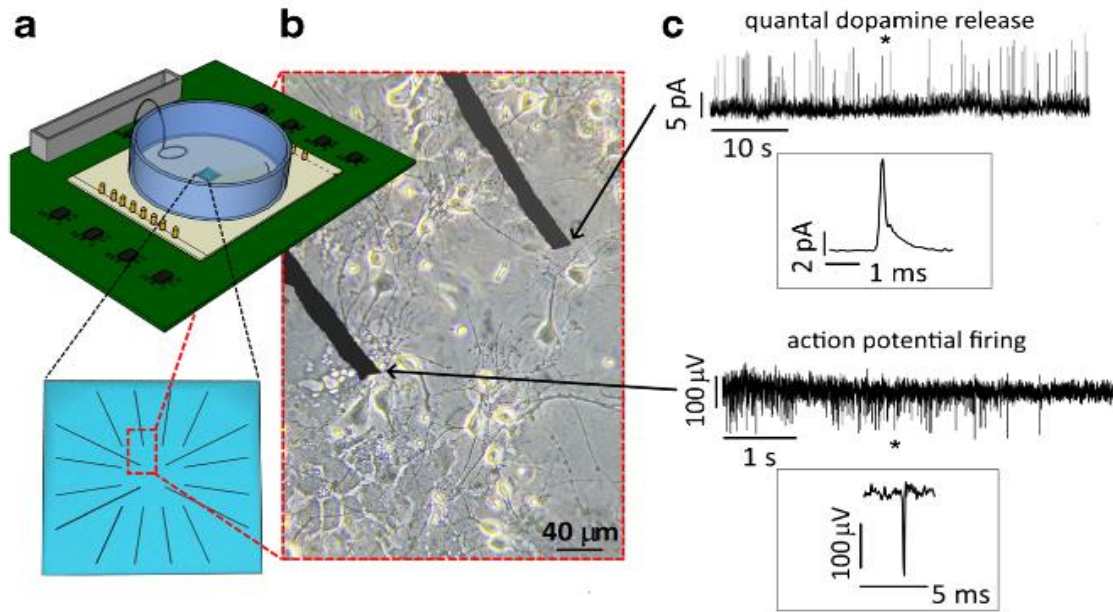


Figure 9. Micrographitized diamond MEA for simultaneous potentiometric and amperometric recording. A Scheme of the recording apparatus of micrographitized diamond MEA. Bottom: detail of the array geometry. B Midbrain neurons cultured on the micrographitized diamond MEA. C Simultaneous recordings of exocytosis and neuronal excitability using a micrographitized diamond MEA. Quantal dopamine release from midbrain dopaminergic neurons (upper trace) and action potential firing (lower trace) have been simultaneously detected from two graphitic electrodes of the 4×4 array. Insets show single events (amperometric spike and extracellular action potential, respectively) on a higher magnification scale (Pflugers Arch - Eur J Physiol (2021) 473:15–36) [242].

Chapter 7

Discussion

1.0 Monitoring the maturation of the dopaminergic network maturation

I started by studying how the firing frequency changes over time as the circuit develops. I observed that there is a significant change in the firing pattern.

Cultured midbrain neurons are characterized by isolated peaks up to 9 DIV, with a reduced number of active channels, after 14 DIV, the number of spikes not only increases progressively, but gives way to a mainly bursty network. This increase in the number of bursts over time is a parameter that indicates how the network evolves and matures. I observed that from 14 DIV onwards there are no more significant variations in firing, so it is possible to define the mature network from this age.

Another very interesting parameter that has been observed is that by distributing the amplitude of the peaks before and after 14 DIV, different amplitude distributions are observed. In fact, when the network is young (7-9 DIV), a single-peak distribution is found, while since 14 DIV onwards, three peak distributions are revealed. This is an indication of the network maturation and, besides the increased firing, burst and synchronism parameters, also signal amplitude increases. Various hypothesis can be made to explain this last issue:

- As reported in [262]–[265], the signal amplitude varies according to the part of the neuron (soma, axon or dendrites) which is in contact with the electrode. The observation of different peaks may be due to the fact that from an electrode it is possible to detect signals originating from different areas of different neurons;
- remodelling of the ion conductance's, associated with the development of the network;
- burst activity increases over time, infact bursts develop towards 11 DIV and stabilizes since 14 DIV onwards.

2.0 Dopaminergic neurons are affected by GABAergic and glutamatergic control

Dopamine (DA) and γ -aminobutyric acid (GABA) are the two main neurotransmitters that mediate the signal processing of the nigro-striatal circuit involved in motor control and several other functions. Most neurons in the *substantia nigra pars compacta* (SNc) are dopaminergic and project onto the *striatum* where they release DA onto striato-nigral and striato-pallidal neurons. In turn, from the *striatum* and *globus pallidus* there is a convergence of GABAergic signals with the *substantia nigra pars reticulata* (SNr). The GABAergic neurons of the SNr would control the release of striatal DA through the collaterals of the axons projecting onto the SNc, as demonstrated by the suppressive effect of SNr stimulation on the firing of the DA neurons. A subpopulation of GABAergic neurons in the CNS is expected to regulate the transmission of DA through a local circuit. The neurons of the substantia nigra have a tonic firing and are controlled by both GABAergic and glutamatergic afferents. GABAergic input is provided by the striatal afferents and *globus pallidus*, while glutamatergic input is mainly provided by the *subthalamic nucleus*.

My experimental model was obtained by enzymatic dissociation of the midbrain: the first objective was to study the *in vitro* reorganization of the network and to evaluate its development over time and its modulation by GABAergic and glutamatergic inputs.

I had shown that the suppression of the activities of GABAergic neurons, by means of the selective blocker picrotoxin (100 μ M), produces a disinhibition of the network which appears as an increase in the firing activity of the bursts and synchronism parameters.

Dopaminergic neurons, *in vitro*, are mainly characterized by regular spontaneous activation, characterized by single spikes [175], [266], [267].

Thus excitatory synaptic inputs play several roles in this control mechanism:

- NMDA (N-methyl-D-aspartic acid) plays an essential role in the discharge pattern of these cells principally *in vivo* experiments [268], [269]; the continuous activation of NMDA receptors transforms the typical pacemaker-like discharge

typical of dopaminergic neurons into bursting mode in vitro [270], [271]. Clearly this may not be the only component present. In the data showed the NMDA contribution is not that significant.

- AMPA (α-amino-3-hydroxy-5-methyl-4-isoxazolepropionic acid) and kainate seem to be more involved in these mechanisms. In particular, the AMPA ionotropic receptor, recently found in the glutamatergic synapse of SNc, is characterized by an electrical stimulation of glutamatergic axons that can induce burst-type peaks in dopaminergic neurons of the CNS that depend on specific AMPAR receptors. [272].

The fact that firing was not totally suppressed after the total blockade of inhibitory and excitatory synapses, unlike what happens with other neuronal networks, such as *hippocampus* or *cortex*, suggests that the remaining electrical activity following the silencing of GABAergic and glutamatergic synapses, is attributable to dopaminergic neurons, coming from the SNc and VTA.

These data therefore demonstrate that the experimental model that I have developed can constitute a coherent method for monitoring dopaminergic neurons and their GABAergic and glutamatergic modulations.

I have also demonstrated, as reported in Berretta et al. [11], that the remaining firing has the same physiological characteristics observed in sliced dopaminergic neurons.

The presence of dopaminergic neurons in the preparation was confirmed by a series of specific experiments, aimed at studying the modulation of the firing frequency by exogenous dopamine.

3.0 Synchronization is regulated by the GABAergic and glutamatergic activity

After demonstrating, as expected, that with the maturation of the network also the network synchronism increases, due to the growth and development of neuronal connections, I evaluated the contribution of inhibitory and excitatory components in balancing the synchronism.

In fact, the overall activity of the network depends on the balance between GABAergic inhibition and the glutamatergic excitatory component [273].

My data clearly showed that by blocking the inhibitory component, the degree of synchronization significantly increases. Conversely, by blocking the AMPA and kainate component, the synchronization is drastically reduced. These data were in agreement with the fact that in the adult brain, the balance between neuronal excitation and inhibition is an essential condition to avoid the onset of pathological conditions. In fact, by blocking the GABAergic synapses, convulsions are generated, as well as the excessive activation of the glutamatergic synapses can have devastating effects since only the component that inhibits remains active.

The result obtained strengthens the theory that this preparation of dissociated dopaminergic neurons represents a valid experimental model to study the functionality of dopaminergic neurons, in physiological and pathological conditions, since it has been observed that dopaminergic neurons, *in vivo*, are subject to a significant GABAergic control.

Alterations in the tonic activity of GABAergic afferents are a potential mechanism extrinsic that triggers a firing mainly characterized by bursts interspersed with pauses. This firing behaviour was observed in slice experiments conducted by Lobb et al. in 2010 [274] and confirmed in the experiments that I conducted on dissociated dopaminergic neurons (chapter 3).

I have also observed that by blocking the inhibitory component the typical peak of the crosscorrelogram is not centered around 0 ms, but it can be shifted either to the right or to the left. This implies that depending on which neuron is the target and which is the referent, one fires faster than the other and *vice versa*. This variation is presumably due to the fact that picrotoxin alters the balance within the network.

4.0 Cav_{1.3} and Cav_{2.3} can play an important role in neuroprotection in PD

Although it is an already known effect, I reported that Cav_{1.3} play a significant role in sustaining the firing activity of DA neurons. In current-clamp conditions, 3 μ M isradipine was sufficient to reduce the spontaneous firing frequency by approximately 60-70% and the AP peak amplitude by 15%.

An important neuroprotective role of these calcium channels has been claimed for some time, unfortunately the recent failure of the L-type Ca²⁺ channel blocker isradipine in the STEADY-PD study (Parkinson Study Group, 2020) to prevent disease progression in patients with early stage PD indicates that inhibition of Cav_{1.3} alone may not be sufficient in the neuroprotection. But there are recent preclinical results that identify Cav_{2.3} channels as a new possible drug targets for the neuroprotective therapy of PD. To this end, the important effect of R-type calcium channels as the contribution of SNX-482-sensitive Cav_{2.3} currents to activity-dependent somatic Ca²⁺ oscillations in SN DA neurons in brain sections has been demonstrated [14], but also to the pacemaker rate in cultured DA neurons.

It has already been previously demonstrated that Cav_{2.3} knockout mice are protected from the selective loss of SN DA neurons in the chronic MPTP / probenecid PD model [14]. In this rodent PD model, the observed protection provides strong evidence for the role of these channels in PD pathology.

I have shown that in cultured mouse DA neurons, Cav_{2.3} channels can contribute to pacemaking. A possible objection could be that SNX-482 (Cav_{2.3} blocker) is also a powerful Kv4.3 channel blocker [275] underlying K⁺ type A (IA) currents. Therefore, it can be argued that in current clamp recordings, a concentration between 50-300 nM of SNX-482 could alter the pacemaker or AP shape by effectively blocking Kv4.3 channels. However, the results obtained on the spontaneous activation of DA neurons show very clearly that 100 nM SNX-482 causes a shortening and reduced frequency of spontaneous APs, while a block of IA channels typically induces an enlargement of APs in different neuronal preparations [276] and an increase in frequency in DA neurons [21].

Thus, pharmacological inhibition of Cav_{2.3} in addition to Cav_{1.3} may be required for clinically meaningful neuroprotection. However, Cav_{2.3}-mediated R-type currents are known to be drug resistant [277]. Thanks to these results it will be possible to expand and spend greater efforts to define an effective Cav_{2.3} drug, or to define a joint pharmacological protocol on the selective block Cav_{2.3} and Cav_{1.3}.

5.0 μ G-SCD-MEAs are efficient to monitor quantal release and electrical activity

I demonstrated that the μ G-SCD-MEAs, the diamond prototype that I developed in collaboration with the Physic Department in these years, are efficient as carbon fiber electrodes (CFEs) to monitor the exocytotic activity in real time.

I started with a simple experimental model, the PC12 cells, defined by Westerink et al., [242] "*The PC12 cells as model for neurosecretion*". The amperometric detection can be performed simultaneously by 16 graphite electrodes: together with the portability of the instrument, this is one of its greatest strengths, combined with the fact that data acquisition is enormously faster, and, being the cells placed on the multielectrodes, this avoids mechanical stimulation as may occur using carbon fiber electrodes.

I also demonstrated the reliability of μ G-SCD-MEAs to carry out pharmacological activities, aimed at monitoring the alterations in kinetics and amplitude of quantum secretory events. For example, I showed that cell incubation with L-DOPA causes significant changes in the shape of the amperometric spikes. These results are consistent with those performed by Pothos et al. [232]. In the cited work, 1 h of incubation with 50 μ M of L-DOPA increases the quantal release by 250%; in my case, I incubated PC12 cells for 1 h at 20 μ M and obtained a 120% increase.

The reason for these changes in the shape of the amperometric spikes is quite complex [244], however some hypotheses can be advanced. It has been hypothesized that L-DOPA favors more fusion events (i.e. fusion between two or more vesicles before exocytosis). Alternatively, Colliver et al. [245] from the TEM images observed that after incubation with L-DOPA there is a significant increase in the diameter and volume of the vesicles,

these pharmacological studies have shown that this increase is mediated by the vesicular monoamine transporter (VMT).

6.0 L-DOPA induced down-modulation of spontaneous firing and the effect is reverted by D₂ autoreceptor antagonist

The μ G-SCD-MEAs, in addition to detecting the quantal release of dopamine, can be exploited to measure the electrical activity of neuronal cultures of the midbrain. Network activity becomes detectable in both devices in most electrodes (70%) when the network is mature (14 DIV).

Neuronal firing of SN DA neurons is inhibited by autoreceptor-mediated D₂-activation of GIRK and is prevented by the D₂ antagonist sulpiride [28], [278]. To evaluate the sensitivity of μ G-SCD-MEAs, I tested this inhibitory pathway in TH-GFP neurons cultured for 2 weeks on μ G-SCD-MEA and conventional MEAs. Autocrine inhibition is induced by the addition of L-DOPA, which is converted into dopamine (DA) and then released by dopaminergic neurons.

In most neurons L-DOPA blocked the current, a reduction in firing rate was observed together with a slow membrane hyperpolarization and an increase in AP amplitude which was subsequently restored by sulpiride, the selective antagonist of the D₂ autoreceptor. Both MEAs device revealed the reduced rate of firing and increased phase-boosting AP, which was restored by the sulpiride.

From a physiological point of view, both measurements are in excellent agreement and suggest a sustained recruitment of NaV channels due to the greater cellular hyperpolarization induced by the activation of the GIRK channel. Sustained cellular hyperpolarizations increase the recruitment rate of NaV channels from steady state inactivation [252], [254], while the recruitment of different Nav channel isoforms which are characterized by a lower activation threshold it cannot be excluded.

For what concerns the opposite effect observed in a minority of neurons, in which L-DOPA increased the peak of activity, variable responses have also been described in *substantia nigra pars compacta* (SNc) neurons, using MEA recordings from midbrain sections [11]. In

that case, neurons that fired at high frequency (> 5 Hz) were insensitive to DA, while neurons at low frequency were either highly or weakly inhibited by DA.

In my experimental conditions, where mesencephalic neurons have been grown for weeks on the microarray, the signals arrive from different DA subpopulations [35], [259], either from non-dopaminergic neurons or from neighbouring DA neurons of *ventral tegmental area* (VTA). Indeed, the excitatory effects of L-DOPA on dopaminergic nigral neurons was mentioned by Berretta et al. on slices [11], I was able to reproduce for the first time this effect on the culture of dopaminergic neurons and recently it was also demonstrated by Liss et al. [279] on a slice.

Finally, for what concerns the fraction of neurons that have been inhibited by L-DOPA and have not undergone a membrane potential with a relevant hyperpolarization, different causes may be responsible for this modulation, based on the involvement of other K⁺ channels of GIRK [260]. This dopamine-mediated lack of inhibition observed in some cases could also be caused by desensitization of D₂ receptors (as argued by Dragicevic et al., 2014 [28]) or by the action of DOPA-quinone, a metabolite produced in the conversion of tyrosine to melanin, which counteracts the inhibition of the firing of dopaminergic neurons of the SNc induced by the opening of GIRK in response to D₂ stimulation [280]. These experiments represent a valid in vitro investigation model of the maturation of the mesencephalic network and the determination of its regulatory components, and may represent a starting point for future studies aimed at understanding the mechanisms responsible for the alteration of dopaminergic neurons.

7.0 μ G-SCD-MEAs are suitable tools for simultaneously performing amperometric and potentiometric measurements

Our data demonstrate that μ G-SCD-MEAs are highly reliable as a long-term multifunctional detection multiarray both for neuronal activity recordings and for measuring secretion from multiple electrodes simultaneously. Compared to conventional approaches, real-time measurements of quantum exocytosis and neuronal firing make

μ G-SCD-MEA a promising biosensor for the in vitro investigation of neuronal circuit properties, as well as a valuable tool for studying deactivated neurotransmission in neurodegenerative disorders. The new goal that was achieved was to realize a first simultaneous measurement of amperometry and potentiometry from the same neuronal network. Currently this is the first simultaneous measurement performed by a multi-electrode device.

8.0 MVIIC restores the impaired firing rates by aSyn

The sinucleinopathies are neurodegenerative diseases characterized by the abnormal accumulation of aggregates of α -synuclein (aSyn) protein in neurons, nerve fibers or glial cells. Among the most common synucleinopathies are Parkinson's disease (PD) and Lewy body dementia (LBD). In both of these diseases, the aSyn protein aggregates into amyloid fibrils which are deposited in characteristic inclusions, i.e. bodies Lewy and Lewy neuritis. The relationship between the aggregation of aSyn, the formation of inclusions of the amyloid protein, the clearance of aggregates, and the development of the disease remains to be understood. The protein is constantly secreted into the extracellular space. Extracellular monomers and aSyn aggregates can be absorbed by other cells. This absorption probably contributes to the diffusion of aSyn aggregation throughout the nervous system. In healthy cells, the function of the protein is associated with synaptic activity, in which it appears to regulate the pool of synaptic vesicles through the rearrangement of the vesicles after endocytosis, although several studies are still underway for a better understanding of its physiological role.

A protein concentration of ~ 100 - 200 mg/mL, this corresponds to a physiological protein concentration of 35 - 70 μ M in the human brain and ~ 40 μ M in the rat brain [196]. In pathological conditions, intracellular concentrations well above 100 μ M are possible [281].

It has been shown that an extracellular administration of aggregated aSyn induces in turn the aggregation of intracellular aSyn [282]. aSyn can be found in the extracellular environment not only in the form of a monomer but also as an oligomer that can be internalized by neuronal cells, through a clathrin mediated endocytotic pathway [283].

Recent evidence shows that these endogenous oligomers are the most cytotoxic in the early stages of disease development [197].

To this end, I exposed dissociated mesencephalic dopaminergic neurons, cultured on MultiElectrodeArray (MEA), to extracellular aSyn with the aim of studying the possible damaging effects of extracellular synuclein on firing activity and network synchronization. The formation of these aggregated oligomers starting from the monomer form after 48 hours of incubation was demonstrated through the AFM technique.

After observing a reduction in the firing frequency proportional to concentration of α Syn of 1 and 70 μ M and an absence of effect at concentrations lower than 0.3 and 0.5 μ M, it is possible to state that the phenomenon of attenuation of the frequency of electrical activity is dose-dependent. These data are in agreement with other experimental evidences, even if obtained on a different preparation (cortical neurons): it has been shown that high concentrations of extracellular aSyn lead to a reduction in the firing frequency of the neuronal network by interrupting the synaptic transmission, while the neuronal capacity to generate action potential remains intact [196]. Among the observed effects there are also a reduction in the number of bursts, while for each burst the number of spikes and the duration increase. This means that aSyn acts by reducing the total number of events generated by the network by altering their distribution, as the number of bursts is reduced, but each of these becomes longer and with a higher percentage of spikes than in the control condition.

Even synchronization is reduced after incubation with aSyn, at the moment it was evaluated in the absence of synapse blockers, it will be interesting to understand, through the use of synapse blockers, how synchronization behaves of the dopaminergic component in the presence of the protein at an extracellular level.

A very interesting result, but which undoubtedly needs further investigation is the effect that aSyn has on a young network (9 DIV). Unlike the case of the mature network (14 DIV), no significant variation was observed in the firing rate. This result could be linked to the fact that extracellular aSyn plays an important role on the synapse, which is not developed at such an early stage of neuronal development, but as mentioned other experiments will be needed to major understand this interesting phenomenon.

In parallel, single-cell dopaminergic tests were developed in current-clamp and using synapse blockers. It emerges that in the absence of stimulation (constant current at 0 pA) the frequency is drastically reduced, confirming the results with MEAs device.

This could be caused by an increase in the influx of calcium into the cell induced by the direct interaction of the extracellular protein with the Cav_{2.2}, as observed by Adamczyk et al., 2006 and by Ronzitti et al., 2014 [206], [208]. The increase in intracellular Ca²⁺ increases the firing of the dopaminergic cells of the SNc and therefore the secretion of dopamine, which through the D₂ autoreceptor reduces the firing frequency by activating a potassium channel (GIRK) via a G-dependent protein mechanism. The reduction in firing could also be due to the interaction between aSyn and DAT: according to the studies by Wawer et al., Luk et al. and Wakamatsu et al. [115], [284], [285], exogenous aSyn causes a decrease in the gene expression of DAT, which is responsible for the reuptake of dopamine from the synaptic space, therefore a reduction of its action leads to an increase in the concentration of dopamine in the synapses and increased dopaminergic stimulation, binding to the D₂ receptor. For these reasons I blocked Cav_{2.1} and Cav_{2.2}, I observed a recovery of the firing frequency compatible with the control condition. It is therefore possible to state that Cav_{2.1} and Cav_{2.2} may play a role in signal recovery. Future experiments could confirm this hypothesis, for by applying both MVIC but also sulpiride, a selective blocker of the D₂ autoreceptor.

These experiments therefore imply the need to carry out further tests to understand at the molecular level the mechanism of action of aSyn on neuronal activity. It is necessary to understand which dopaminergic receptors are most expressed on the neurons of the *substantia nigra pars compacta* in order to explain what was observed at the MEA and in these preliminary current clamp experiments with the current set at 0 pA.

Another particularly interesting result derives from what was observed by applying a depolarizing pulse of 20 pA. It is observed differently from the non-stimulated condition that the frequency increases in a statistically significant way after having incubated for 48 h with aSyn. Also the rising phase, that is the phase of ascent of the action potential, increased with the stimulation > + 20 pA. But when the current pulse delivered reaches 60 pA the activity decreases as the cell adapts earlier than the control condition. In the control condition the firing frequency gradually increases proportionally to the pulse

amplitude; by comparing the two situations it is clear that aSyn induces an uncontrolled increase in cellular activity, inducing higher frequency and earlier adaptation.

The increase in the rising phase could be due to an expression of channels that induce the entry of depolarizing cationic currents. To test this hypothesis, future experiments could be carried out with the same method but in the presence of sodium or calcium channel blockers.

The increase in firing frequency observed under stimulation is in agreement with the observation of Lin et al., 2021 [286]: this study states that in the presence of over-expressed aSyn, a reduction in the expression of the D₂ receptor occurs in dopaminergic neurons, which causes an increase in the regulation of firing and dopamine secretion, since D₂ is the receptor responsible for inhibiting cellular excitability.

Chapter 8

Bibliography

- [1] C. R. Gerfen and D. J. Surmeier, "Modulation of Striatal Projection Systems by Dopamine," <http://dx.doi.org/10.1146/annurev-neuro-061010-113641>, vol. 34, pp. 441–466, Jun. 2011, doi: 10.1146/ANNUREV-NEURO-061010-113641.
- [2] A. A. Grace, S. B. Floresco, Y. Goto, and D. J. Lodge, "Regulation of firing of dopaminergic neurons and control of goal-directed behaviors," *Trends Neurosci.*, vol. 30, no. 5, pp. 220–227, May 2007, doi: 10.1016/J.TINS.2007.03.003.
- [3] E. Dragicevic, J. Schiemann, and B. Liss, "Dopamine midbrain neurons in health and Parkinson's disease: emerging roles of voltage-gated calcium channels and ATP-sensitive potassium channels," *Neuroscience*, vol. 284, pp. 798–814, Jan. 2015, doi: 10.1016/J.NEUROSCIENCE.2014.10.037.
- [4] T. K. Lee and E. L. Yankee, "Review Open Access Neuroimmunology and Neuroinflammation A review on Parkinson's disease treatment," doi: 10.20517/2347-8659.2020.58.
- [5] J. L. Lanciego, N. Luquin, and J. A. Obeso, "Functional Neuroanatomy of the Basal Ganglia," *Cold Spring Harb. Perspect. Med.*, vol. 2, no. 12, 2012, doi: 10.1101/CSHPERSPECT.A009621.
- [6] A. M. Graybiel, T. Aosaki, A. W. Flaherty, and M. Kimura, "The Basal Ganglia and Adaptive Motor Control," *Science (80-.)*, vol. 265, no. 5180, pp. 1826–1831, Sep. 1994, doi: 10.1126/SCIENCE.8091209.
- [7] R. L. Albin, A. B. Young, and J. B. Penney, "The functional anatomy of basal ganglia disorders," *Trends Neurosci.*, vol. 12, no. 10, pp. 366–375, Jan. 1989, doi: 10.1016/0166-2236(89)90074-X.
- [8] E. Guatteo, M. L. Cucchiaroni, and N. B. Mercuri, "Substantia Nigra Control of

- Basal Ganglia Nuclei," *J. Neural Transm. Suppl.*, no. 73, pp. 91–101, 2009, doi: 10.1007/978-3-211-92660-4_7.
- [9] G. Tomagra *et al.*, "Quantal release of dopamine and action potential firing detected in midbrain neurons by multifunctional diamond-based microarrays," *Front. Neurosci.*, 2019, doi: 10.3389/fnins.2019.00288.
- [10] P. D. Shepard and B. S. Bunney, "Repetitive firing properties of putative dopamine-containing neurons in vitro: regulation by an apamin-sensitive Ca(2+)-activated K+ conductance," *Exp. brain Res.*, vol. 86, no. 1, pp. 141–150, 1991, doi: 10.1007/BF00231048.
- [11] N. Berretta, G. Bernardi, and N. B. Mercuri, "Firing properties and functional connectivity of substantia nigra pars compacta neurones recorded with a multi-electrode array in vitro," *J. Physiol.*, vol. 588, no. 10, pp. 1719–1735, May 2010, doi: 10.1113/JPHYSIOL.2010.189415.
- [12] A. A. Grace and B. S. Bunney, "The control of firing pattern in nigral dopamine neurons: single spike firing," *J. Neurosci.*, vol. 4, no. 11, pp. 2866–2876, 1984.
- [13] A. A. Grace and S.-P. Onn, "Morphology and Electrophysiological Properties of Immunocytochemically Identified Rat Dopamine Neurons Recorded in vitro," *J. Neurosci.*, vol. 9, no. 10, p. 34833481, 1989.
- [14] J. Benkert *et al.*, "Cav2.3 channels contribute to dopaminergic neuron loss in a model of Parkinson's disease," *Nat. Commun.*, vol. 10, no. 1, Dec. 2019, doi: 10.1038/S41467-019-12834-X.
- [15] J. Striessnig, "Getting a handle on CaV2.2 (N-type) voltage-gated Ca²⁺ channels," *Proc. Natl. Acad. Sci.*, vol. 115, no. 51, pp. 12848–12850, Dec. 2018, doi: 10.1073/PNAS.1818608115.
- [16] N. B. Mercuri, A. Bond, P. Calabresi, F. Stratta, A. Stefani, and G. Bernardi, "Effects of dihydropyridine calcium antagonists on rat midbrain dopaminergic neurones," *Br. J. Pharmacol.*, vol. 113, no. 3, pp. 831–838, Nov. 1994, doi: 10.1111/J.1476-5381.1994.TB17068.X.

- [17] I. Putzier, P. Kullmann, ... J. H.-J. of, and undefined 2009, "Cav1. 3 channel voltage dependence, not Ca²⁺ selectivity, drives pacemaker activity and amplifies bursts in nigral dopamine neurons," *Soc Neurosci.*, 2009, doi: 10.1523/JNEUROSCI.4742-09.2009.
- [18] J. N. Guzman, J. Sánchez-Padilla, C. S. Chan, and D. J. Surmeier, "Robust pacemaking in substantia nigra dopaminergic neurons," *Soc Neurosci.*, 2009, doi: 10.1523/JNEUROSCI.2519-09.2009.
- [19] M. Puopolo, E. Raviola, and B. P. Bean, "Roles of subthreshold calcium current and sodium current in spontaneous firing of mouse midbrain dopamine neurons," *J. Neurosci.*, vol. 27, no. 3, pp. 645–656, Jan. 2007, doi: 10.1523/JNEUROSCI.4341-06.2007.
- [20] C. S. Chan *et al.*, "'Rejuvenation' protects neurons in mouse models of Parkinson's disease," *Nat. 2007 4477148*, vol. 447, no. 7148, pp. 1081–1086, Jun. 2007, doi: 10.1038/nature05865.
- [21] B. Liss, O. Franz, S. Sewing, R. Bruns, H. Neuhoff, and J. Roeper, "Tuning pacemaker frequency of individual dopaminergic neurons by Kv4.3L and KChip3.1 transcription," *EMBO J.*, vol. 20, no. 20, pp. 5715–5724, Oct. 2001, doi: 10.1093/EMBOJ/20.20.5715.
- [22] J. Wolfart, H. Neuhoff, O. F.-J. of Neuroscience, and undefined 2001, "Differential expression of the small-conductance, calcium-activated potassium channel SK3 is critical for pacemaker control in dopaminergic midbrain neurons," *Soc Neurosci.*, 2001, Accessed: Dec. 14, 2021. [Online]. Available: <https://www.jneurosci.org/content/21/10/3443.short>.
- [23] K. F. Herrik, P. Christophersen, and P. D. Shepard, "Pharmacological modulation of the gating properties of small conductance Ca²⁺-activated K⁺ channels alters the firing pattern of dopamine neurons in vivo," *J. Neurophysiol.*, vol. 104, no. 3, pp. 1726–1735, Sep. 2010, doi: 10.1152/JN.01126.2009.
- [24] J. Deignan, R. Luján, C. Bond, A. Riegel, M. W.- Neuroscience, and undefined 2012, "SK2 and SK3 expression differentially affect firing frequency and precision

- in dopamine neurons," *Elsevier*, Accessed: Dec. 14, 2021. [Online]. Available: <https://www.sciencedirect.com/science/article/pii/S0306452212004150>.
- [25] T. Kimm, Z. M. Khaliq, and B. P. Bean, "Differential Regulation of Action Potential Shape and Burst-Frequency Firing by BK and Kv2 Channels in Substantia Nigra Dopaminergic Neurons," *J. Neurosci.*, vol. 35, no. 50, pp. 16404–16417, Dec. 2015, doi: 10.1523/JNEUROSCI.5291-14.2015.
- [26] M. J. Wanat, I. Willuhn, J. J. Clark, and P. E. M. Phillips, "Phasic dopamine release in appetitive behaviors and drug abuse," *Curr. Drug Abuse Rev.*, vol. 2, no. 2, p. 195, Jun. 2009, doi: 10.2174/1874473710902020195.
- [27] P. F. Marcott, A. A. Mamaligas, and C. P. Ford, "Phasic Dopamine Release Drives Rapid Activation of Striatal D2-Receptors," *Neuron*, vol. 84, no. 1, pp. 164–176, Oct. 2014, doi: 10.1016/J.NEURON.2014.08.058.
- [28] E. Dragicevic *et al.*, "Cav1.3 channels control D2-autoreceptor responses via NCS-1 in substantia nigra dopamine neurons," *Brain*, vol. 137, no. 8, pp. 2287–2302, 2014, doi: 10.1093/brain/awu131.
- [29] M. G. Lacey, N. B. Mercuri, and R. A. North, "Dopamine acts on D2 receptors to increase potassium conductance in neurones of the rat substantia nigra zona compacta.," *J. Physiol.*, vol. 392, no. 1, pp. 397–416, Nov. 1987, doi: 10.1113/jphysiol.1987.sp016787.
- [30] L. L. Iversen, "Dopamine handbook," p. 615, Accessed: Dec. 14, 2021. [Online]. Available: https://books.google.com/books/about/Dopamine_Handbook.html?hl=it&id=3pK1-LxtFV4C.
- [31] G. Morris, D. Arkadir, A. Nevet, E. Vaadia, and H. Bergman, "Coincident but Distinct Messages of Midbrain Dopamine and Striatal Tonically Active Neurons," *Neuron*, vol. 43, no. 1, pp. 133–143, Jul. 2004, doi: 10.1016/J.NEURON.2004.06.012.
- [32] J. F. Atherton and M. D. Bevan, "Ionic Mechanisms Underlying Autonomous Action Potential Generation in the Somata and Dendrites of GABAergic Substantia

- Nigra Pars Reticulata Neurons In Vitro,” *J. Neurosci.*, vol. 25, no. 36, pp. 8272–8281, Sep. 2005, doi: 10.1523/JNEUROSCI.1475-05.2005.
- [33] F. W. Zhou, S. G. Matta, and F. M. Zhou, “Constitutively Active TRPC3 Channels Regulate Basal Ganglia Output Neurons,” *J. Neurosci.*, vol. 28, no. 2, pp. 473–482, Jan. 2008, doi: 10.1523/JNEUROSCI.3978-07.2008.
- [34] T. A. Zhang, A. N. Placzek, and J. A. Dani, “In Vitro Identification and Electrophysiological Characterization of Dopamine Neurons in the Ventral Tegmental Area,” *Neuropharmacology*, vol. 59, no. 6, p. 431, Nov. 2010, doi: 10.1016/J.NEUROPHARM.2010.06.004.
- [35] S. Lammel, A. Hetzel, O. Häckel, I. Jones, B. Liss, and J. Roeper, “Unique Properties of Mesoprefrontal Neurons within a Dual Mesocorticolimbic Dopamine System,” *Neuron*, vol. 57, no. 5, pp. 760–773, Mar. 2008, doi: 10.1016/J.NEURON.2008.01.022.
- [36] L. A. Chiodo, M. J. Bannon, A. A. Grace, R. H. Roth, and B. S. Bunney, “Evidence for the absence of impulse-regulating somatodendritic and synthesis-modulating nerve terminal autoreceptors on subpopulations of mesocortical dopamine neurons,” *Neuroscience*, vol. 12, no. 1, pp. 1–16, May 1984, doi: 10.1016/0306-4522(84)90133-7.
- [37] M. Kawano *et al.*, “Particular subpopulations of midbrain and hypothalamic dopamine neurons express vesicular glutamate transporter 2 in the rat brain,” *J. Comp. Neurol.*, vol. 498, no. 5, pp. 581–592, Oct. 2006, doi: 10.1002/CNE.21054.
- [38] L. Descarries, N. Bérubé-Carrière, M. Riad, G. D. Bo, J. A. Mendez, and L. É. Trudeau, “Glutamate in dopamine neurons: Synaptic versus diffuse transmission,” *Brain Res. Rev.*, vol. 58, no. 2, pp. 290–302, Aug. 2008, doi: 10.1016/J.BRAINRESREV.2007.10.005.
- [39] N. Chuhma, W. Y. Choi, S. Mingote, and S. Rayport, “Dopamine neuron glutamate cotransmission: frequency-dependent modulation in the mesoventromedial projection,” *Neuroscience*, vol. 164, no. 3, pp. 1068–1083, Dec. 2009, doi: 10.1016/J.NEUROSCIENCE.2009.08.057.

- [40] P. W. Kalivas, "Neurotransmitter regulation of dopamine neurons in the ventral tegmental area," *Brain Res. Rev.*, vol. 18, no. 1, pp. 75–113, Jan. 1993, doi: 10.1016/0165-0173(93)90008-N.
- [41] J. D. Fernstrom and M. H. Fernstrom, "Tyrosine, Phenylalanine, and Catecholamine Synthesis and Function in the Brain," *J. Nutr.*, vol. 137, no. 6, pp. 1539S-1547S, Jun. 2007, doi: 10.1093/JN/137.6.1539S.
- [42] T. NAGATSU, M. LEVITT, and S. UDENFRIEND, "Tyrosine Hydroxylase: THE INITIAL STEP IN NOREPINEPHRINE BIOSYNTHESIS," *J. Biol. Chem.*, vol. 239, no. 9, pp. 2910–2917, Sep. 1964, doi: 10.1016/S0021-9258(18)93832-9.
- [43] A. Mishra, S. Singh, and S. Shukla, "Physiological and Functional Basis of Dopamine Receptors and Their Role in Neurogenesis: Possible Implication for Parkinson's disease," *J. Exp. Neurosci.*, vol. 12, p. 1179069518779829, Jan. 2018, doi: 10.1177/1179069518779829.
- [44] A. Bonci and F. W. Hopf, "The dopamine D2 receptor: new surprises from an old friend," *Neuron*, vol. 47, no. 3, pp. 335–338, Aug. 2005, doi: 10.1016/J.NEURON.2005.07.015.
- [45] A. Ledonne and N. B. Mercuri, "Current concepts on the physiopathological relevance of dopaminergic receptors," *Front. Cell. Neurosci.*, vol. 11, p. 27, Feb. 2017, doi: 10.3389/FNCEL.2017.00027/BIBTEX.
- [46] J. Y. Jang *et al.*, "Regulation of dopaminergic neuron firing by heterogeneous dopamine autoreceptors in the substantia nigra pars compacta," *J. Neurochem.*, vol. 116, no. 6, pp. 966–974, Mar. 2011, doi: 10.1111/J.1471-4159.2010.07107.X.
- [47] J. A. Bourne, "SCH 23390: The first selective dopamine D1-like receptor antagonist," *CNS Drug Rev.*, vol. 7, no. 4, pp. 399–414, 2001, doi: 10.1111/J.1527-3458.2001.TB00207.X/FORMAT/PDF.
- [48] C. Missale, S. Russel Nash, S. W. Robinson, M. Jaber, and M. G. Caron, "Dopamine receptors: From structure to function," *Physiol. Rev.*, vol. 78, no. 1, pp. 189–225, 1998, doi: 10.1152/PHYSREV.1998.78.1.189/ASSET/IMAGES/LARGE/JNP.JA09F3.JPEG.

- [49] A. V. Kravitz *et al.*, "Regulation of parkinsonian motor behaviours by optogenetic control of basal ganglia circuitry," *Nat.* 2010 4667306, vol. 466, no. 7306, pp. 622–626, Jul. 2010, doi: 10.1038/nature09159.
- [50] C. P. Ford, S. C. Gantz, P. E. M. Phillips, and J. T. Williams, "Control of Extracellular Dopamine at Dendrite and Axon Terminals," *J. Neurosci.*, vol. 30, no. 20, pp. 6975–6983, May 2010, doi: 10.1523/JNEUROSCI.1020-10.2010.
- [51] A. Björklund and O. Lindvall, "Dopamine in dendrites of substantia nigra neurons: suggestions for a role in dendritic terminals," *Brain Res.*, vol. 83, no. 3, pp. 531–537, Jan. 1975, doi: 10.1016/0006-8993(75)90849-5.
- [52] D. Sulzer, S. J. Cragg, and M. E. Rice, "Striatal dopamine neurotransmission: Regulation of release and uptake," *Basal Ganglia*, vol. 6, no. 3, pp. 123–148, Aug. 2016, doi: 10.1016/J.BAGA.2016.02.001.
- [53] A. Anzalone *et al.*, "Dual Control of Dopamine Synthesis and Release by Presynaptic and Postsynaptic Dopamine D2 Receptors," *J. Neurosci.*, vol. 32, no. 26, pp. 9023–9034, Jun. 2012, doi: 10.1523/JNEUROSCI.0918-12.2012.
- [54] J. W. De Jong *et al.*, "Reducing Ventral Tegmental Dopamine D2 Receptor Expression Selectively Boosts Incentive Motivation," *Neuropsychopharmacol.* 2015 409, vol. 40, no. 9, pp. 2085–2095, Mar. 2015, doi: 10.1038/npp.2015.60.
- [55] E. S. Calipari *et al.*, "Amphetamine Self-Administration Attenuates Dopamine D2 Autoreceptor Function," *Neuropsychopharmacol.* 2014 398, vol. 39, no. 8, pp. 1833–1842, Feb. 2014, doi: 10.1038/npp.2014.30.
- [56] M. Santiago and B. H. C. Westerink, "Characterization and Pharmacological Responsiveness of Dopamine Release Recorded by Microdialysis in the Substantia Nigra of Conscious Rats," *J. Neurochem.*, vol. 57, no. 3, pp. 738–747, Sep. 1991, doi: 10.1111/J.1471-4159.1991.TB08214.X.
- [57] M. E. Rice and J. C. Patel, "Somatodendritic dopamine release: Recent mechanistic insights," *Philos. Trans. R. Soc. B Biol. Sci.*, vol. 370, no. 1672, pp. 1–14, 2015, doi: 10.1098/rstb.2014.0185.

- [58] D. J. Surmeier, P. T. Schumacker, J. D. Guzman, E. Ilijic, B. Yang, and E. Zampese, "Calcium and Parkinson's disease," *Biochem. Biophys. Res. Commun.*, vol. 483, no. 4, pp. 1013–1019, Feb. 2017, doi: 10.1016/J.BBRC.2016.08.168.
- [59] E. Guatteo *et al.*, "Functional alterations of the dopaminergic and glutamatergic systems in spontaneous α -synuclein overexpressing rats," *Exp. Neurol.*, vol. 287, 2017, doi: 10.1016/j.expneurol.2016.10.009.
- [60] V. M. Nemani *et al.*, "Increased expression of alpha-synuclein reduces neurotransmitter release by inhibiting synaptic vesicle reclustering after endocytosis," *Neuron*, vol. 65, no. 1, pp. 66–79, Jan. 2010, doi: 10.1016/J.NEURON.2009.12.023.
- [61] P. Garcia-Reitboeck *et al.*, "Endogenous alpha-synuclein influences the number of dopaminergic neurons in mouse substantia nigra," *Exp. Neurol.*, vol. 248, pp. 541–545, Oct. 2013, doi: 10.1016/J.EXPNEUROL.2013.07.015.
- [62] C. J. Wilson and J. C. Callaway, "Coupled oscillator model of the dopaminergic neuron of the substantia nigra," *J. Neurophysiol.*, vol. 83, no. 5, pp. 3084–3100, 2000, doi: 10.1152/JN.2000.83.5.3084/ASSET/IMAGES/LARGE/9K0500976012.JPEG.
- [63] H. Neuhoff, A. Neu, B. Liss, and J. Roeper, "Ih Channels Contribute to the Different Functional Properties of Identified Dopaminergic Subpopulations in the Midbrain," *J. Neurosci.*, vol. 22, no. 4, pp. 1290–1302, Feb. 2002, doi: 10.1523/JNEUROSCI.22-04-01290.2002.
- [64] B. P. Bean, "The action potential in mammalian central neurons," *Nat. Rev. Neurosci.* 2007 86, vol. 8, no. 6, pp. 451–465, Jun. 2007, doi: 10.1038/nrn2148.
- [65] J. Sanchez-Padilla *et al.*, "Mitochondrial oxidant stress in locus coeruleus is regulated by activity and nitric oxide synthase," *Nat. Neurosci.* 2014 176, vol. 17, no. 6, pp. 832–840, May 2014, doi: 10.1038/nn.3717.
- [66] R. C. Foehring, X. F. Zhang, J. C. F. Lee, and J. C. Callaway, "Endogenous calcium buffering capacity of substantia nigral dopamine neurons," *J. Neurophysiol.*, vol. 102, no. 4, pp. 2326–2333, Oct. 2009, doi:

- 10.1152/JN.00038.2009/ASSET/IMAGES/LARGE/Z9K0100997280003.JPEG.
- [67] W. Xu and D. Lipscombe, "Neuronal CaV1.3 α 1 L-Type Channels Activate at Relatively Hyperpolarized Membrane Potentials and Are Incompletely Inhibited by Dihydropyridines," *J. Neurosci.*, vol. 21, no. 16, pp. 5944–5951, Aug. 2001, doi: 10.1523/JNEUROSCI.21-16-05944.2001.
- [68] D. C. GERMAN, K. F. MANAYE, P. K. SONSALLA, and B. A. BROOKS, "Midbrain Dopaminergic Cell Loss in Parkinson's Disease and MPTP-Induced Parkinsonism: Sparing of Calbindin-D25k—Containing Cells," *Ann. N. Y. Acad. Sci.*, vol. 648, no. 1, pp. 42–62, May 1992, doi: 10.1111/J.1749-6632.1992.TB24523.X.
- [69] P. Gaspar, N. Ben Jelloun, and A. Febvret, "Sparing of the dopaminergic neurons containing calbindin-D28k and of the dopaminergic mesocortical projections in weaver mutant mice," *Neuroscience*, vol. 61, no. 2, pp. 293–305, 1994, doi: 10.1016/0306-4522(94)90232-1.
- [70] J. Follett, B. Darlow, M. B. Wong, J. Goodwin, and D. L. Pountney, "Potassium depolarization and raised calcium induces α -synuclein aggregates," *Neurotox. Res.*, vol. 23, no. 4, pp. 378–392, May 2013, doi: 10.1007/S12640-012-9366-Z/FIGURES/6.
- [71] A. Mouatt-Prigent, Y. Agid, and E. C. Hirsch, "Does the calcium binding protein calretinin protect dopaminergic neurons against degeneration in Parkinson's disease?," *Brain Res.*, vol. 668, no. 1–2, pp. 62–70, Dec. 1994, doi: 10.1016/0006-8993(94)90511-8.
- [72] M. J. Hurley, B. Brandon, S. M. Gentleman, and D. T. Dexter, "Parkinson's disease is associated with altered expression of CaV1 channels and calcium-binding proteins," *Brain*, vol. 136, no. 7, pp. 2077–2097, Jul. 2013, doi: 10.1093/BRAIN/AWT134.
- [73] S. V. Zaichick, K. M. McGrath, and G. Caraveo, "The role of Ca²⁺ signaling in Parkinson's disease," *Dis. Model. Mech.*, vol. 10, no. 5, p. 519, May 2017, doi: 10.1242/DMM.028738.
- [74] A. Koschak *et al.*, " α 1D (Cav1.3) Subunits Can Form L-type Ca²⁺ Channels

- Activating at Negative Voltages *," *J. Biol. Chem.*, vol. 276, no. 25, pp. 22100–22106, Jun. 2001, doi: 10.1074/JBC.M101469200.
- [75] J. Bendor, T. Logan, R. E.- Neuron, and undefined 2013, "The function of α -synuclein," *Elsevier*, Accessed: Dec. 03, 2021. [Online]. Available: <https://www.sciencedirect.com/science/article/pii/S0896627313008027>.
- [76] V. Lee, J. T.- Neuron, and undefined 2006, "Mechanisms of Parkinson's disease linked to pathological α -synuclein: new targets for drug discovery," *Elsevier*, Accessed: Dec. 03, 2021. [Online]. Available: <https://www.sciencedirect.com/science/article/pii/S0896627306007331>.
- [77] P. H. Weinreb, W. Zhen, A. W. Poon, K. A. Conway, and P. T. Lansbury, "NACP, A Protein Implicated in Alzheimer's Disease and Learning, Is Natively Unfolded†," *Biochemistry*, vol. 35, no. 43, pp. 13709–13715, 1996, doi: 10.1021/BI961799N.
- [78] J. Burré, S. Vivona, J. Diao, M. Sharma, A. T. Brunger, and T. C. Südhof, "Properties of native brain α -synuclein," *Nat. 2013 4987453*, vol. 498, no. 7453, pp. E4–E6, Jun. 2013, doi: 10.1038/nature12125.
- [79] S. Chandra, X. Chen, J. Rizo, R. Jahn, and T. C. Südhof, "A Broken α -Helix in Folded α -Synuclein *," *J. Biol. Chem.*, vol. 278, no. 17, pp. 15313–15318, Apr. 2003, doi: 10.1074/JBC.M213128200.
- [80] J. Burré, M. Sharma, and T. C. Südhof, "Cell Biology and Pathophysiology of α -Synuclein," *Cold Spring Harb. Perspect. Med.*, vol. 8, no. 3, Mar. 2018, doi: 10.1101/CSHPERSPECT.A024091.
- [81] L. D. Bernal-Conde *et al.*, "Alpha-Synuclein Physiology and Pathology: A Perspective on Cellular Structures and Organelles," *Front. Neurosci.*, vol. 13, p. 1399, Jan. 2020, doi: 10.3389/FNINS.2019.01399/BIBTEX.
- [82] J. E. Payton, R. J. Perrin, W. S. Woods, and J. M. George, "Structural Determinants of PLD2 Inhibition by α -Synuclein," *J. Mol. Biol.*, vol. 337, no. 4, pp. 1001–1009, Apr. 2004, doi: 10.1016/J.JMB.2004.02.014.
- [83] J. M. Jenco, A. Rawlingson, B. Daniels, and A. J. Morris, "Regulation of

- Phospholipase D2: Selective Inhibition of Mammalian Phospholipase D Isoenzymes by α - and β -Synuclein[†],” *Biochemistry*, vol. 37, no. 14, pp. 4901–4909, Apr. 1998, doi: 10.1021/BI972776R.
- [84] O. S. Gorbatyuk *et al.*, “ α -synuclein expression in rat substantia nigra suppresses phospholipase D2 toxicity and nigral neurodegeneration,” *Mol. Ther.*, vol. 18, no. 10, pp. 1758–1768, Oct. 2010, doi: 10.1038/MT.2010.137/ATTACHMENT/AB27B0D9-D3EE-480E-8172-FC6564D88C02/MMC5.
- [85] M. M. Ouberai *et al.*, “ α -Synuclein Senses Lipid Packing Defects and Induces Lateral Expansion of Lipids Leading to Membrane Remodeling *,” *J. Biol. Chem.*, vol. 288, no. 29, pp. 20883–20895, Jul. 2013, doi: 10.1074/JBC.M113.478297.
- [86] F. Kamp and K. Beyer, “Binding of α -Synuclein Affects the Lipid Packing in Bilayers of Small Vesicles *,” *J. Biol. Chem.*, vol. 281, no. 14, pp. 9251–9259, Apr. 2006, doi: 10.1074/JBC.M512292200.
- [87] N. Ostrerova *et al.*, “ α -Synuclein Shares Physical and Functional Homology with 14-3-3 Proteins,” *J. Neurosci.*, vol. 19, no. 14, pp. 5782–5791, Jul. 1999, doi: 10.1523/JNEUROSCI.19-14-05782.1999.
- [88] J. M. Souza, B. I. Giasson, Q. Chen, V. M. Y. Lee, and H. Ischiropoulos, “Dityrosine Cross-linking Promotes Formation of Stable α -Synuclein Polymers: IMPLICATION OF NITRATIVE AND OXIDATIVE STRESS IN THE PATHOGENESIS OF NEURODEGENERATIVE SYNUCLEINOPATHIES *,” *J. Biol. Chem.*, vol. 275, no. 24, pp. 18344–18349, Jun. 2000, doi: 10.1074/JBC.M000206200.
- [89] A. Rekas *et al.*, “Interaction of the Molecular Chaperone α B-Crystallin with α -Synuclein: Effects on Amyloid Fibril Formation and Chaperone Activity,” *J. Mol. Biol.*, vol. 340, no. 5, pp. 1167–1183, Jul. 2004, doi: 10.1016/J.JMB.2004.05.054.
- [90] T. D. Kim, S. R. Paik, and C. H. Yang, “Structural and Functional Implications of C-Terminal Regions of α -Synuclein[†],” *Biochemistry*, vol. 41, no. 46, pp. 13782–13790, Nov. 2002, doi: 10.1021/BI026284C.
- [91] T. D. Kim, S. R. Paik, C.-H. Yang, and J. Kim, “Structural changes in α -synuclein

- affect its chaperone-like activity in vitro," *Protein Sci.*, vol. 9, no. 12, pp. 2489–2496, Jan. 2000, doi: 10.1110/PS.9.12.2489.
- [92] M. Ahn, S. B. Kim, M. Kang, Y. Ryu, and T. Doohun Kim, "Chaperone-like activities of α -synuclein: α -Synuclein assists enzyme activities of esterases," *Biochem. Biophys. Res. Commun.*, vol. 346, no. 4, pp. 1142–1149, Aug. 2006, doi: 10.1016/J.BBRC.2006.05.213.
- [93] S. Kanda, J. F. Bishop, M. A. Eglitis, Y. Yang, and M. M. Mouradian, "Enhanced vulnerability to oxidative stress by α -synuclein mutations and C-terminal truncation," *Neuroscience*, vol. 97, no. 2, pp. 279–284, Apr. 2000, doi: 10.1016/S0306-4522(00)00077-4.
- [94] C. A. Da Costa, K. Ancolio, and F. Checler, "Wild-type but Not Parkinson's Disease-related Ala-53 \rightarrow Thr Mutant α -Synuclein Protects Neuronal Cells from Apoptotic Stimuli *," *J. Biol. Chem.*, vol. 275, no. 31, pp. 24065–24069, Aug. 2000, doi: 10.1074/JBC.M002413200.
- [95] S. Yu *et al.*, "Inhibition of tyrosine hydroxylase expression in α -synuclein-transfected dopaminergic neuronal cells," *Neurosci. Lett.*, vol. 367, no. 1, pp. 34–39, Aug. 2004, doi: 10.1016/J.NEULET.2004.05.118.
- [96] R. G. Perez, J. C. Waymire, E. Lin, J. J. Liu, F. Guo, and M. J. Zigmond, "A Role for α -Synuclein in the Regulation of Dopamine Biosynthesis," *J. Neurosci.*, vol. 22, no. 8, pp. 3090–3099, Apr. 2002, doi: 10.1523/JNEUROSCI.22-08-03090.2002.
- [97] E. Masliah *et al.*, "Dopaminergic Loss and Inclusion Body Formation in α -Synuclein Mice: Implications for Neurodegenerative Disorders," *Science (80-.)*, vol. 287, no. 5456, pp. 1265–1269, Feb. 2000, doi: 10.1126/SCIENCE.287.5456.1265.
- [98] D. Kirik *et al.*, "Parkinson-Like Neurodegeneration Induced by Targeted Overexpression of α -Synuclein in the Nigrostriatal System," *J. Neurosci.*, vol. 22, no. 7, pp. 2780–2791, Apr. 2002, doi: 10.1523/JNEUROSCI.22-07-02780.2002.
- [99] M. J. Baptista *et al.*, "Co-ordinate transcriptional regulation of dopamine synthesis genes by α -synuclein in human neuroblastoma cell lines," *J. Neurochem.*, vol. 85, no. 4, pp. 957–968, May 2003, doi: 10.1046/J.1471-4159.2003.01742.X.

- [100] L. Maroteaux, J. T. Campanelli, and R. H. Scheller, "Synuclein: a neuron-specific protein localized to the nucleus and presynaptic nerve terminal," *J. Neurosci.*, vol. 8, no. 8, pp. 2804–2815, Aug. 1988, doi: 10.1523/JNEUROSCI.08-08-02804.1988.
- [101] R. J. Perrin, W. S. Woods, D. F. Clayton, and J. M. George, "Interaction of Human α -Synuclein and Parkinson's Disease Variants with Phospholipids: STRUCTURAL ANALYSIS USING SITE-DIRECTED MUTAGENESIS *," *J. Biol. Chem.*, vol. 275, no. 44, pp. 34393–34398, Nov. 2000, doi: 10.1074/JBC.M004851200.
- [102] J. Burré, M. Sharma, T. Tsetsenis, V. Buchman, M. R. Etherton, and T. C. Südhof, " α -Synuclein promotes SNARE-complex assembly in vivo and in vitro," *Science (80-.)*, vol. 329, no. 5999, pp. 1663–1667, 2010, doi: 10.1126/science.1195227.
- [103] D. L. Fortin, V. M. Nemani, S. M. Voglmaier, M. D. Anthony, T. A. Ryan, and R. H. Edwards, "Neural Activity Controls the Synaptic Accumulation of α -Synuclein," *J. Neurosci.*, vol. 25, no. 47, pp. 10913–10921, Nov. 2005, doi: 10.1523/JNEUROSCI.2922-05.2005.
- [104] L. Wang, U. Das, D. A. Scott, Y. Tang, P. J. McLean, and S. Roy, " α -Synuclein multimers cluster synaptic vesicles and attenuate recycling," *Curr. Biol.*, vol. 24, no. 19, pp. 2319–2326, Oct. 2014, doi: 10.1016/J.CUB.2014.08.027/ATTACHMENT/89F262AE-5A35-4D2E-9880-2E967399077E/MMC1.PDF.
- [105] J. Burré, M. Sharma, and T. C. Südhof, " α -Synuclein assembles into higher-order multimers upon membrane binding to promote SNARE complex formation," *Proc. Natl. Acad. Sci. U. S. A.*, vol. 111, no. 40, pp. E4274–E4283, Oct. 2014, doi: 10.1073/PNAS.1416598111/-/DCSUPPLEMENTAL.
- [106] S. Paillusson, T. Clairembault, M. Biraud, M. Neunlist, and P. Derkinderen, "Activity-dependent secretion of alpha-synuclein by enteric neurons," *J. Neurochem.*, vol. 125, no. 4, pp. 512–517, May 2013, doi: 10.1111/JNC.12131.
- [107] H. J. Lee, S. Patel, and S. J. Lee, "Intravesicular Localization and Exocytosis of α -Synuclein and its Aggregates," *J. Neurosci.*, vol. 25, no. 25, pp. 6016–6024, Jun. 2005, doi: 10.1523/JNEUROSCI.0692-05.2005.

- [108] W. Zhang *et al.*, "Aggregated α -synuclein activates microglia: a process leading to disease progression in Parkinson's disease," *FASEB J.*, vol. 19, no. 6, pp. 533–542, Apr. 2005, doi: 10.1096/FJ.04-2751COM.
- [109] J. Y. Sung, J. Kim, S. R. Paik, J. H. Park, Y. S. Ahn, and K. C. Chung, "Induction of Neuronal Cell Death by Rab5A-dependent Endocytosis of α -Synuclein *," *J. Biol. Chem.*, vol. 276, no. 29, pp. 27441–27448, Jul. 2001, doi: 10.1074/JBC.M101318200.
- [110] K. J. Ahn, S. R. Paik, K. C. Chung, and J. Kim, "Amino acid sequence motifs and mechanistic features of the membrane translocation of α -synuclein," *J. Neurochem.*, vol. 97, no. 1, pp. 265–279, Apr. 2006, doi: 10.1111/J.1471-4159.2006.03731.X.
- [111] K. A. Conway, S.-J. Lee, J.-C. Rochet, T. T. Ding, R. E. Williamson, and P. T. Lansbury, "Acceleration of oligomerization, not fibrillization, is a shared property of both α -synuclein mutations linked to early-onset Parkinson's disease: implications for," *Natl. Acad. Sci.*, Accessed: Dec. 03, 2021. [Online]. Available: <https://www.pnas.org/content/97/2/571.short>.
- [112] T. T. Ding, S. J. Lee, J. C. Rochet, and P. T. Lansbury, "Annular α -Synuclein Protofibrils Are Produced When Spherical Protofibrils Are Incubated in Solution or Bound to Brain-Derived Membranes[†]," *Biochemistry*, vol. 41, no. 32, pp. 10209–10217, Aug. 2002, doi: 10.1021/BI020139H.
- [113] Z. S. Martin *et al.*, " α -Synuclein oligomers oppose long-term potentiation and impair memory through a calcineurin-dependent mechanism: Relevance to human synucleopathic diseases," *J. Neurochem.*, vol. 120, no. 3, pp. 440–452, 2012, doi: 10.1111/j.1471-4159.2011.07576.x.
- [114] H. G. Wang *et al.*, "Ca²⁺-induced apoptosis through calcineurin dephosphorylation of BAD," *Science*, vol. 284, no. 5412, pp. 339–343, Apr. 1999, doi: 10.1126/SCIENCE.284.5412.339.
- [115] K. C. Luk *et al.*, "Exogenous α -synuclein fibrils seed the formation of Lewy body-like intracellular inclusions in cultured cells," *Natl. Acad. Sci.*, Accessed: Dec. 03,

2021. [Online]. Available: <https://www.pnas.org/content/106/47/20051.short>.
- [116] L. Volpicelli-Daley, K. Luk, T. Patel, S. T.- Neuron, and undefined 2011, "Exogenous α -synuclein fibrils induce Lewy body pathology leading to synaptic dysfunction and neuron death," *Elsevier*, Accessed: Dec. 03, 2021. [Online]. Available: <https://www.sciencedirect.com/science/article/pii/S0896627311008440>.
- [117] S. Blumenstock *et al.*, "Seeding and transgenic overexpression of alpha-synuclein triggers dendritic spine pathology in the neocortex," *EMBO Mol. Med.*, vol. 9, no. 5, pp. 716–731, May 2017, doi: 10.15252/EMMM.201607305.
- [118] J. M. Froula *et al.*, " α -Synuclein fibril-induced paradoxical structural and functional defects in hippocampal neurons," *Acta Neuropathol. Commun.*, vol. 6, no. 1, p. 35, May 2018, doi: 10.1186/S40478-018-0537-X.
- [119] B. A. Hijaz and L. A. Volpicelli-Daley, "Initiation and propagation of α -synuclein aggregation in the nervous system," *Mol. Neurodegener.*, vol. 15, no. 1, pp. 1–12, Mar. 2020, doi: 10.1186/S13024-020-00368-6/FIGURES/2.
- [120] W. Peelaerts, L. Bousset, A. V. der P.- Nature, and undefined 2015, " α -Synuclein strains cause distinct synucleinopathies after local and systemic administration," *nature.com*, Accessed: Dec. 03, 2021. [Online]. Available: https://idp.nature.com/authorize/casa?redirect_uri=https://www.nature.com/articles/nature14547&casa_token=3DEpwQaBVusAAAAA:uXlycTMqBdXm7GzBVTvXog_eWHT1X1vS0SV6PI7xk_uNr9ugAdpkkKxEqvJqOfyDi7-QwTLi7rRRKaQD.
- [121] S. Kim, S. Kwon, T. Kam, N. P.- Neuron, and undefined 2019, "Transneuronal propagation of pathologic α -synuclein from the gut to the brain models Parkinson's disease," *Elsevier*, Accessed: Dec. 03, 2021. [Online]. Available: <https://www.sciencedirect.com/science/article/pii/S089662731930488X>.
- [122] J. I. Ayers *et al.*, "Robust Central Nervous System Pathology in Transgenic Mice following Peripheral Injection of α -Synuclein Fibrils," *J. Virol.*, vol. 91, no. 2, pp. 2095–2111, Jan. 2017, doi: 10.1128/JVI.02095-16/ASSET/EBB6D5FE-0586-4077-91CD-81284302C2BF/ASSETS/GRAPHIC/ZJV9991822800006.JPEG.

- [123] B. K. Choi *et al.*, "Large α -synuclein oligomers inhibit neuronal SNARE-mediated vesicle docking," *Proc. Natl. Acad. Sci. U. S. A.*, vol. 110, no. 10, pp. 4087–4092, Mar. 2013, doi: 10.1073/PNAS.1218424110/-/DCSUPPLEMENTAL/PNAS.201218424SI.PDF.
- [124] P. Desplats *et al.*, "Inclusion formation and neuronal cell death through neuron-to-neuron transmission of alpha-synuclein," *Proc. Natl. Acad. Sci. U. S. A.*, vol. 106, no. 31, pp. 13010–13015, Aug. 2009, doi: 10.1073/PNAS.0903691106.
- [125] N. L. Rey, G. H. Petit, L. Bousset, R. Melki, and P. Brundin, "Transfer of human α -synuclein from the olfactory bulb to interconnected brain regions in mice," *Acta Neuropathol.*, vol. 126, no. 4, p. 555, Oct. 2013, doi: 10.1007/S00401-013-1160-3.
- [126] K. C. Luk *et al.*, "Pathological α -Synuclein Transmission Initiates Parkinson-like Neurodegeneration in Non-transgenic Mice," *Science*, vol. 338, no. 6109, p. 949, Nov. 2012, doi: 10.1126/SCIENCE.1227157.
- [127] J. Pruzak, L. Just, O. Isacson, and G. Nikkhah, "Isolation and Culture of Ventral Mesencephalic Precursor Cells and Dopaminergic Neurons from Rodent Brains," *Curr. Protoc. Stem Cell Biol.*, vol. 11, no. 1, pp. 2D.5.1-2D.5.21, Dec. 2009, doi: 10.1002/9780470151808.SC02D05S11.
- [128] N. Matsushita, H. Okada, Y. Yasoshima, K. Takahashi, K. Kiuchi, and K. Kobayashi, "Dynamics of tyrosine hydroxylase promoter activity during midbrain dopaminergic neuron development," *J. Neurochem.*, vol. 82, no. 2, pp. 295–304, 2002, doi: 10.1046/J.1471-4159.2002.00972.X/FORMAT/PDF.
- [129] K. Sawamoto *et al.*, "Generation of Dopaminergic Neurons in the Adult Brain from Mesencephalic Precursor Cells Labeled with a nestin-GFP Transgene," *J. Neurosci.*, vol. 21, no. 11, p. 3895, Jun. 2001, doi: 10.1523/JNEUROSCI.21-11-03895.2001.
- [130] C. W. Hui, Y. Zhang, and K. Herrup, "Non-Neuronal Cells Are Required to Mediate the Effects of Neuroinflammation: Results from a Neuron-Enriched Culture System," *PLoS One*, vol. 11, no. 1, Jan. 2016, doi: 10.1371/JOURNAL.PONE.0147134.
- [131] P. H. Patterson and L. L. Y. Chun, "The Influence of Non-Neuronal Cells on

- Catecholamine and Acetylcholine Synthesis and Accumulation in Cultures of Dissociated Sympathetic Neurons (cell culture/cell-cell interaction),” vol. 71, no. 9, pp. 3607–3610, 1974.
- [132] T. Fath, Y. D. Ke, P. Gunning, J. Götz, and L. M. Ittner, “Primary support cultures of hippocampal and substantia nigra neurons,” *Nat. Protoc.* 2009 41, vol. 4, no. 1, pp. 78–85, Dec. 2008, doi: 10.1038/nprot.2008.199.
- [133] C. Solsona, B. Innocenti, and J. M. Fernández, “Regulation of exocytotic fusion by cell inflation,” *Biophys. J.*, vol. 74, no. 2 Pt 1, pp. 1061–1073, 1998, doi: 10.1016/S0006-3495(98)74030-5.
- [134] L. J. Gentet, G. J. Stuart, J. D. Clements, and J. Curtin, “Direct Measurement of Specific Membrane Capacitance in Neurons,” *Biophys. J.*, vol. 79, pp. 314–320, 2000, doi: 10.1016/S0006-3495(00)76293-X.
- [135] P. Chen and K. D. Gillis, “The noise of membrane capacitance measurements in the whole-cell recording configuration,” *Biophys. J.*, vol. 79, no. 4, pp. 2162–2170, 2000, doi: 10.1016/S0006-3495(00)76464-2.
- [136] T. Sakaba, A. Hazama, and Y. Maruyama, “Patch-Clamp Capacitance Measurements,” pp. 277–286, 2012, doi: 10.1007/978-4-431-53993-3_17.
- [137] K. D. Gillis, “Techniques for Membrane Capacitance Measurements,” *Single-Channel Rec.*, pp. 155–198, 1995, doi: 10.1007/978-1-4419-1229-9_7.
- [138] M. Lindau and E. Neher, “Patch-clamp techniques for time-resolved capacitance measurements in single cells,” *Pflügers Arch.* 1988 4112, vol. 411, no. 2, pp. 137–146, Feb. 1988, doi: 10.1007/BF00582306.
- [139] C. G. Zoski, “Handbook of electrochemistry,” *Handb. Electrochem.*, 2007, doi: 10.1016/B978-0-444-51958-0.X5000-9.
- [140] “Electrochemical Methods: Fundamentals and Applications, 2nd Edition | Wiley.” <https://www.wiley.com/en-be/Electrochemical+Methods:+Fundamentals+and+Applications,+2nd+Edition-p-9780471043720> (accessed Nov. 26, 2021).

- [141] D. J. Chesney, "Laboratory Techniques in Electroanalytical Chemistry, 2nd Edition Edited by Peter T. Kissinger and William R. Heineman.," *J. Am. Chem. Soc.*, vol. 118, no. 44, pp. 10946–10946, 1996, Accessed: Nov. 26, 2021. [Online]. Available: <https://www.hoepli.it/libro/laboratory-techniques-in-electroanalytical-chemistry-second-edition-revised-and-expanded/9780824794453.html>.
- [142] A. J. Bard and L. R. Faulkner, "Basic Potential Step Methods," *Electrochem. Methods Fundam. Appl.*, pp. 156–225, Dec. 2001, Accessed: Mar. 24, 2022. [Online]. Available: <https://books.google.com.mx/books?id=kv56QgAACAAJ>.
- [143] M. J. O'Donovan, "The origin of spontaneous activity in developing networks of the vertebrate nervous system," *Curr. Opin. Neurobiol.*, vol. 9, no. 1, pp. 94–104, Feb. 1999, doi: 10.1016/S0959-4388(99)80012-9.
- [144] S. J. Eglén, E. Cotterill, and S. J. Eglén, "Burst detection methods CMA Cumulative Moving Average IQR Inter-Quartile Range IRT ISI Rank Threshold ISI InterSpike Interval LTD Long Term Depression LTP Long Term Potentiation MEA MultiElectrode Array MI Max Interval PS Poisson Surprise RS Rank Surprise," *Adv. Neurobiol.*, vol. 22, pp. 185–206, 2018.
- [145] E. Cotterill, P. Charlesworth, C. W. Thomas, O. Paulsen, and S. J. Eglén, "A comparison of computational methods for detecting bursts in neuronal spike trains and their application to human stem cell-derived neuronal networks," *J. Neurophysiol.*, vol. 116, no. 2, pp. 306–321, Aug. 2016, doi: 10.1152/JN.00093.2016/ASSET/IMAGES/LARGE/Z9K0071637090008.JPEG.
- [146] M. Abeles, "Quantification, smoothing, and confidence limits for single-units' histograms," *J. Neurosci. Methods*, 1982, doi: 10.1016/0165-0270(82)90002-4.
- [147] I. Sugihara, E. J. Lang, and R. Llinás, "Serotonin Modulation of Inferior Olivary Oscillations and Synchronicity: A Multiple-electrode Study in the Rat Cerebellum," *Eur. J. Neurosci.*, vol. 7, no. 4, pp. 521–534, 1995, doi: 10.1111/j.1460-9568.1995.tb00657.x.
- [148] X. Liu, Y. Tong, and P. P. Fang, "Recent development in amperometric measurements of vesicular exocytosis," *TrAC Trends Anal. Chem.*, vol. 113, pp.

- 13–24, Apr. 2019, doi: 10.1016/J.TRAC.2019.01.013.
- [149] R. M. Wightman *et al.*, “Temporally resolved catecholamine spikes correspond to single vesicle release from individual chromaffin cells,” *Proc. Natl. Acad. Sci.*, vol. 88, no. 23, pp. 10754–10758, Dec. 1991, doi: 10.1073/PNAS.88.23.10754.
- [150] E. N. Pothos, V. Davila, and D. Sulzer, “Presynaptic Recording of Quanta from Midbrain Dopamine Neurons and Modulation of the Quantal Size,” 1998.
- [151] F. Picollo *et al.*, “All-carbon multi-electrode array for real-time in vitro measurements of oxidizable neurotransmitters,” *Sci. Reports 2016 61*, vol. 6, no. 1, pp. 1–8, Feb. 2016, doi: 10.1038/srep20682.
- [152] F. Picollo *et al.*, “Development and characterization of a diamond-insulated graphitic multi electrode array realized with ion beam lithography,” *Sensors (Switzerland)*, vol. 15, no. 1, pp. 515–528, Aug. 2016, doi: 10.3390/s150100515.
- [153] P. Olivero *et al.*, “Direct fabrication of three-dimensional buried conductive channels in single crystal diamond with ion microbeam induced graphitization,” *Diam. Relat. Mater.*, vol. 18, no. 5–8, pp. 870–876, May 2009, doi: 10.1016/J.DIAMOND.2008.10.068.
- [154] F. Picollo *et al.*, “Fabrication and electrical characterization of three-dimensional graphitic microchannels in single crystal diamond,” *New J. Phys.*, vol. 14, May 2012, doi: 10.1088/1367-2630/14/5/053011.
- [155] F. Picollo *et al.*, “A New Diamond Biosensor with Integrated Graphitic Microchannels for Detecting Quantal Exocytic Events from Chromaffin Cells,” *Adv. Mater.*, vol. 25, no. 34, pp. 4696–4700, Sep. 2013, doi: 10.1002/ADMA.201300710.
- [156] V. Carabelli *et al.*, “Nanocrystalline diamond microelectrode arrays fabricated on sapphire technology for high-time resolution of quantal catecholamine secretion from chromaffin cells,” *Biosens. Bioelectron.*, vol. 26, no. 1, pp. 92–98, Sep. 2010, doi: 10.1016/J.BIOS.2010.05.017.
- [157] G. Tomagra *et al.*, “Simultaneous multisite detection of quantal release from PC12

- cells using micro graphitic-diamond multi electrode arrays," *Biophys. Chem.*, vol. 253, 2019, doi: 10.1016/j.bpc.2019.106241.
- [158] G. Tomagra *et al.*, "Diamond-based multi electrode arrays for monitoring neurotransmitter release," *Lect. Notes Electr. Eng.*, vol. 539, pp. 125–134, 2019, doi: 10.1007/978-3-030-04324-7_17.
- [159] S. Ditalia Tchernij *et al.*, "Electrical characterization of a graphite-diamond-graphite junction fabricated by MeV carbon implantation," *Diam. Relat. Mater.*, vol. C, no. 74, pp. 125–131, Apr. 2017, doi: 10.1016/J.DIAMOND.2017.02.019.
- [160] M. G. Lacey, N. B. Mercuri, and R. A. North, "Two cell types in rat substantia nigra zona compacta distinguished by membrane properties and the actions of dopamine and opioids," *J. Neurosci.*, 1989, doi: 10.1523/jneurosci.09-04-01233.1989.
- [161] J. Roeper, "Dissecting the diversity of midbrain dopamine neurons," *Trends Neurosci.*, vol. 36, no. 6, pp. 336–342, Jun. 2013, doi: 10.1016/J.TINS.2013.03.003.
- [162] E. B. Margolis, A. R. Coker, J. R. Driscoll, A.-I. Lemaître, and H. L. Fields, "Reliability in the Identification of Midbrain Dopamine Neurons," *PLoS One*, vol. 5, no. 12, p. e15222, 2010, doi: 10.1371/JOURNAL.PONE.0015222.
- [163] H. Kita, "Parvalbumin-immunopositive neurons in rat globus pallidus: a light and electron microscopic study," *Brain Res.*, vol. 657, no. 1–2, pp. 31–41, Sep. 1994, doi: 10.1016/0006-8993(94)90950-4.
- [164] S. ID and G. AA, "Role of the subthalamic nucleus in the regulation of nigral dopamine neuron activity," *Synapse*, vol. 12, no. 4, pp. 287–303, 1992, doi: 10.1002/SYN.890120406.
- [165] Y. Smith and J. P. Bolam, "The output neurones and the dopaminergic neurones of the substantia nigra receive a GABA-Containing input from the globus pallidus in the rat," *J. Comp. Neurol.*, vol. 296, no. 1, pp. 47–64, Jun. 1990, doi: 10.1002/CNE.902960105.
- [166] T. Yamaguchi, H.-L. Wang, X. Li, T. H. Ng, and M. Morales, "Mesocorticolimbic

- Glutamatergic Pathway," *J. Neurosci.*, vol. 31, no. 23, pp. 8476–8490, Jun. 2011, doi: 10.1523/JNEUROSCI.1598-11.2011.
- [167] C. Gold, D. A. Henze, C. Koch, and G. Buzsáki, "On the origin of the extracellular action potential waveform: A modeling study," *J. Neurophysiol.*, vol. 95, no. 5, pp. 3113–3128, 2006, doi: 10.1152/jn.00979.2005.
- [168] A. N. Opalka, W. qiang Huang, J. Liu, H. Liang, and D. V. Wang, "Hippocampal Ripple Coordinates Retrosplenial Inhibitory Neurons during Slow-Wave Sleep," *Cell Rep.*, vol. 30, no. 2, pp. 432-441.e3, 2020, doi: 10.1016/j.celrep.2019.12.038.
- [169] R. Maex, B. P. Vos, and E. De Schutter, "Weak common parallel fibre synapses explain the loose synchrony observed between rat cerebellar Golgi cells," *J. Physiol.*, 2000, doi: 10.1111/j.1469-7793.2000.t01-1-00175.x.
- [170] F. Zeldenrust, W. J. Wadman, and B. Englitz, "Neural coding with bursts—Current state and future perspectives," *Front. Comput. Neurosci.*, vol. 12, no. July, pp. 1–14, 2018, doi: 10.3389/fncom.2018.00048.
- [171] J. M. Tepper and C. R. Lee, "GABAergic control of substantia nigra dopaminergic neurons," *Progress in Brain Research*. 2007, doi: 10.1016/S0079-6123(06)60011-3.
- [172] L. Chen, Y. Deng, W. Luo, Z. Wang, and S. Zeng, "Detection of bursts in neuronal spike trains by the mean inter-spike interval method," *Prog. Nat. Sci.*, vol. 19, no. 2, pp. 229–235, Feb. 2009, doi: 10.1016/J.PNSC.2008.05.027.
- [173] R. J. I. N, and K. ST, "Electrophysiological characteristics of substantia nigra neurons in organotypic cultures: spontaneous and evoked activities," *Neuroscience*, vol. 97, no. 4, pp. 703–714, 2000, doi: 10.1016/S0306-4522(00)00046-4.
- [174] J. M. Tepper, L. P. Martin, and D. R. Anderson, "GABAA receptor-mediated inhibition of rat substantia nigra dopaminergic neurons by pars reticulata projection neurons," *J. Neurosci.*, vol. 15, no. 4, pp. 3092–3103, Apr. 1995, doi: 10.1523/JNEUROSCI.15-04-03092.1995.
- [175] S. Prisco, S. Natoli, G. Bernardi, and N. B. Mercuri, "Group I metabotropic

- glutamate receptors activate burst firing in rat midbrain dopaminergic neurons,” *Neuropharmacology*, vol. 42, pp. 289–296, 2002, Accessed: Dec. 21, 2021. [Online]. Available: www.elsevier.com/locate/neuropharm.
- [176] Guang Jian Wang, R. D. Randall, and S. A. Thayer, “Glutamate-induced intracellular acidification of cultured hippocampal neurons demonstrates altered energy metabolism resulting from Ca²⁺ loads,” <https://doi.org/10.1152/jn.1994.72.6.2563>, vol. 72, no. 6, pp. 2563–2569, 1994, doi: 10.1152/JN.1994.72.6.2563.
- [177] S. W. Johnson, V. Seutin, and R. A. North, “Burst Firing in Dopamine Neurons Induced by N-Methyl-D-aspartate: Role of Electrogenic Sodium Pump,” *Science (80-.)*, vol. 258, no. 5082, pp. 665–667, Oct. 1992, doi: 10.1126/SCIENCE.1329209.
- [178] J. Rohrbacher, N. Ichinohe, and S. T. Kitai, “Electrophysiological characteristics of substantia nigra neurons in organotypic cultures: spontaneous and evoked activities,” *Neuroscience*, vol. 97, no. 4, pp. 703–714, 2000, doi: 10.1016/S0306-4522(00)00046-4.
- [179] A. Dobi, E. B. Margolis, H. L. Wang, B. K. Harvey, and M. Morales, “Glutamatergic and Nonglutamatergic Neurons of the Ventral Tegmental Area Establish Local Synaptic Contacts with Dopaminergic and Nondopaminergic Neurons,” *J. Neurosci.*, vol. 30, no. 1, p. 218, Jan. 2010, doi: 10.1523/JNEUROSCI.3884-09.2010.
- [180] D. Poli, V. P. Pastore, and P. Massobrio, “Functional connectivity in in vitro neuronal assemblies,” *Front. Neural Circuits*, vol. 9, no. OCT, p. 57, Oct. 2015, doi: 10.3389/FNCIR.2015.00057.
- [181] A. W. Wiegner and M. M. Wierzbicka, “A method for assessing significance of peaks in cross-correlation histograms,” *J. Neurosci. Methods*, vol. 22, no. 2, pp. 125–131, 1987, doi: [https://doi.org/10.1016/0165-0270\(87\)90006-9](https://doi.org/10.1016/0165-0270(87)90006-9).
- [182] C. Shen, “Analysis of detrended time-lagged cross-correlation between two nonstationary time series,” *Phys. Lett. A*, vol. 379, no. 7, pp. 680–687, Mar. 2015, doi: 10.1016/J.PHYSLETA.2014.12.036.

- [183] “Cross correlation.”
https://www.usna.edu/Users/oceano/pguth/md_help/html/time0alq.htm
(accessed Dec. 17, 2021).
- [184] J. D. Olden and B. D. Neff, “Cross-correlation bias in lag analysis of aquatic time series.”
- [185] D. Gavello, J. Rojo-Ruiz, A. Marcantoni, C. Franchino, E. Carbone, and V. Carabelli, “Leptin counteracts the hypoxia-induced inhibition of spontaneously firing hippocampal neurons: A microelectrode array study,” *PLoS One*, vol. 7, no. 7, Jul. 2012, doi: 10.1371/JOURNAL.PONE.0041530.
- [186] A. Peyrache *et al.*, “Spatiotemporal dynamics of neocortical excitation and inhibition during human sleep,” *Proc. Natl. Acad. Sci. U. S. A.*, vol. 109, no. 5, pp. 1731–1736, 2012, doi: 10.1073/pnas.1109895109.
- [187] E. Cohen, M. Ivenshitz, V. Amor-Baroukh, V. Greenberger, and M. Segal, “Determinants of spontaneous activity in networks of cultured hippocampus,” *Brain Res.*, 2008, doi: 10.1016/j.brainres.2008.06.022.
- [188] E. F. Vastola, “Biological signal detection by the autocorrelogram and a recurrence frequency method,” *Electroencephalogr. Clin. Neurophysiol.*, vol. 40, no. 1, pp. 89–96, Jan. 1976, doi: 10.1016/0013-4694(76)90182-6.
- [189] J. Lautenschläger, C. F. Kaminski, and G. S. Kaminski Schierle, “ α -Synuclein – Regulator of Exocytosis, Endocytosis, or Both?,” *Trends Cell Biol.*, vol. 27, no. 7, pp. 468–479, Jul. 2017, doi: 10.1016/J.TCB.2017.02.002.
- [190] K. J. Vargas, S. Makani, T. Davis, C. H. Westphal, P. E. Castillo, and S. S. Chandra, “Synucleins Regulate the Kinetics of Synaptic Vesicle Endocytosis,” *J. Neurosci.*, vol. 34, no. 28, pp. 9364–9376, Jul. 2014, doi: 10.1523/JNEUROSCI.4787-13.2014.
- [191] M. T. Lin and M. F. Beal, “Mitochondrial dysfunction and oxidative stress in neurodegenerative diseases,” *Nature*, vol. 443, no. 7113, pp. 787–795, Oct. 2006, doi: 10.1038/NATURE05292.
- [192] M. R. Cookson and M. Van Der Brug, “Building 35, Room 1A116, MSC 3707, 35

- Convent Drive," *Exp Neurol*, vol. 209, no. 1, pp. 5–11, 2008.
- [193] J. T. Bendor, T. P. Logan, and R. H. Edwards, "The Function of α -Synuclein," *Neuron*, vol. 79, no. 6, pp. 1044–1066, Sep. 2013, doi: 10.1016/J.NEURON.2013.09.004.
- [194] M. X. Henderson, J. Q. Trojanowski, and V. M. Y. Lee, "alpha-Synuclein Pathology in Parkinson's Disease and Related alpha-Synucleinopathies," *Neurosci. Lett.*, vol. 709, p. 134316, Sep. 2019, doi: 10.1016/J.NEULET.2019.134316.
- [195] L. A. Volpicelli-Daley *et al.*, "Exogenous α -synuclein fibrils induce Lewy body pathology leading to synaptic dysfunction and neuron death," *Neuron*, vol. 72, no. 1, pp. 57–71, Oct. 2011, doi: 10.1016/J.NEURON.2011.08.033.
- [196] G. C. Hassink *et al.*, "Exogenous α -synuclein hinders synaptic communication in cultured cortical primary rat neurons," *PLoS One*, vol. 13, no. 3, Mar. 2018, doi: 10.1371/JOURNAL.PONE.0193763.
- [197] A. Tozzi *et al.*, "Alpha-Synuclein Produces Early Behavioral Alterations via Striatal Cholinergic Synaptic Dysfunction by Interacting With GluN2D N-Methyl-D-Aspartate Receptor Subunit," *Biol. Psychiatry*, vol. 79, no. 5, pp. 402–414, 2016, doi: 10.1016/j.biopsych.2015.08.013.
- [198] F. van Diggelen *et al.*, "Two conformationally distinct α -synuclein oligomers share common epitopes and the ability to impair long-term potentiation," *PLoS One*, vol. 14, no. 3, p. e0213663, Mar. 2019, doi: 10.1371/JOURNAL.PONE.0213663.
- [199] G. Bhak *et al.*, "Morphological Evaluation of Meta-stable Oligomers of α -Synuclein with Small-Angle Neutron Scattering," *Sci. Reports 2018 81*, vol. 8, no. 1, pp. 1–10, Sep. 2018, doi: 10.1038/s41598-018-32655-0.
- [200] S. Emadi, S. Kasturirangan, M. S. Wang, P. Schulz, and M. R. Sierks, "Detecting Morphologically Distinct Oligomeric Forms of α -Synuclein," *J. Biol. Chem.*, vol. 284, no. 17, p. 11048, Apr. 2009, doi: 10.1074/JBC.M806559200.
- [201] A. Mendyk, P. K. Tuszyński, S. Polak, and R. Jachowicz, "Generalized in vitro-in vivo relationship (IVIVR) model based on artificial neural networks," *Drug Des. Devel.*

- Ther.*, vol. 7, pp. 223–232, 2013, doi: 10.2147/DDDT.S41401.
- [202] G. La Camera, M. Giugliano, W. Senn, and S. Fusi, “The response of cortical neurons to in vivo-like input current: Theory and experiment: I. Noisy inputs with stationary statistics,” *Biol. Cybern.*, vol. 99, no. 4–5, pp. 279–301, Nov. 2008, doi: 10.1007/S00422-008-0272-7.
- [203] W. A. Catterall and A. P. Few, “Calcium Channel Regulation and Presynaptic Plasticity,” *Neuron*, vol. 59, no. 6, pp. 882–901, Sep. 2008, doi: 10.1016/J.NEURON.2008.09.005.
- [204] R. E. Westenbroek, J. W. Hell, C. Warner, S. J. Dubel, T. P. Snutch, and W. A. Catterall, “Biochemical properties and subcellular distribution of an N-type calcium channel $\alpha 1$ subunit,” *Neuron*, vol. 9, no. 6, pp. 1099–1115, Dec. 1992, doi: 10.1016/0896-6273(92)90069-P.
- [205] G. W. Zamponi, J. Striessnig, A. Koschak, and A. C. Dolphin, “The physiology, pathology, and pharmacology of voltage-gated calcium channels and their future therapeutic potential,” *Pharmacol. Rev.*, vol. 67, no. 4, pp. 821–870, 2015, doi: 10.1124/pr.114.009654.
- [206] G. Ronzitti *et al.*, “Exogenous α -Synuclein Decreases Raft Partitioning of Cav2.2 Channels Inducing Dopamine Release,” *J. Neurosci.*, vol. 34, no. 32, p. 10603, Aug. 2014, doi: 10.1523/JNEUROSCI.0608-14.2014.
- [207] G. Ronzitti, G. Bucci, G. Stephens, and E. Chieregatti, “Raft-partitioning of calcium channels regulates their function,” *Channels*, vol. 9, no. 4, pp. 169–170, 2015, doi: 10.1080/19336950.2015.1063285.
- [208] A. Adamczyk and J. B. Strosznajder, “Alpha-synuclein potentiates Ca^{2+} influx through voltage-dependent Ca^{2+} channels,” *Neuroreport*, vol. 17, no. 18, pp. 1883–1886, Dec. 2006, doi: 10.1097/WNR.0B013E3280115185.
- [209] J. Striessnig, A. Pinggera, G. Kaur, G. Bock, and P. Tuluc, “L-type Ca^{2+} channels in heart and brain,” *Wiley Interdiscip. Rev. Membr. Transp. Signal.*, vol. 3, no. 2, p. 15, Mar. 2014, doi: 10.1002/WMTS.102.

- [210] Y. Liu *et al.*, “Ca v 1.2 and Ca v 1.3 L-type calcium channels regulate dopaminergic firing activity in the mouse ventral tegmental area,” *J Neurophysiol*, vol. 112, pp. 1119–1130, 2014, doi: 10.1152/jn.00757.2013.-Dopaminergic.
- [211] C. Catoni, T. Calì, and M. Brini, “Calcium, Dopamine and Neuronal Calcium Sensor 1: Their Contribution to Parkinson’s Disease,” *Front. Mol. Neurosci.*, vol. 0, p. 55, Feb. 2019, doi: 10.3389/FNMOL.2019.00055.
- [212] J. N. Guzman *et al.*, “Systemic isradipine treatment diminishes calcium-dependent mitochondrial oxidant stress,” *J. Clin. Invest.*, vol. 128, no. 6, pp. 2266–2280, Jun. 2018, doi: 10.1172/JCI95898.
- [213] B. Liss and J. Striessnig, “The Potential of L-Type Calcium Channels as a Drug Target for Neuroprotective Therapy in Parkinson’s Disease,” *Annu. Rev. Pharmacol. Toxicol.*, vol. 59, no. 1, pp. 263–289, Jan. 2019, doi: 10.1146/annurev-pharmtox-010818-021214.
- [214] R. C. Evans, M. Zhu, and Z. M. Khaliq, “Dopamine Inhibition Differentially Controls Excitability of Substantia Nigra Dopamine Neuron Subpopulations through T-Type Calcium Channels,” *J. Neurosci.*, vol. 37, no. 13, pp. 3704–3720, Mar. 2017, doi: 10.1523/JNEUROSCI.0117-17.2017.
- [215] S. Y. Branch, R. Sharma, and M. J. Beckstead, “Aging Decreases L-Type Calcium Channel Currents and Pacemaker Firing Fidelity in Substantia Nigra Dopamine Neurons,” *J. Neurosci.*, vol. 34, no. 28, p. 9310, 2014, doi: 10.1523/JNEUROSCI.4228-13.2014.
- [216] F. Philippart, G. Destreel, P. Merino-Sepúlveda, P. Henny, D. Engel, and V. Seutin, “Differential Somatic Ca²⁺ Channel Profile in Midbrain Dopaminergic Neurons,” *J. Neurosci.*, vol. 36, no. 27, pp. 7234–7245, Jul. 2016, doi: 10.1523/JNEUROSCI.0459-16.2016.
- [217] J. N. Guzman *et al.*, “Oxidant stress evoked by pacemaking in dopaminergic neurons is attenuated by DJ-1,” *Nature*, vol. 468, no. 7324, pp. 696–700, Dec. 2010, doi: 10.1038/NATURE09536.
- [218] A. J. Laude and A. W. M. Simpson, “Compartmentalized signalling: Ca²⁺

- compartments, microdomains and the many facets of Ca²⁺ signalling,” *FEBS J.*, vol. 276, no. 7, pp. 1800–1816, Apr. 2009, doi: 10.1111/J.1742-4658.2009.06927.X.
- [219] D. J. Surmeier, J. N. Guzman, J. Sanchez-Padilla, and J. A. Goldberg, “The origins of oxidant stress in parkinson’s disease and therapeutic strategies,” *Antioxidants and Redox Signaling*, vol. 14, no. 7. Mary Ann Liebert, Inc. 140 Huguenot Street, 3rd Floor New Rochelle, NY 10801 USA , pp. 1289–1301, Apr. 01, 2011, doi: 10.1089/ars.2010.3521.
- [220] N. J. Ortner *et al.*, “Lower affinity of isradipine for L-type Ca²⁺ channels during substantia nigra dopamine neuron-like activity: Implications for neuroprotection in parkinson’s disease,” *J. Neurosci.*, vol. 37, no. 28, pp. 6761–6777, Jul. 2017, doi: 10.1523/JNEUROSCI.2946-16.2017.
- [221] T. S. Anekonda, J. F. Quinn, C. Harris, K. Frahler, T. L. Wadsworth, and R. L. Woltjer, “L-type voltage-gated calcium channel blockade with isradipine as a therapeutic strategy for Alzheimer’s disease,” *Neurobiol Dis*, vol. 41, no. 1, pp. 62–70, 2011, doi: 10.1016/j.nbd.2010.08.020.
- [222] P. Durante, C. G. Cardenas, J. A. Whittaker, S. T. Kitai, and R. S. Scroggs, “Low-Threshold L-type Calcium Channels in Rat Dopamine Neurons,” *J. Neurophysiol.*, vol. 91, no. 3, pp. 1450–1454, Mar. 2004, doi: 10.1152/JN.01015.2003/ASSET/IMAGES/LARGE/Z9K0040437460003.JPEG.
- [223] A. Verma and V. Ravindranath, “CaV1.3 L-Type Calcium Channels Increase the Vulnerability of Substantia Nigra Dopaminergic Neurons in MPTP Mouse Model of Parkinson’s Disease,” *Front. Aging Neurosci.*, vol. 11, p. 382, Jan. 2020, doi: 10.3389/FNAGI.2019.00382/BIBTEX.
- [224] A. Bonci, P. Grillner, N. B. Mercuri, and G. Bernardi, “L-Type Calcium Channels Mediate a Slow Excitatory Synaptic Transmission in Rat Midbrain Dopaminergic Neurons,” *J. Neurosci.*, vol. 18, no. 17, pp. 6693–6703, Sep. 1998, doi: 10.1523/JNEUROSCI.18-17-06693.1998.
- [225] B. T. Chen, K. A. Moran, M. V. Avshalumov, and M. E. Rice, “Limited regulation of

- somatodendritic dopamine release by voltage-sensitive Ca²⁺ channels contrasted with strong regulation of axonal dopamine release," *J. Neurochem.*, vol. 96, no. 3, pp. 645–655, 2006, doi: 10.1111/j.1471-4159.2005.03519.x.
- [226] Y. Kim, M. K. Park, and S. Chung, "Voltage-operated Ca²⁺ channels regulate dopamine release from somata of dopamine neurons in the substantia nigra pars compacta," *Biochem. Biophys. Res. Commun.*, vol. 373, no. 4, pp. 665–669, 2008, doi: 10.1016/j.bbrc.2008.06.099.
- [227] R. De La Fuente-Fernández, M. Schulzer, E. Mak, D. B. Calne, and A. J. Stoessl, "Presynaptic mechanisms of motor fluctuations in Parkinson's disease: A probabilistic model," *Brain*, vol. 127, no. 4, pp. 888–899, Apr. 2004, doi: 10.1093/brain/awh102.
- [228] M. Stacy and A. Galbreath, "Optimizing long-term therapy for Parkinson disease: Levodopa, dopamine agonists, and treatment-associated dyskinesia," *Clin. Neuropharmacol.*, vol. 31, no. 1, pp. 51–56, Jan. 2008, doi: 10.1097/WNF.0b013e318065b088.
- [229] R. Katzenschlager and A. J. Lees, "Treatment of Parkinson's disease: Levodopa as the first choice," *J. Neurol. Suppl.*, vol. 249, no. 2, 2002, doi: 10.1007/s00415-002-1204-4.
- [230] M. C. Mauri, S. Bravin, A. Bitetto, R. Rudelli, and G. Invernizzi, "A risk-benefit assessment of sulpiride in the treatment of schizophrenia," *Drug Safety*, vol. 14, no. 5. Springer International Publishing, pp. 288–298, Oct. 27, 1996, doi: 10.2165/00002018-199614050-00003.
- [231] M. R. Luquin, O. Scipioni, J. Vaamonde, O. Gershanik, and J. A. Obeso, "Levodopa-induced dyskinesias in Parkinson's disease: Clinical and pharmacological classification," *Mov. Disord.*, vol. 7, no. 2, pp. 117–124, Jan. 1992, doi: 10.1002/mds.870070204.
- [232] E. Pothos, M. Desmond, and D. Sulzer, "l-3,4-Dihydroxyphenylalanine Increases the Quantal Size of Exocytotic Dopamine Release In Vitro," *J. Neurochem.*, vol. 66, no. 2, pp. 629–636, Nov. 2002, doi: 10.1046/j.1471-4159.1996.66020629.x.

- [233] N. B. Mercuri and G. Bernardi, "The 'magic' of L-dopa: Why is it the gold standard Parkinson's disease therapy?," *Trends Pharmacol. Sci.*, vol. 26, no. 7, pp. 341–344, 2005, doi: 10.1016/j.tips.2005.05.002.
- [234] Y. Misu, Y. Goshima, H. Ueda, and H. Okamura, "Neurobiology of L-DOPAergic systems," *Prog. Neurobiol.*, vol. 49, no. 5, pp. 415–454, 1996, doi: 10.1016/0301-0082(96)00025-1.
- [235] A. Hasbi, B. F. O'dowd, and S. R. George, "Dopamine D1-D2 receptor heteromer signaling pathway in the brain: emerging physiological relevance," 2011. doi: 10.1186/1756-6606-4-26.
- [236] J.-H. Baik, "Dopamine signaling in reward-related behaviors," 2013, doi: 10.3389/fncir.2013.00152.
- [237] Y. Schmitz, M. Benoit-Marand, F. Gonon, and D. Sulzer, "Presynaptic regulation of dopaminergic neurotransmission," *J. Neurochem.*, vol. 87, no. 2, pp. 273–289, Oct. 2003, doi: 10.1046/J.1471-4159.2003.02050.X.
- [238] K. T. Kawagoe, J. A. Jankowski, and R. Mark Wightman, "Etched Carbon-Fiber Electrodes as Amperometric Detectors of Catecholamine Secretion from Isolated Biological Cells," *Buck, R. P. IEEE Trans. Elec. Devices ED*, vol. 63, no. 13, pp. 1455–1458, 1991, Accessed: Dec. 19, 2021. [Online]. Available: <https://pubs.acs.org/sharingguidelines>.
- [239] R. H. S. Westerink, A. de Groot, and H. P. M. Vijverberg, "Heterogeneity of Catecholamine-Containing Vesicles in PC12 Cells," *Biochem. Biophys. Res. Commun.*, vol. 270, no. 2, pp. 625–630, 2000, doi: <https://doi.org/10.1006/bbrc.2000.2470>.
- [240] D. Bruns, "Detection of transmitter release with carbon fiber electrodes," *Methods*, vol. 33, no. 4, pp. 312–321, 2004, doi: <https://doi.org/10.1016/j.ymeth.2004.01.004>.
- [241] S. E. Zerby and A. G. Ewing, "Electrochemical monitoring of individual exocytotic events from the varicosities of differentiated PC12 cells," *Brain Res.*, vol. 712, no. 1, pp. 1–10, 1996, doi: [https://doi.org/10.1016/0006-8993\(95\)01383-0](https://doi.org/10.1016/0006-8993(95)01383-0).

- [242] R. H. S. Westerink and A. G. Ewing, "The PC12 cell as model for neurosecretion," *Acta Physiol. (Oxf)*, vol. 192, no. 2, p. 273, Feb. 2008, doi: 10.1111/J.1748-1716.2007.01805.X.
- [243] K. D. Kozminski, D. A. Gutman, V. Davila, D. Sulzer, and A. G. Ewing, "Voltammetric and pharmacological characterization of dopamine release from single exocytotic events at rat pheochromocytoma (PC12) cells," *Anal. Chem.*, vol. 70, no. 15, pp. 3123–3130, Aug. 1998, doi: 10.1021/ac980129f.
- [244] L. A. Sombers *et al.*, "The Effects of Vesicular Volume on Secretion through the Fusion Pore in Exocytotic Release from PC12 Cells," *J. Neurosci.*, vol. 24, no. 2, pp. 303–309, Jan. 2004, doi: 10.1523/JNEUROSCI.1119-03.2004.
- [245] T. L. Colliver, S. J. Pyott, M. Achalabun, and A. G. Ewing, "VMAT-Mediated Changes in Quantal Size and Vesicular Volume," 2000.
- [246] H. Fathali and A. S. Cans, "Amperometry methods for monitoring vesicular quantal size and regulation of exocytosis release," *Pflugers Archiv European Journal of Physiology*, vol. 470, no. 1. Springer Verlag, pp. 125–134, Jan. 01, 2018, doi: 10.1007/s00424-017-2069-9.
- [247] M. A. Mena, V. Davila, J. Bogaluvsky, and D. Sulzer, "A Synergistic Neurotrophic Response to L-Dihydroxyphenylalanine and Nerve Growth Factor," 1998. [Online]. Available: <http://www.molpharm.org>.
- [248] N. B. Mercuri, P. Calabresi, and G. Bernardi, "Responses of rat substantia nigra compacta neurones to L-DOPA," *Br. J. Pharmacol.*, vol. 100, no. 2, pp. 257–260, Jun. 1990, doi: 10.1111/j.1476-5381.1990.tb15792.x.
- [249] G. K. Aghajanian and B. S. Bunney, "Dopamine 'Autoreceptors': Pharmacological characterization by microiontophoretic single cell recording studies," *Naunyn. Schmiedebergs. Arch. Pharmacol.*, vol. 297, no. 1, pp. 1–7, Mar. 1977, doi: 10.1007/BF00508803.
- [250] E. Guatteo *et al.*, "Dual effects of L-DOPA on nigral dopaminergic neurons," *Exp. Neurol.*, vol. 247, pp. 582–594, Sep. 2013, doi: 10.1016/j.expneurol.2013.02.009.

- [251] J. Duda, C. Pötschke, and B. Liss, "Converging roles of ion channels, calcium, metabolic stress, and activity pattern of Substantia nigra dopaminergic neurons in health and Parkinson's disease," *Journal of Neurochemistry*, vol. 139, no. Suppl Suppl 1. Blackwell Publishing Ltd, pp. 156–178, Oct. 01, 2016, doi: 10.1111/jnc.13572.
- [252] D. H. F. Vandael, A. Zuccotti, J. Striessnig, and E. Carbone, "CaV1.3-driven SK channel activation regulates pacemaking and spike frequency adaptation in mouse chromaffin cells," *J. Neurosci.*, vol. 32, no. 46, pp. 16345–16359, Nov. 2012, doi: 10.1523/JNEUROSCI.3715-12.2012.
- [253] A. Marcantoni, E. F. Raymond, E. Carbone, and H. Marie, "Firing properties of entorhinal cortex neurons and early alterations in an Alzheimer's disease transgenic model," *Pflugers Arch. Eur. J. Physiol.*, vol. 466, no. 7, pp. 1437–1450, 2014, doi: 10.1007/s00424-013-1368-z.
- [254] L. Guarina *et al.*, "Nanodiamonds-induced effects on neuronal firing of mouse hippocampal microcircuits," *Sci. Rep.*, vol. 8, no. 1, pp. 1–14, Dec. 2018, doi: 10.1038/s41598-018-20528-5.
- [255] P. Fromherz, A. Offenhäusser, T. Vetter, and J. Weis, "A neuron-silicon junction: A Retzius cell of the leech on an insulated-gate field-effect transistor," *Science (80-.)*, vol. 252, no. 5010, pp. 1290–1293, May 1991, doi: 10.1126/science.1925540.
- [256] P. Fromherz, "Extracellular recording with transistors and the distribution of ionic conductances in a cell membrane," *Eur. Biophys. J.*, 1999, doi: 10.1007/s002490050206.
- [257] A. Marcantoni, P. Baldelli, J. M. Hernandez-Guijo, V. Comunanza, V. Carabelli, and E. Carbone, "L-type calcium channels in adrenal chromaffin cells: Role in pacemaking and secretion," *Cell Calcium*, vol. 42, no. 4–5, pp. 397–408, 2007, doi: 10.1016/j.ceca.2007.04.015.
- [258] F. Yasumoto, T. Negishi, Y. Ishii, S. Kyuwa, Y. Kuroda, and Y. Yoshikawa, "Endogenous Dopamine Maintains Synchronous Oscillation of Intracellular Calcium in Primary Cultured-Mouse Midbrain Neurons," *Cell. Mol. Neurobiol.*, vol.

- 24, no. 1, pp. 51–61, Feb. 2004, doi: 10.1023/B:CEMN.0000012724.79184.b6.
- [259] B. Liss and J. Roeper, “A new tool for your novelty centre,” *Journal of Physiology*, vol. 588, no. 12. J Physiol, pp. 2013–2013, Jun. 2010, doi: 10.1113/jphysiol.2010.192203.
- [260] J. Yang, M. Ye, C. Tian, M. Yang, Y. Wang, and Y. Shu, “Dopaminergic modulation of axonal potassium channels and action potential waveform in pyramidal neurons of prefrontal cortex,” *J. Physiol.*, vol. 591, no. 13, pp. 3233–3251, Jul. 2013, doi: 10.1113/jphysiol.2013.251058.
- [261] D. J. Surmeier, J. Ding, M. Day, Z. Wang, and W. Shen, “D1 and D2 dopamine-receptor modulation of striatal glutamatergic signaling in striatal medium spiny neurons,” *Trends in Neurosciences*, vol. 30, no. 5. Trends Neurosci, pp. 228–235, May 2007, doi: 10.1016/j.tins.2007.03.008.
- [262] H. Lindén, E. Hagen, S. Łeski, E. S. Norheim, K. H. Pettersen, and G. T. Einevoll, “LFPy: A tool for biophysical simulation of extracellular potentials generated by detailed model neurons,” *Front. Neuroinform.*, vol. 7, no. JAN, 2014, doi: 10.3389/fninf.2013.00041.
- [263] J. Müller *et al.*, “High-resolution CMOS MEA platform to study neurons at subcellular, cellular, and network levels,” *Lab Chip*, vol. 15, no. 13, pp. 2767–2780, 2015, doi: 10.1039/c5lc00133a.
- [264] M. E. J. Obien, K. Deligkaris, T. Bullmann, D. J. Bakkum, and U. Frey, “Revealing neuronal function through microelectrode array recordings,” *Front. Neurosci.*, vol. 9, no. JAN, p. 423, 2015, doi: 10.3389/fnins.2014.00423.
- [265] D. J. Bakkum *et al.*, “The Axon Initial Segment is the Dominant Contributor to the Neuron’s Extracellular Electrical Potential Landscape,” *Adv. Biosyst.*, vol. 3, no. 2, pp. 1–11, 2019, doi: 10.1002/adbi.201800308.
- [266] S. W. Johnson and R. A. North, “Two types of neurone in the rat ventral tegmental area and their synaptic inputs,” *J. Physiol.*, vol. 450, no. 1, pp. 455–468, May 1992, doi: 10.1113/JPHYSIOL.1992.SP019136.

- [267] A. A. Grace and S. P. Onn, "Morphology and electrophysiological properties of immunocytochemically identified rat dopamine neurons recorded in vitro," *J. Neurosci.*, vol. 9, no. 10, pp. 3463–3481, 1989, doi: 10.1523/JNEUROSCI.09-10-03463.1989.
- [268] Z. Y. Tong, P. G. Overton, and D. Clark, "Stimulation of the prefrontal cortex in the rat induces patterns of activity in midbrain dopaminergic neurons which resemble natural burst events.," *Synapse*, vol. 22, no. 3, pp. 195–208, Mar. 1996, doi: 10.1002/(SICI)1098-2396(199603)22:3<195::AID-SYN1>3.0.CO;2-7.
- [269] K. Chergui, H. Akaoka, P. J. Charléty, C. F. Saunier, M. Buda, and G. Chouvet, "Subthalamic nucleus modulates burst firing of nigral dopamine neurones via NMDA receptors," *Neuroreport*, vol. 5, no. 10, pp. 1185–1188, 1994, doi: 10.1097/00001756-199406020-00006.
- [270] S. Johnson, V. Seutin, R. N.- Science, and undefined 1992, "Burst firing in dopamine neurons induced by N-methyl-D-aspartate: role of electrogenic sodium pump," *science.sciencemag.org*, Accessed: Dec. 21, 2021. [Online]. Available: <https://science.sciencemag.org/content/258/5082/665.abstract>.
- [271] N. Omelchenko and S. R. Sesack, "Glutamate Synaptic Inputs to Ventral Tegmental Area Neurons in the Rat Derive Primarily from Subcortical Sources," *Neuroscience*, vol. 146, no. 3, p. 1259, May 2007, doi: 10.1016/J.NEUROSCIENCE.2007.02.016.
- [272] F. Georges and G. Aston-Jones, "Activation of Ventral Tegmental Area Cells by the Bed Nucleus of the Stria Terminalis: A Novel Excitatory Amino Acid Input to Midbrain Dopamine Neurons," *J. Neurosci.*, vol. 22, no. 12, pp. 5173–5187, Jun. 2002, doi: 10.1523/JNEUROSCI.22-12-05173.2002.
- [273] Y. Shu, A. Hasenstaub, and D. A. McCormick, "Turning on and off recurrent balanced cortical activity," *Nat. 2003 4236937*, vol. 423, no. 6937, pp. 288–293, May 2003, doi: 10.1038/nature01616.
- [274] C. J. Lobb, C. J. Wilson, and C. A. Paladini, "A dynamic role for GABA receptors on the firing pattern of midbrain dopaminergic neurons," *J. Neurophysiol.*, vol. 104, no. 1, pp. 403–413, Jul. 2010, doi:

- 10.1152/JN.00204.2010/ASSET/IMAGES/LARGE/Z9K0071001900006.JPEG.
- [275] T. Kimm and B. P. Bean, "Inhibition of A-type potassium current by the peptide toxin SNX-482," *J. Neurosci.*, vol. 34, no. 28, pp. 9182–9189, 2014, doi: 10.1523/JNEUROSCI.0339-14.2014.
- [276] J. Kim, D. S. Wei, and D. A. Hoffman, "Kv4 potassium channel subunits control action potential repolarization and frequency-dependent broadening in rat hippocampal CA1 pyramidal neurones," *J. Physiol.*, vol. 569, no. 1, pp. 41–57, Nov. 2005, doi: 10.1113/JPHYSIOL.2005.095042.
- [277] T. Schneider, M. Dibué, and J. Hescheler, "How 'Pharmacoresistant' is Cav2.3, the Major Component of Voltage-Gated R-type Ca²⁺ Channels?," *Pharmaceuticals*, vol. 6, no. 6, p. 759, 2013, doi: 10.3390/PH6060759.
- [278] N. B. Mercuri, P. Calabresi, and G. Bernardi, "The electrophysiological actions of dopamine and dopaminergic drugs on neurons of the substantia nigra pars compacta and ventral tegmental area," *Life Sciences*, vol. 51, no. 10, p. 1992, 1992, doi: 10.1016/0024-3205(92)90479-9.
- [279] N. Mannal, K. Kleiner, M. Fauler, A. Dougalis, C. Poetschke, and B. Liss, "Multi-Electrode Array Analysis Identifies Complex Dopamine Responses and Glucose Sensing Properties of Substantia Nigra Neurons in Mouse Brain Slices," *Front. Synaptic Neurosci.*, vol. 13, p. 635050, Feb. 2021, doi: 10.3389/FNSYN.2021.635050/FULL.
- [280] B. M. Bizzarri *et al.*, "L-DOPA-quinone Mediated Recovery from GIRK Channel Firing Inhibition in Dopaminergic Neurons," *ACS Med. Chem. Lett.*, vol. 10, no. 4, pp. 431–436, Apr. 2019, doi: 10.1021/ACSMEDCHEMLETT.8B00477/SUPPL_FILE/ML8B00477_SI_001.PDF.
- [281] T. Brudek *et al.*, "Autoimmune antibody decline in Parkinson's disease and Multiple System Atrophy; a step towards immunotherapeutic strategies," *Mol. Neurodegener.*, vol. 12, no. 1, Jun. 2017, doi: 10.1186/S13024-017-0187-7.
- [282] A. C. Hoffmann *et al.*, "Extracellular aggregated alpha synuclein primarily triggers lysosomal dysfunction in neural cells prevented by trehalose," *Sci. Reports 2019*

- 91, vol. 9, no. 1, pp. 1–18, Jan. 2019, doi: 10.1038/s41598-018-35811-8.
- [283] K. Yamada and T. Iwatsubo, “Extracellular α -synuclein levels are regulated by neuronal activity,” *Mol. Neurodegener.*, vol. 13, no. 1, Feb. 2018, doi: 10.1186/S13024-018-0241-0.
- [284] A. Wawer, I. Joniec-Maciejak, A. Sznejder-Pachotek, J. Schwenkgrub, A. Ciesielska, and D. Mirowska-Guzel, “Exogenous α -Synuclein Monomers Alter Dopamine Metabolism in Murine Brain,” *Neurochem. Res.*, vol. 41, no. 8, pp. 2102–2109, Aug. 2016, doi: 10.1007/S11064-016-1923-Z/FIGURES/3.
- [285] M. Wakamatsu *et al.*, “Selective loss of nigral dopamine neurons induced by overexpression of truncated human α -synuclein in mice,” *Neurobiol. Aging*, vol. 29, no. 4, pp. 574–585, Apr. 2008, doi: 10.1016/J.NEUROBIOLAGING.2006.11.017.
- [286] M. Lin *et al.*, “In Parkinson’s patient-derived dopamine neurons, the triplication of α -synuclein locus induces distinctive firing pattern by impeding D2 receptor autoinhibition,” *Acta Neuropathol. Commun.*, vol. 9, no. 1, pp. 1–25, Dec. 2021, doi: 10.1186/S40478-021-01203-9/FIGURES/12.